The Molecular Mechanism of BRPF Proteins for the Reversion of Taxane Resistance in Prostate Cancer

by

Beyza Dedeoğlu Aydın

A Dissertation Submitted to the
Graduate School of Sciences and Engineering

in Partial Fulfillment of the Requirements for

the Degree of

Master of Science

in

Molecular Biology and Genetics

June 20, 2023

The Molecular Mechanism of BRPF Proteins for the Reversion of Taxane Resistance in Prostate Cancer

Koç University

Graduate School of Sciences and Engineering

This is to certify that I have examined this copy of a master's thesis by

Beyza Dedeoğlu Aydın

and have found that it is complete and satisfactory in all respects,
and that any and all revisions required by the final
examining committee have been made.

Committee Members:

Prof. Ceyda Açılan Ayhan (Advisor)

Prof. Tuğba Bağcı Önder

Assoc. Prof. NC Tolga Emre

Date: June 20, 2023

To my parents for their endless support and love and to my husband for being a constant source of motivation.

ABSTRACT

The Molecular Mechanism of BRPF Proteins for the Reversion of Taxane Resistance in Prostate Cancer

Beyza Dedeoğlu Aydın

Master of Science in Molecular Biology and Genetics

June 20, 2023

Prostate cancer (PCa) is a major cause of cancer-related death in men. Localized PCa can be treated with androgen suppression and surgery, nonetheless, many patients progress to the castration-resistant PCa (CRPCa), which is more aggressive and/or metastatic. The standard of care for CRPCa patients are taxanes (namely Docetaxel and Cabazitaxel), however resistance against these drugs develops over time. Taxane resistance makes clinical application of taxanes inefficient. Epigenetic regulation of cancer not only affects tumor development and progression but also resistance for chemotherapy. Hence, targeting these mechanisms appears as an alternative strategy to overcome drug resistance. Previous studies using an epigenetic drug library and epi-targeted CRISPR screens using taxane resistant CRPCa cells (Du145 and 22Rv1) have shown that inhibition of BRPF proteins (epigenetic reader proteins containing bromodomain group) efficiently reverses taxane resistance. To this end, we aimed to elucidate the molecular pathways involved in the reversion of taxane resistance through BRPFs in CRPCa cells.

In this thesis, several approaches were combined including RNA sequencing, chromatin immunoprecipitation, bioinformatics and genome editing methods in order to characterize the biological significance of the BRPF proteins in taxane-resistant CRPCa. BRPF inhibition with small molecules resensitized taxane-resistant CRPCa cells to both taxanes under study. Efficient silencing of both BRPF1 and -2 were able to revert taxane resistance, albeit only mildly. On the other hand, knockout of BRPF2 effectively reversed taxane-resistance and induced cell death. BRPF1 was essential for the viability of resistant cells, hence BRPF1 knockout in resistant cells could not be generated despite several attempts. Furthermore, silencing or knocking out of BRPFs led to downregulation of *ABCB1*, which encodes a permeability glycoprotein (Pgp), and suppressed its function, potentially explaining how cells may be resensitized to taxane treatment. This supression seems to involve direct binding of BRPF1 to the *ABCB1* promoter, as determined by ChIP-qPCR analysis. Furthermore, we observed that the promoter region of *ABCB1* in taxane-resistant CRPCa cells exhibited occupancy by H3K27ac. Taken together, our results uncovered molecular players involved in BRPF mediated drug resistance. BRPF inhibition appears as a promising anticancer strategy in taxane resistant CRPCa and the mechanism seems to involve inhibition of drug efflux. BRPF inhibition can be utilized in the development of effective therapies against taxane resistant CRPCa.

Keywords: BRPF, castration-resistant prostate cancer, drug resistance, epigenetics, taxane resistance.

ÖZETÇE

BRPF Proteinlerinin Prostat Kanserinde Taksan Direncini Geri Çevirmedeki Moleküler Mekanizması

Beyza Dedeoğlu Aydın

Moleküler Biyoloji ve Genetik, Yüksek Lisans

20 Haziran 2023

Prostat kanseri (PKa), erkeklerde kansere bağlı ölümlerin önemli bir nedenidir. Lokalize PKa, androjen baskılama ve cerrahi ile tedavi edilebilir, ancak birçok hasta kastrasyona dirençli PKa (KDPKa) aşamasına ilerler, bu da daha agresif ve/veya metastatik bir durumdur. KDPKa hastaları için standart tedavi yöntemi taksanlardır (özellikle Doksetaksel ve Kabazitaksel), ancak bu ilaçlara karşı direnç zamanla gelişir. Taksan direnci, taksanların klinik uygulamasını etkisiz hale getirir. Kanserdeki epigenetik düzenlemeler, tümör gelişimi ve ilerlemesini etkilediği gibi kemoterapiye karşı direnci de etkiler. Bu nedenle, epigenetik mekanizmalara yönelik hedefleme, ilaç direncinin önüne geçmek için alternatif bir strateji olarak görünmektedir. Daha önce yapılan çalışmalar, bir epigenetik ilaç kütüphanesi ve epi-hedefli CRISPR taramaları kullanarak, BRPF proteinlerinin (bromodomain grubu içeren epigenetik okuyucu proteinler) inhibisyonunun, taksan direncini, taksan dirençli KDPKa hücrelerde (Du145 ve 22Rv1) etkin bir şekilde tersine çevirdiğini göstermiştir. Bu amaçla, BRPF'ler aracılığıyla taksan direncinin tersine çevrilmesinde yer alan moleküler yolları, taksana dirençli KDPKa hücrelerinde aydınlatmayı amaçladık.

Bu tezde, RNA dizileme, kromatin immünopresipitasyonu, biyoinformatik ve genom düzenleme yöntemleri gibi çeşitli yaklaşımlar, BRPF proteinlerinin taksana dirençli KDPKa'daki biyolojik önemini karakterize etmek için kullanıldı. Küçük moleküllerle BRPF inhibisyonu, taksana dirençli KDPKa hücrelerini hem Doksetaksel hem de Kabazitaksel'e tekrar duyarlı hale getirdi. Hem BRPF1 hem de BRPF2'nin etkin bir şekilde susturulması, taksan direncini tersine çevirmeye yardımcı oldu, ancak sadece hafif bir etki gözlendi. Öte yandan, BRPF2'nin genetik knockout'u etkin bir şekilde taksan direncini tersine çevirdi. BRPF1, dirençli hücrelerin hayatta kalması için önemliydi, bu nedenle dirençli hücrelerde BRPF1 knockout'u çeşitli denemelere rağmen gerçekleştirilemedi. Ayrıca, BRPF'lerin sessizleştirilmesi veya knockout'u, permeabilite glikoprotein (Pgp) kodlayan *ABCB1*'in ifadesini düşürdü ve fonksiyonunu baskıladı, bu da hücrelerin taksan tedavisine yeniden duyarlı hale gelmesinin potansiyel bir açıklaması olabilir. Bu baskılama, ChIP-qPCR analizi doğrultusunda BRPF1'in doğrudan *ABCB1* promotörüne bağlanmasıyla açıklanabilir. Ayrıca, taksana dirençli KDPKa hücrelerinde *ABCB1*'in promotör bölgesinde H3K27 asetilasyonunun mevcut olduğunu gözlemledik. Sonuç olarak, bu çalışmada BRPF aracılı ilaç direncinde yer alan moleküler oyuncular

ortaya çıkarılmıştır. BRPF inhibisyonu, taksan direnci gösteren KDPKa'da umut verici bir kanser karşıtı strateji olarak görünmekte ve mekanizma, taksanın hücre dışına pompalanmasının inhibisyonunu içermektedir. BRPF inhibisyonu, taksana dirençli KDPKa'ya karşı etkili tedavilerin geliştirilmesinde kullanılabilir.

Anahtar kelimeler: BRPF, kastrasyona dirençli prostat kanseri, ilaç direnci, epigenetik, taksan direnci.

ACKNOWLEDGEMENTS

I would like to express my sincere gratitude to all those who have supported and contributed to the completion of my thesis. First and foremost, I would like to express my gratitude to my advisor Prof. Ceyda Açılan Ayhan for her guidance, mentorship, and unwavering support throughout this research journey. I would like to extend my gratitude to my mentor Dr. Buse Cevatemre. Her knowledge, encouragement, and invaluable feedback have been instrumental in shaping the direction of my work.

I am deeply thankful to Prof. Tuğba Bağcı Önder, Assoc. Prof. Tolga Emre and professors and faculty members whose expertise and insights have contributed to the development of my research. Their valuable suggestions and discussions have broadened my understanding and enriched my work. I am thankful to Dr. Hamzah Syed and and Dr. Özlem Yedier Bayram who generously provided me knowledge and materials for my research. I would like to express my heartfelt appreciation to my intern, Caroline Uslucan, for her invaluable support, positive energy and constant presence throughout my master's journey. I am grateful to my labmates for creating a collaborative and enjoyable research environment. Their intellectual discussions, and willingness to help have made the lab work not only easier but also immensely enjoyable. Their friendship and support have been a constant source of motivation.

This thesis is the output of the research project titled “Investigating the Roles of BRPF Epigenetic Regulators in Reversing Taxane Resistance in Castration Resistant Prostate Cancer in vitro and in vivo.” supported by the TÜBİTAK Career Support Program with project number 120S776. I would like to express my gratitude to TÜBİTAK for their support. Their financial support has enabled me to conduct experiments, attend conferences, significantly enhancing the quality and scope of my work. I would also like to acknowledge TÜBİTAK for granting me BIDEB 2210 scholarship.

Finally, I want to express my deepest appreciation to my family and my husband for their love, encouragement, and continuous support throughout this journey. Your support, encouragement, and contributions have been invaluable, and I am truly grateful for your presence in my life.

Thank you all.

Beyza Dedeoğlu Aydın

TABLE OF CONTENTS

LIST OF TABLES

LIST OF FIGURES

ABBREVIATIONS

ABC	Atp Binding Cassette
ABCB	Atp Binding Cassette Subfamily B Member
ABCG	Atp Binding Cassette Subfamily G Member
ADT	Androgen Deprivation Therapy
AKT	Akt Serine/Threonine Kinase
AML	Acute Myelogenous Leukemia
ANKRD	Ankyrin Repeat Domain
AR	Androgen Receptor
ATP	Adenosine Triphosphate
AUC	Area Under The Curve
BAM	Binary Alignment Map
BCA	Bicinchoninic Acid
BCL	B-Cell Lymphoma
BD	Bromo Domain
BET	The Bromodomain And Extra-Terminal Domain
BN	BRPF-Specific N-Terminal
BRD	Bromo Domain
BRPF	Bromodomain And PHD Finger Containing Protein
BSA	Bovine Serum Albumin
CBP	CREB-Binding Protein
CBX	Chromobox Protein
CBZ	Cabazitaxel
CBZ-R	Cabazitaxel-Resistant
ChIP	Chromatin Immunoprecipitation
CR	Castration Resistance
CREB	Camp-Response Element Binding Protein
CRISPR	Clustered Regularly Interspaced Short Palindromic Repeats
CRPC	Castration Resistant Prostate Cancer
CTG	Celltiter-Glo
CXCL	Chemokine (C-X-C Motif) Ligand
DAPI	4′,6-Diamidino-2-Phenylindole
DEG	Differentially Expressed Gene
DMEM	Dulbecco's Modified Eagle Medium
DMSO	Dimethyl Sulfoxide
DNA	Deoxyribonucleic Acid
DNMT	DNA (Cytosine-5)-Methyltransferase
DTX	Docetaxel
DTX-R	Docetaxel-Resistant
EAF	ELL-Associated Factor
EDTA	Etheylenediaminetetraacetic Acid
EGF	Epidermal Growth Factor

EGFR	Epidermal Growth Factor Receptor
EGR	Early Growth Response Protein
EGTA	Ethylene Glycol-Bis(B-Aminoethyl Ether)-N,N,N′,N′-Tetraacetic Acid
EMT	Epithelial-Mesenchymal-Transition
EPC	Enhancer Of Polycomb
ES	Enrichment Scores
EZH	Enhancer Of Zeste Homolog
FBS	Fetal Bovine Serum
FC	Fold Change
FDR	False Discovery Rate
FOSL	Fos-Related Antigen
FRET	Fluorescence Resonance Energy Transfer
GAPDH	Glyceraldehyde-3-Phosphate Dehydrogenase
GFP	Green Fluorescence Protein
GGPPS	Geranylgeranyl Diphosphate Synthases
GREAT	Genomic Regions Enrichment Of Annotations Tool
GSEA	Gene Set Enrichment Analysis
GTP	Guanosine-5'-Triphosphate
HA	Hemagglutinin
HAT	Histone Acetyltransferases
HCC	Hepatocellular Carcinoma
HDAC	Histone Deacetylases
HEPES	4-(2-Hydroxyethyl)-1-Piperazineethanesulfonic Acid
HIV	Human Immunodeficiency Virus
HMT	Histone Methyltransferases
HRP	Horseradish Peroxidase
HSPA	Heat Shock Protein
IC50	Half-Maximal Inhibitory Concentration
IGF	Insulin Like Growth Factor Binding Protein Like 1
IGFBPL	Transmembrane Protein 59 Like
IL	Interleukin
ING	Inhibitor Of Growth
IP	Immunoprecipitation
JAK	Janus-Family Tyrosine Kinase
JNK	Jun N-Terminal Kinase
KAT	Lysine Acetyltransferase
LHRH	Luteinizing Hormone-Releasing Hormone
MDR	Multidrug Resistance
MEAF	MYST/Esa1 Associated Factor
MLL	Mixed Lineage Leukemia
M-MLV	Moloney Murine Leukemia Virus
NEK	NIMA Related Kinase

NFDM	Nonfat Dry Milk
NFKB	Nuclear Factor Kappa B
NLS	Nuclear Localization Signal
NP-40	Nonylphenoxypolyethoxyethanol
NTN	Netrin
PBS	Phosphate-Buffered Saline
PCA	Principal Component Analysis
PCR	Polymerase Chain Reaction
PDB	Protein Data Bank
PEG	Polyethylene Glycol
PHD	Plant Homeodomain
PI	Protease Inhibitor
PMSF	Phenylmethylsulfonyl Fluoride
PNK	Polynucleotide Kinase
PRC	Polycomb Repressive Complex
PRMT	Protein Arginine Methyltransferase
PTM	Post-Translational Modifications
PVDF	Polyvinylidene Fluoride
PWWP	Proline–Tryptophan–Tryptophan–Proline
PZP	PHD-Zincknuckle-PHD
RIPA	Radioimmunoprecipitation Assay
RNA	Ribonucleic Acid
ROC	Receiver Operating Characteristic
RP	Precision-Recall
RPMI	Roswell Park Memorial Institute
RT	Room Temperature
RUNX	Runt-Related Transcription Factor
SAMD	Sterile Alpha Motif Domain Containing
SD	Standard Deviation
SDS	Sodium Dodecyl Sulfate
SIK	Serine/Threonine-Protein Kinase
SIRT	Sirtuin
SLC	Solute Carrier
SOD	Superoxide Dismutase
SRB	Sulforhodamine B
SZ	Sfp1-Like C2H2 Zinc Finger
TBST	Tris Buffered Saline Tween-20
TCA	Trichloroacetic Acid
TEB	Triton Extraction Buffer
TF	Transcription Factor
TGF	Transforming Growth Factor
TGFA	Transforming Growth Factor-Alpha
TNBC	Triple Negative Breast Cancer

TNF	Tumor Necrosis Factor
TNFA	Tumor Necrosis Factor Alpha
TNFRSF	Tumor Necrosis Factor Receptor Superfamily
TRAF	TNF Receptor Associated Factor Protein
TSS	Transcription Start Site
TTS	Transcription Termination Site
UCSC	University Of California, Santa Cruz
UPR	Unfolded Protein Response
USP	Universal Stress Protein
UTR	Untranslated Region
VEGFA	Vascular Endothelial Growth Factor A
WB	Western Blot
ZNF	Zinc Finger

Chapter 1:
INTRODUCTION

1.1 Prostate Cancer

Cancer is a significant source of morbidity and mortality worldwide. Prostate cancer (PCa) is a major cause of cancer-related death in men (Siegel et al., 2022). Cancer pathology's genetic, epigenetic, and metabolic elements contribute to developing tumor phenotype. Hormone-sensitive PCa has a high incidence rate, but because it progresses slowly and is detected early, it is often effectively treated (Rebello et al., 2021). Localized PCa is curable via primary interventions such as androgen deprivation therapy (ADT). Androgen suppression therapy is the standard of care for newly diagnosed PCa patients. Nonetheless, some patients still progress to the lethal castration-resistant stage of the disease. ADT refers to surgical (bilateral orchiectomy) or chemical (pharmaceutical) therapies that lower serum testosterone levels or block the androgen receptor (AR), such as Luteinizing hormone-releasing hormone (LHRH) agonists and antagonists. Flutamide, enzalutamide, and apalutamide are antiandrogens used in conjunction with chemical or surgical castration but are not considered ADT (Choi et al., 2022).

1.1.1 Castration-Resistant Prostate Cancer

PCa that recurs after hormonal treatment is known as castration-resistant PCa (CRPCa). CRPCa is resistant to hormone therapy – the standard treatment for PCa. CRPCa is more aggressive and/or metastatic than primary PCa. Numerous patients develop CRPCa. In CRPCa, cytotoxic chemotherapy using taxanes such as docetaxel and cabazitaxel is an important therapeutic option. Taxanes prevent microtubule depolymerization by binding to the free β-tubulin subunit in the cytoplasm. This results in mitotic arrest, cell death, and blockage of cellular trafficking (Thadani-Mulero et al., 2012).

1.1.2 Taxane Resistance in Prostate Cancer

While there have been significant advances in the treatment of PCa, the development of new treatments has been hampered by the emergence of drug resistance. This is particularly important in the case of castration-resistant PCa (CRPCa). Chemotherapy is preferred as the second line of defense to treat CRPCa. Nonetheless, some patients acquire resistance to chemotherapy. The average lifespan of taxane-resistant CRPCa is about 18 to 19 months. 80% of patients have been reported to have rapid disease progression following an initial response to docetaxel (Sella et al., 2007).

Although there have been advancements in the field of surgery, chemotherapy, and radiotherapy in recent times, chemotherapy resistance is a significant obstacle to treating PCa in clinics, as it results in treatment failure and the progress of the disease (Semenas

et al., 2012). Over time, the acquisition of resistance to taxanes can occur, as depicted in the diagram in Figure 1.1.

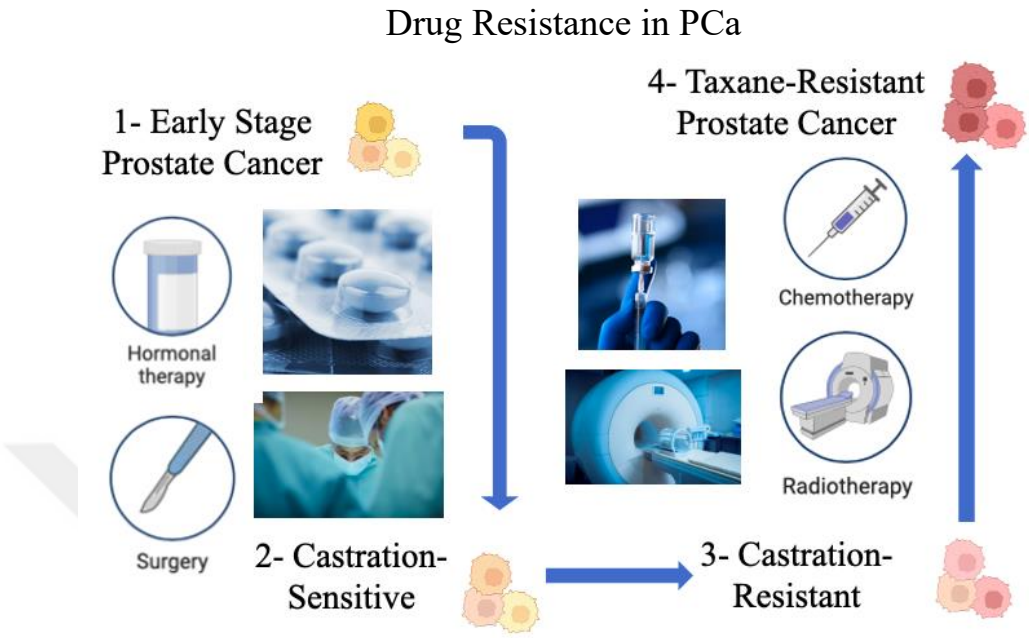

Figure 1.1: Schematic representation of the emergence of taxane resistance in prostate cancer. Figure created in biorender.com.

The development of resistance involves various mechanisms, such as genetic alterations, epigenetic changes, activation of survival pathways, and altered drug efflux mechanisms (Y. Liu et al., 2021). Ultimately, the emergence of taxane resistance allows cancer cells to persist, leading to tumor progression, increased aggressiveness, and the potential for metastasis to distant organs. Some of the most well-known processes linked to the emergence of taxane resistance are as the following: structural and functional alterations in microtubules (overexpression or mutations), upregulation of the drug efflux transporters, altered AR signaling, activation of antioxidant response (high expression of BMI1, SOD2, and IGF-1 signaling), and activation of survival pathways/escape from apoptosis (Maloneyi et al., 2020; Sánchez et al., 2011; Terry et al., 2009; G. Zhang et al., 2015). One of these processes is the activation of anti-apoptotic proteins such as the BCL2 family and clusterin (Zhong et al., 2010). Other examples are the activation of the GATA2-IGF axis, PI3K/AKT, Notch, Hedgehog, JNK and WNT/β-Catenin, p53, NFKB and IL-6/STAT3 signaling pathways (Domingo-Domenech et al., 2012; Kosaka et al., 2011; C. Liu et al., 2013; Maloney et al., 2020; Singh et al., 2019; Vidal et al., 2015).

Drug influx/efflux pumps determine the intracellular concentrations of Docetaxel. The effects of taxanes may be greatly impacted by the overexpression or downregulation of drug influx/efflux pumps (de Morrée et al., 2016). ATP-binding cassette (ABC) transporters (a family of integral membrane proteins) function in the ATP-dependent translocation of many substrates across membranes and lead to multidrug resistance (Rees

et al., 2009). *ABCB1* (ATP binding cassette subfamily B member 1) gene showed a notable increase in expression in PCa (Zhu et al., 2013) and, esophageal cancer cell lines that were resistant to taxane (R. Wang et al., 2016). Additionally, using siRNA to knock down *ABCB1* effectively restored the sensitivity to both paclitaxel and docetaxel in drug-resistant PCa (Zhu et al., 2013) and esophageal cancer cell lines (R. Wang et al., 2016).

Multidrug resistance (MDR) is a term depicting acquired resistance in cancer cells to a wide variety of chemotherapeutic agents following exposure (J. Wang et al., 2017). One of the most common causes of chemotherapy failure is intrinsic or acquired MDR, which leads to the return of malignant tumors and, eventually, patient relapse or death (J. Wang et al., 2017). MDR has been linked to several processes, including increased drug efflux (as depicted in Figure 1.2), increased DNA damage repair, decreased apoptosis, raised autophagy, and changed drug metabolism (J. Wang et al., 2017).

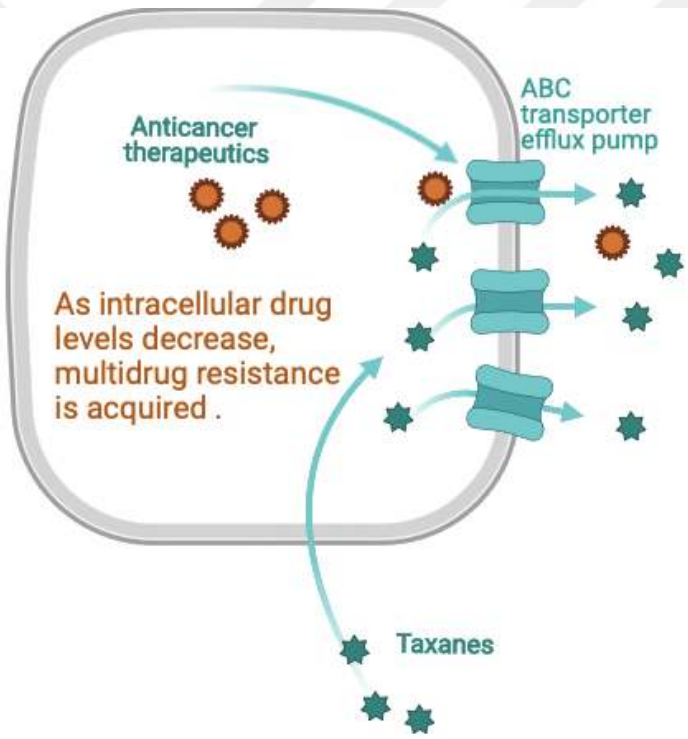

Figure 1.2: Schematic representation of acquired multidrug resistance via ABC transporter efflux pumps. Figure created in biorender.com.

1.1.3 Overcoming Taxane Resistance

In recent years, there has been an increasing focus on finding ways to overcome drug resistance in cancer. While effective strategies for improving taxane resistant PCa therapy have not yet been established, there were alternative approaches to increase immunotherapy response in patients with mCRPCa. The current treatment approach is to design clinical trials that combine agents with complementary anti-tumor activity. The novel combinatorial approaches could lead to synergy and thus improve responses in

patients. With technological advances in genomics, personalized therapies are currently being tested in PCa and will likely be utilized with increasing frequency in future clinical trials. Over the last decade, the genomic and transcriptomic landscapes of CRPCa have been extensively studied. However, the epigenetic landscape of taxane-resistant CRPCa remains largely unknown.

Over the last few decades, therapies reversing MDR have been investigated to increase the efficacy of chemotherapy. Verapamil, valspodar (PSC833), biricodar (VX710), tariquidar (XR9576), and laniquidar (R101933) are frequently studied MDR reversal drugs (J. Wang et al., 2017). Clinical studies of these drugs have shown limited evidence of significant survival advantages, mostly due to toxicities (Genovese et al., 2017). This is because of the critical functions of ABC transporters in a variety of normal tissues such as physiological disposal of toxins such as catabolites and xenobiotics (KP, 2016). Several studies have recently shown that combinational therapies can selectively target resistant cells while leaving healthy cells unharmed (Blagosklonny, 2003). BKM1972, AR antagonist enzalutamide, and RORγ antagonist SR2211 are also shown to enhance Docetaxel efficacy via blocking ABCB1 (Y. Wang et al., 2020). More effective therapeutic strategies for patients with PCa can be achieved by targeting the epigenetic mechanisms involved in drug resistance.

The challenges in PCa research are developing new effective systemic therapies and identifying drug resistance mechanisms. Tumor cells might acquire resistance to the taxanes, via genetic and epigenetic changes that lead to the activation of intrinsic resistance mechanisms in cancer cells (Maloney et al., 2020). The molecular and epigenetic mechanisms by which taxane resistance develops are yet to be precisely established. It is believed that taxane resistance is multifactorial. Taxane-resistant PCa is a complex and heterogeneous disease, making it difficult to identify effective targets for new treatments. Understanding the mechanisms of taxane resistance may result in improvements in CRPC treatment. There is an urgent need for novel strategies to combat taxane resistance in CRPCa. These include investigating the underlying mechanisms of drug resistance and developing new drugs and combination therapies. In this thesis, the epigenetic mechanisms underlying taxane resistance and therapeutic methods are studied for improving survival in taxane-resistant CRPCa via studying the epigenetic changes from taxane sensitive cells to resistant cells as described in Figure 1.3.

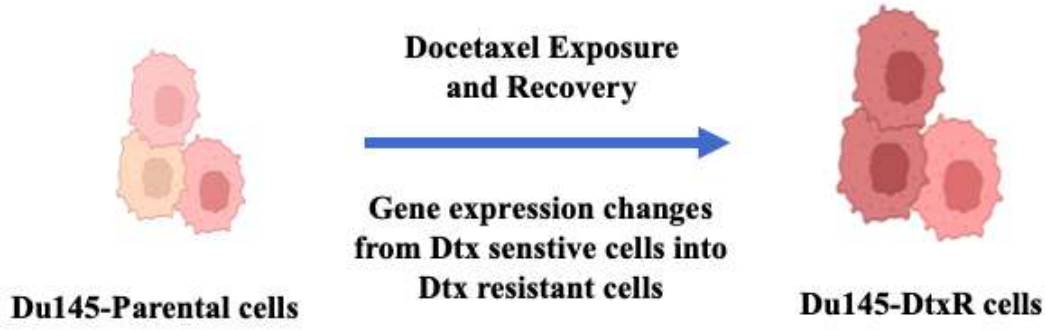

Figure 1.3: Model for acquired taxane resistance. Figure created in biorender.com.

1.2 Epigenetics

1.2.1 The Significance of the Epigenetic Modifications in Cancer

Nuclear DNA is packed into chromatin in a certain manner that results in a distinct pattern of gene expression (X-J Yang & Ullah, 2007). Histone modifications, nucleosome positioning, and the three-dimensional (3D) architecture of the chromatin inside the nucleus are all considered to be components of chromatin structure (Taverna et al. 2007). The human genome is wrapped around nucleosomes, which are made up of key histone proteins (H2A, H2B, H3, and H4), to compact and organise it. The negatively charged DNA is stabilized by the positively charged proteins known as histones. The globular domain and flexible N-terminal tail of each core histone are collectively referred to as the histone tail. Epigenetic regulation, which controls gene expression without altering the DNA sequence, primarily occurs through reversible chemical modifications of DNA or histone proteins. These modifications influence the accessibility and readout of the genetic information. Additionally, epigenetic changes can occur through the exchange of variant histones, the assembly and disassembly of chromatin structure facilitated by histone chaperones, or ATP-dependent chromatin remodeling by proteins like those belonging to the Swi/Snf family (Loyola & Almouzni, 2004; Peterson & Tamkun, 1995).

Through coordinating DNA accessibility and transcriptional activity, various chromatin states, nucleosome positioning, and histone post-translational modifications (PTMs) alter the chromatin structure (Biswas & Rao, 2018). Histone modifications, including acetylation, methylation, phosphorylation, ubiquitination, and sumoylation, play a crucial role in regulating chromatin structure and gene expression. Acetylation of histones is typically associated with transcriptionally active chromatin, while methylation of histones can either activate or repress gene expression, depending on the specific residue and degree of methylation. These alterations, generally known as the “histone code”, are essential for defining the outcome of gene expression (Alberts et al., 2002).

By recruiting scaffolding proteins like bromo- and chromodomain proteins, which specifically recognize and bind to acetylated and methylated lysine residues, respectively,

the histone code is known to control gene expression (Taverna et al., 2007). A variety of chromatin states are produced by various combinations of histone modifications, with constitutively silent regions producing "heterochromatin" and actively transcribed regions generating "euchromatin." These alterations play a crucial role in determining the genome's transcriptional state (Taverna et al., 2007).

Chromatin structure is a complex and dynamic phenomenon that involves a multitude of mechanisms and factors. Epigenetic modifications undergo substantial changes during various developmental processes, such as germ cell development and stem cell differentiation. They also play a significant role in pathological processes like tumorigenesis (Jones & Baylin, 2007). Understanding the intricate mechanisms of epigenetic control provides insights into gene regulation and its implications in development, disease, and potential therapeutic interventions.

There are three main categories of epigenetic proteins: writers, readers, and erasers as shown in Figure 1.4.

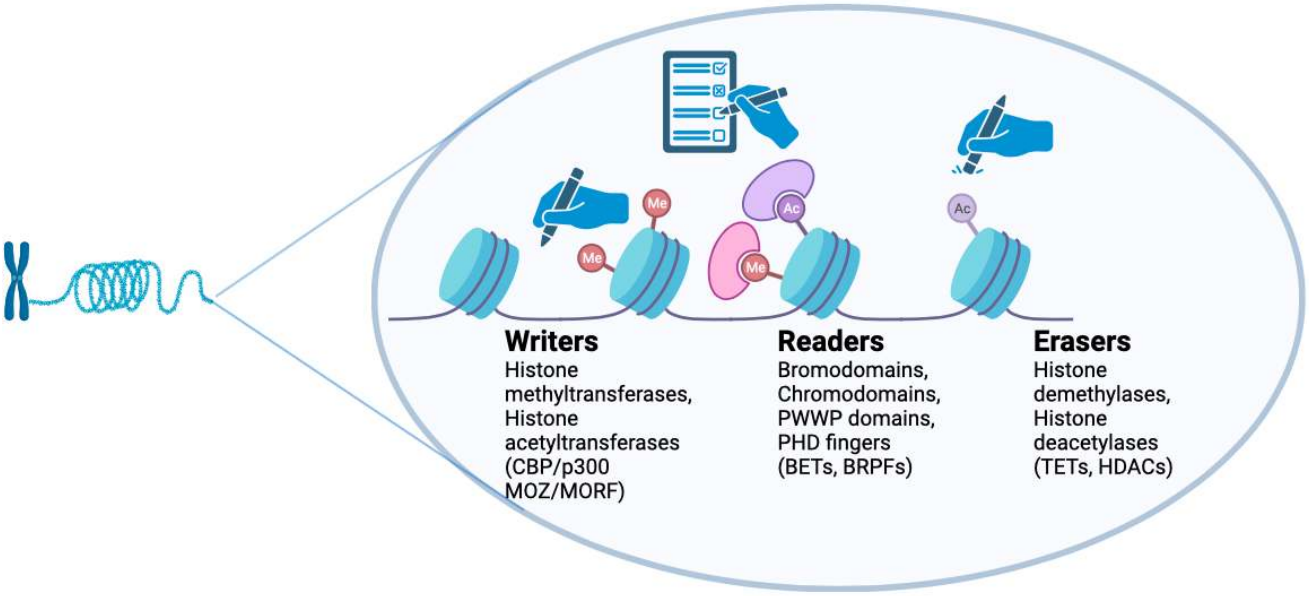

Figure 1.4: Subgroups of epigenetic modifier enzymes: Writers, erasers and readers. Figure created in biorender.com.

1.2.2 Histone Modifications

Epigenetic writers catalyze both active and repressive marks on DNA or histones. DNMTs, enhancer of zeste homolog 2 (EZH2), and disruptor of telomeric silencing 1-like (DOT1L) have emerged as the most attractive targets for therapeutic research among the writer proteins, which also include histone acetyltransferases (HATs) and histone methyltransferases (HMTs) (Feng & De Carvalho, 2022). DNMT1 inhibitor DAC has been shown to treat CRPCa patients by inhibiting the DNMT1-TRAF6-EZH2 pathway

(Li et al., 2022). The lncRNA PCAT1, which also promotes NF-B signaling, upregulates *c-Myc*, and enhances AKT and NF-B signaling, disrupts the PHLPP/FKBP51/IKK complex. LncRNA-PCAT1 expression and CRPC development are closely connected (Shang et al., 2019). In a study, it was shown that the polycomb group (PcG) family of transcriptional repressors may be responsible for epigenetic dysregulation that accelerates PCa development (Varambally et al., 2002). The PRC1 and PRC2 polycomb repressive complexes are composed of PcG proteins. The trimethylation of histone H3 at lysine 27 (H3K27me3) by PRC2 is facilitated by the enzymatic activity of EZH2, which causes transcriptional inactivation (Cao et al., 2002). Another study suggests that BMI1, a member of PRC1, promotes docetaxel resistance through its antioxidant role (Crea et al., 2011).

1.2.3 Epigenetic Readers

Epigenetic readers contain domains that can recognize particular post-translational alterations to DNA or histones (Feng & De Carvalho, 2022). Examples include the identification of methylated lysines by chromodomains, acetylated histone residues by bromodomains, and methylated CpGs by methylated CpG-binding domains. Drug development has focused on the BRD and extraterminal domain (BET) family, which has essential roles in carcinogenesis (Feng & De Carvalho, 2022).

The N-terminal chromodomain of PRC1-member CBX proteins (CBX2, 4, 6, 7, and 8) may then identify the H3K27me3 mark. Through protein-protein interactions, CBX proteins can draw PRC1 to the chromatin after binding H3K27me3. Through a number of processes, including histone H2A ubiquitination and chromatin compaction, PRC1 recruitment further increases transcriptional suppression (Cao et al., 2002). According to recent studies, metastatic and androgen-independent PCa cells overexpress chromatin reader CBX2, and increased CBX2 expression indicates a poor prognosis (Berezovska et al., 2006; Clermont et al., 2016; Z. Gao et al., 2012).

Bromodomains, as epigenetic readers found in chromatin-modifying complexes, bind to the acetyl lysine residues, and allow the recruitment of protein complexes (Obi et al., 2020). Bromodomain-containing proteins are dysregulated in numerous pathological conditions such as cancer and neurological disorders. Some HATs have bromodomains, such as p300, and CBP (Cheng et al., 2021). p300 binds to the adenovirus-E1a oncoprotein and CREB-binding protein (CBP) binds to the transcription factor CREB. p300/CBP are acetyltransferases and transcriptional coactivators of many transcription factors (Kitabayashi et al., 2001). Translocation t (8; 16) (p11; p13) of MOZ gene in patients with acute myeloid leukemia (AML) causes the fusion of the MOZ gene to the CBP gene, resulting in a MOZ-CBP fusion protein, and with translocation t(8;22)(p11;q13), MOZ-p300 fusion protein forms in AML (Borrow et al., 1996). p300-MLL fusion protein forms with the t(11;22) translocation in AML (Kitabayashi et al., 2001).

1.2.4 BRPF Structure and Histone Modifications

Bromodomain-PHD finger proteins (BRPF) scaffolding protein is an epigenetic reader that carries MYST family of HATs to chromatin through its bromodomain (Meier et al., 2017). The MYST family of HATs were named after the four members: MOZ (monocytic leukemic zinc-finger protein, also known as KAT6A), yeast Ybf2 (renamed Sas3, for something about silencing 3), yeast Sas2 and TIP60 (HIV Tat-interacting 60 kDa protein) (Xiang-Jiao Yang, 2015). BRPF1 also known as Peregrin, consists of a bromodomain, a N-terminal plant homeodomain (PHD)-zincknuckle-PHD (PZP), a C-terminal proline-tryptophan-tryptophan-proline (PWWP) domain (Laue et al., 2008). Crystal structure of human BRPF1 PZP bound to histone H3 tail (Klein et al., 2020) and BRPF1 domains (Yan et al., 2020) are displayed in Figure 1.5.

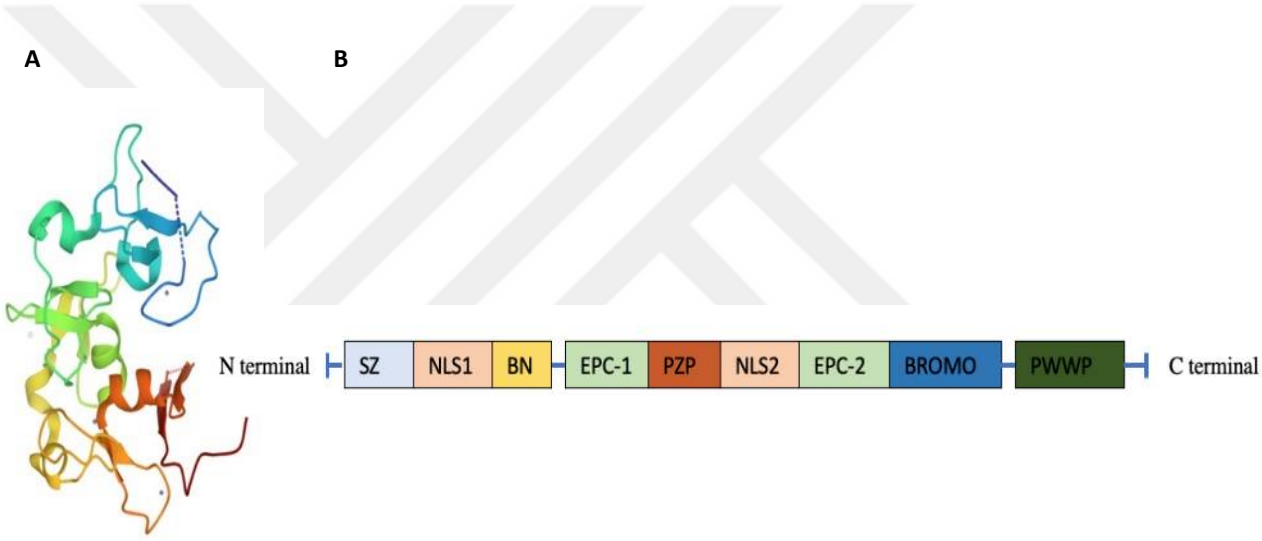

Figure 1.5: Structure of BRPF1 (Klein et al., 2020; Yan et al., 2020).
(A) Crystal structure of human BRPF1 PZP bound to histone H3 tail in ribbon representation PDB accession code 6U04. (Klein et al., 2020) (B) 2D BRPF1 domain structures: Sfp1-like C2H2 zinc finger (SZ); NLS, nuclear localization signal; H1-like, histone H1–like domain; PZP, PHD–zinc knuckle–PHD; bromo, bromodomain; PWWP, Pro-Trp-Trp-Pro containing domain; SM, serine/methionine-rich (Yan et al., 2020).

BRPF1 contains two EPC (enhancer of polycomb)–like motifs. With the contribution of BRPF-specific N-terminal (BN) domain, EPC-I interacts with the MYST domains of MOZ/MORF, whereas the downstream motif EPC-II binds to ING5 (the inhibitor of growth 5 or the paralog ING4) and MEAF6 (MYST/ Esa1-associated factor 6 homolog) (Ullah et al., 2008). BRPF1 contains the PZP domain, bromodomain, and PWWP domain for chromatin association (Yan et al., 2020). In contrast to its paralogs BRPF2 and BRPF3, BRPF1 additionally contains an Sfp1-like C2H2 zinc finger (SZ) (Yan et al., 2020). BRPFs and its binding partners mediate H3K9, H3K14, and H3K23 acetylation for gene activation (Cheng et al., 2021). BRPF1, MOZ, MEAF6, and ING5 form a multi-

subunit HAT complex as it was depicted in Figure 1.6 that acetylates free histones H3, H4, H2A and H2B in vitro (Poplawski et al., 2014) and regulates numerous cellular processes including the self-renewal of leukemic stem cells (You et al., 2016), embryo development, cell proliferation (You et al., 2015) and osteoclast differentiation (Meier et al., 2017).

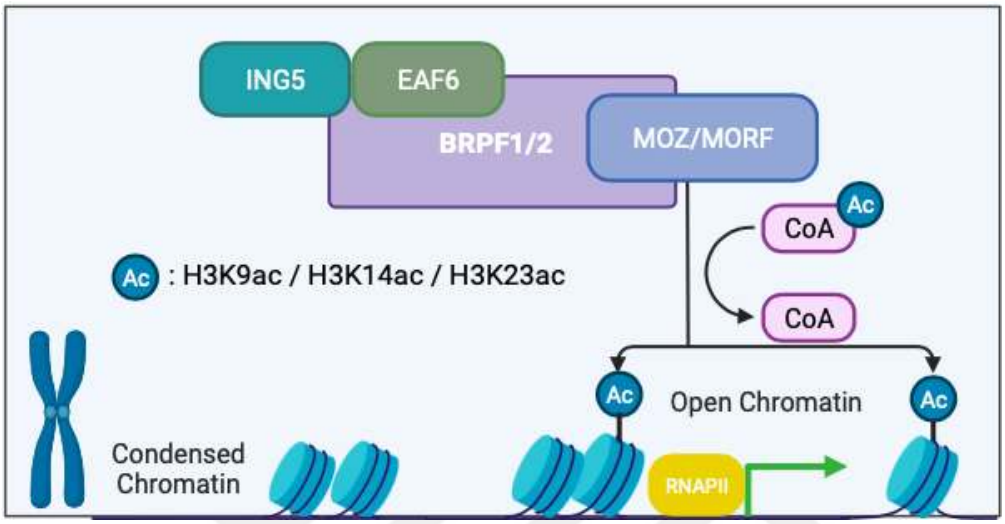

Figure 1.6: BRPFs and its binding partners mediate H3K9, H3K14, and H3K23 acetylation for gene activation (Cheng et al., 2021). Figure created with biorender.com.

BRPF1 is associated with the expression of genes taking part in hematopoiesis and developmental processes, such as Hox genes (Laue et al., 2008). In mice, BRPF1 gene knockout demonstrated that BRPF1 is essential for the growth and proliferation of embryonic fibroblasts and hematopoietic progenitors (You et al., 2015). The HAT activity of the MOZ/MORF HATs increases through the interaction of BRPF1 with the histone acetyltransferase domain. (Ullah et al., 2008)

MOZ is a co-activator of RUNX1 (also known as AML1) which is a regulator of hematopoiesis (Katsumoto et al., 2006). The impaired HAT activity of MOZ is associated with the development of cancer, specifically AML (Carlson & Glass, 2014) MORF (MOZ-related factor, KAT6B) is also crucial for many developmental processes and have been linked with leukemia and other cancers (X-J Yang & Ullah, 2007). BRPF1 mutations are seen in patients with neurodevelopmental disorders that are linked to dysregulated histone H3K23 acetylation (Yan et al., 2017). A mutation in MOZ gene is observed in esophageal adenocarcinoma (Dulak et al., 2013), MORF gene is disrupted in leiomyomata (Moore et al., 2004), mutations in MORF gene are seen in familial breast cancer (Wen et al., 2014), and CRPCa (Grasso et al., 2012). Transcriptome sequencing in another study demonstrated that BRPF1 is a master regulator directing the expression of numerous important oncogenes, such as E2F2 and EZH2 (Cheng et al., 2021). It was shown that BRPF1 promoted promoter H3K14 acetylation via the MOZ/MORF complex, activating the expression of E2F2 and EZH2 (Cheng et al., 2021). Human HCCs usually

have elevated levels of BRPF1, they proposed BRPF1 targeting as a treatment for HCC (Cheng et al., 2021). Deubiquitinase USP16 is shown to act as a novel deubiquitinase of c-Myc which increases CRPCa cell proliferation (Ge et al., 2021). USP35/BRPF1 axis activates malignant characteristics of PCa via stimulating the MVA pathway (Lin et al., 2022). Targeting USP35/BRPF1 might be a novel approach to enhance overall prognosis in PCa patients (Lin et al., 2022).

1.2.5 BRPF Inhibitors

GSK5959, PFI-4, GSK6853, OF-1, and NI-57 are some of the inhibitors of BRPF (Cheng et al., 2019). Their chemical structures are given in Figure 1.7.

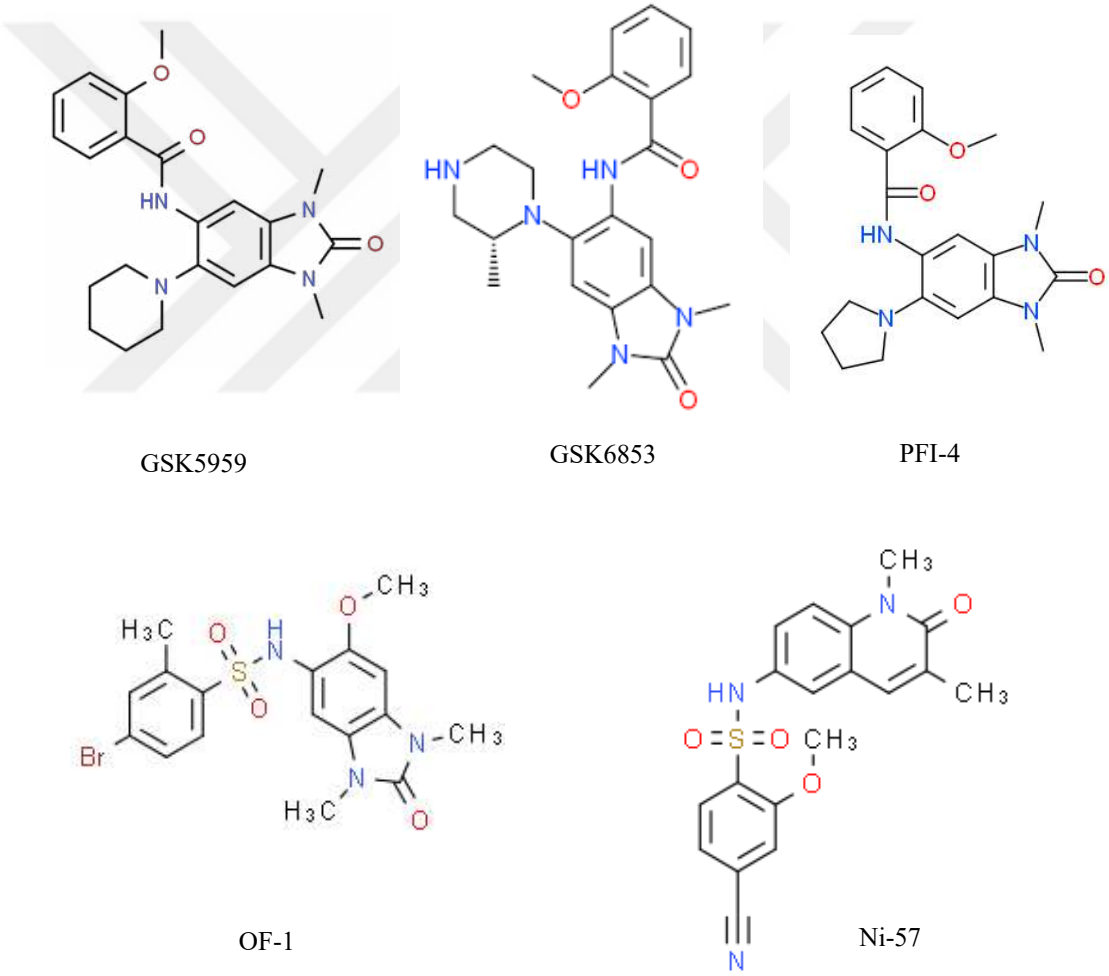

Figure 1.7: Chemical structures of BRPF inhibitors GSK5959, GSK6853, PFI-4, OF-1 and Ni-57.

GSK5959 specifically targets the BRPF1 bromodomain, displaying an IC50 of 80 nM. It exhibits significant selectivity for BRPF1 compared to 35 other bromodomains, such as BRPF2/3 and BET family bromodomains. GSK5959 effectively inhibits the interaction

between BRPF1 and histone H3.3 (Ullah et al., 2008). PFI-4 acts as a potent inhibitor of the BRPF1B bromodomain, exhibiting an IC50 of 172 nM. It displays substantial selectivity for BRPF1 over other bromodomains like BRPF2 (BRD1), BRPF3, and BRD4. PFI-4, similar to GSK5959, effectively disrupts the binding of BRPF1 to histone H3.3 (Ullah et al., 2008). GSK6853 demonstrates selectivity for BRPF1 over other bromodomains, with pIC50 values of 8.1, 5.1/4.8, and 4.7/<4.3 for BRPF1, BRPF2/3, and BRD4, BD1/2, respectively (Bamborough et al., 2016). OF-1 is a selective inhibitor of both BRPF1B and BRPF2 bromodomains, with Kd values of 100 and 500 nM, respectively. It demonstrates a higher selectivity for BRPF1B and BRPF2 over BRD4. Lastly, NI-57 is a pan-BRPF bromodomain inhibitor with Kd values of 31, 108, and 408 nM for BRPF1B, BRPF2, and BRPF3, respectively. It exhibits higher selectivity for BRPFs over BRD9 and other non-Class IV bromodomains (Ullah et al., 2008).

1.2.6 The Importance of Novel Epigenetic Therapies in Taxane Resistance

Understanding the regulation of chromatin structure is crucial for elucidating the molecular basis of gene expression and its dysregulation in various diseases. Many diseases, including cancer, exhibit aberrancy in epigenetic regulation (Feng & De Carvalho, 2022). Certain hematological and solid cancers are now being treated with a variety of epigenetic modifiers including inhibitors of DNA methyltransferase (DNMT) and histone deacetylase (HDAC) (Biswas & Rao, 2018). Due to the frequent epigenetic instability of tumors and the reversible nature of epigenetic changes, cancer cells may be vulnerable to therapy (Feng & De Carvalho, 2022). Epigenetic alterations are now recognized as one of the processes underlying resistance to anti-cancer drugs. Therefore, epigenetic regulators are essential targets of drug-resistant cancers (Biersack et al., 2022). Furthermore, epigenetic regulators are enzymes or proteins that bind to chromatin, making them highly suitable therapeutic targets for small inhibitory molecules. Epigenetic modifiers present valuable therapeutic targets given the reversible nature of epigenetic modifications. Therefore, the combination of chemotherapy and epigenetic inhibitors is regarded as a promising strategy for combating drug resistance in cancer treatment (Clermont et al., 2016; Wu et al., 2004)

In this study, epigenetic changes are evaluated in relation to taxane resistance and how they are becoming more widely recognized as possible mediators of overcoming taxane resistance in PCa. The development of drug resistance constitutes a major problem for the treatment of cancer, especially when taxane-based therapies are used. The effectiveness of taxane treatment is, however, hindered by the emergence of resistance mechanisms, necessitating the investigation of alternate methods to overcome this resistance.

Our primary objective was to gain insight into the molecular mechanisms underpinning BRPF (bromodomain-containing reader proteins) suppression in the reversal of taxane resistance. We used small chemical inhibitors, siRNA, and CRISPR/Cas9 technology to

target BRPF1 and BRPF2 expression in an effort to understand the impact of BRPF inhibition on taxane-resistant cancer cells. To assess the effectiveness of BRPF inhibition, we employed two methods. First, we assessed cell viability using the Sulforhodamine B (SRB) assay. Second, we evaluated the colony formation capacity of the cells via a colonogenic assay, which provides insights into the long-term survival and clonogenic potential of the cells. To gain a comprehensive insight of the molecular changes induced by BRPF inhibition, we employed RNA-sequencing. This approach allowed us to examine the transcriptomic differences between taxane-resistant cells that overexpress *ABCB1*, both with and without BRPF inhibition, revealing potential downstream targets of BRPFs and altered gene expression patterns. Furthermore, to identify direct target genes of BRPFs, we utilized chromatin immunoprecipitation coupled with quantitative PCR (ChIP-qPCR). This technique enabled us to analyze the binding of BRPF proteins to *ABCB1* promoter region and investigate the impact of their inhibition on the expression of target genes. Finally, BRPF inhibition emerges as a promising and innovative therapeutic strategy in the battle against taxane resistance in CRPCa. The findings of this study highlight the significant role of BRPF proteins in mediating taxane resistance and provide evidence that targeting these proteins can effectively reverse resistance through the downregulation of *ABCB1*, and restore sensitivity to taxane treatment.

Chapter 2:
MATERIALS AND METHODS

2.1 Cell Culture and Cell Lines

Du145, 22Rv1, HepG2, Huh7, U2OS, A549, H1299, RPE-1, MDA-MB-231, U373, HEK293T, THP-1, Jurkat, and K-562 cell lines were purchased from ATCC and the MOLM-13 cell line was purchased from DSMZ. T1-160 (Paclitaxel-resistant SUM159PT) cell line was generated by Özlem Yedier Bayram, PhD.

All cell lines were routinely grown at 37℃ in a 5% CO_2 humidified atmosphere. Prostate cancer cell lines 22Rv1, PC-3, DU-145, LNCaP cell lines were grown in RPMI-1640 (Sigma Aldrich, R8758) supplemented with heat-inactivated 10% fetal bovine serum, 100 U/mL of penicillin, and 100 µg/mL of streptomycin. Breast cancer cell lines (MDA-MB-231), brain tumor cell lines (U373), Hepatocellular carcinoma cell lines (HepG2 and Huh7), osteosarcoma cell line U2OS, and HEK293T cells were grown in DMEM (Sigma Aldrich, 51434C) supplemented with heat-inactivated 10% fetal bovine serum, 2 mM L-glutamine, 100 U/mL of penicillin, and 100 µg/mL of streptomycin. Non-small lung cancer cell lines (A549, H1299) and RPE-1 cells were grown in DMEM/F-12 (Gibco, 11320033) supplemented with heat-inactivated 5% fetal bovine serum, 100 U/mL of penicillin, and 100 µg/mL of streptomycin. Leukemia cell lines (Jurkat, K-562, MOLM-13, THP-1 were grown in RPMI-1640 (Sigma Aldrich, R8758) supplemented with heat-inactivated 10% fetal bovine serum (FBS; Biowest, 1810) and 100 U/ml of penicillin, and 100 µg/mL of streptomycin (Life Technologies, 15140122). T1-160 cells were grown in Ham's F12 nutrient mix (Gibco, USA) supplemented with 5% FBS, 5 µg/mL insulin (Sigma Aldrich, USA), 1 µg/mL hydrocortisone (Sigma Aldrich, USA) and 10 mM HEPES (Thermo Fisher, USA).

2.2 Generation and Confirmation of Taxane Resistant Cell Models

The development of mentioned Docetaxel and Cabazitaxel resistant Du145 and 22Rv1 cell lines (Du145-DtxR, Du145-CbzR and 22Rv1-DtxR, 22Rv1-CbzR) belong to the İpek Bulut, MSc. and Buse Cevatemre, PhD. The taxane sensitive cells (Du145-P and 22Rv1-P) were initially allowed to grow for 24 h and subsequently exposed to escalating doses of Docetaxel/Cabazitaxel (Dtx/Cbz) for a duration of 72 h. This process was repeated in a cycle over a period of 8 to 12 months.

2.2.1 Sulforhodamine B (SRB) Cell Viability Assay

Du145 parental (4×10^3) and resistant (7×10^3) cells were seeded on 96-well plates the day prior to drug exposure. At the end of the treatment with increasing doses of Dtx/Cbz for 72 h, cells were fixed with 50% (w/v) TCA (Sigma Aldrich, T6399) at 4°C for 1 h, washed with deionized water and allowed air dry at room temperature. Cells were then stained with 0.4% (w/v) SRB (Santa Cruz, sc-253615) for 30 min and subsequently

washed with 1% acetic acid. SRB dye was extracted using a 10 mM Trizma base (Sigma Aldrich, T1503). Measurements were carried out at 564 nm using a microplate reader (Synergy H1 Hybrid reader, BioTek).

2.2.2 Colony Formation Assay

Du145 parental (3×10^2) and resistant (1×10^3) cells were seeded on 12-well plates the day prior to taxane exposure. At the end of the taxane treatment, the medium was replaced by drug-free medium, and the cells were cultured for an additional 10 days. After this period, the wells were washed with PBS, and the colonies were fixed for 10 min with methanol (Merck, 1.06009). The colonies were stained in 0.5% (w/v) crystal violet (Merck, 1.09218) for 15 min and washed twice with distilled water. Colonies were quantified by using ImageJ (Schneider et al., 2012).

2.2.3 Immunofluorescence Staining

Du145 taxane sensitive and resistant cells grown on coverslips. Cells were fixed with ice cold methanol (Merck, 1.06009) at -20°C for 20 min, permeabilized with 0.1% Triton X-100 at room temperature for 15 min and blocked with %1 BSA at room temperature for 15 min. Cells were incubated with (1:100 diluted in %1 BSA) α-tubulin (Cell Signaling Technologies, DM1A Mouse mAb 3873), β-Actin (Boster Bio, M01263-3), BRPF1 (ab259840), BRPF2 (ab181069) at room temperature for 1 h. After washing twice, Alexa Fluor™ 488 secondary antibody (Invitrogen, A32731) was added and incubated at room temperature for 1 h. Texas Red™-X Phalloidin Actin specific dye, (Thermo Fishcer, T7471) was used for actin staining. 5 µL methanolic stock solution was diluted into 200 µL PBS. To visualize the nuclei the cells were stained with DAPI (Abcam, ab228549). The immunostained cells were observed and collected by a confocal microscope (Leica SP8).

2.3 Understanding The Phenotypic Characteristics Of Resistant Cells

2.3.1 Wound Healing Assay

To assess the migration time of cells towards the center, Du145 taxane sensitive and resistant cells (8×10^4) were seeded on 12-well plates and allowed to adhere. Next day, cell layer was scraped in a straight line using a 10 µL pipette tip. Using phase contrast microscopy, images were taken. An image J plugin for the image analysis of in vitro scratch wound healing assays was used for the analysis (Suarez-Arnedo et al., 2020).

2.3.2 Doubling Time Assay

Du145 taxane sensitive and resistant cells (1×10^5) were seeded on 6-well plates. Cells were trypsinized and counted using trypan blue dye every 48 h until day 6. The doubling time was calculated via the following method.

(t=time, N=cell number)

Doubling time $T_d = (t2 - t1) * \frac{\ln(2)}{2\ln(N2/N1)}$

2.3.3 Cell Adhesion Assay

To determine the time required for cells to adhere, Du145 and 22Rv1 taxane sensitive and resistant cells (4.5×10^4) were seeded on 12-well plates and allowed to adhere. Unattached cells were washed off with PBS and attached cells were fixed with ice-cold methanol (Merck, 1.06009) at 20 min intervals up to 6 h after seeding. Attached cells were stained with 0.5% (w/v) crystal violet (Merck, 1.09218) for 1 h, washed and left to dry. Plates were scanned and particle mean for each well were analyzed using ImageJ software (Schneider et al., 2012).

2.4 Confirmation of Reversion of Taxane Resistance via BRPF inhibition

2.4.1 Previous Studies with Epigenetic Screening

Epigenetics Drug Screening belongs to İpek Bulut, MSc. and Buse Cevatemre, PhD. Epigenetics Screening Library (Cayman, 11076) was used to identify regulators of taxane resistance reversal. Du145-DtxR cells were co-treated with compounds at a concentration of 5 μM and IC25 values of taxanes for 72 h. 145 epidrugs were screened for resistance reverter activity by using the SRB viability assay. Epi-targeted CRISPR Library Screening belongs to Özlem Yedier Bayram, PhD. and Bengül Gökbayrak PhD.

2.4.2 siRNA Silencing of BRPFs

siRNA transfections of taxane resistant Du145 and 22Rv1 cells with Lipofectamine 3000 (Invitrogen, L3000015) were carried out according to manufacturer's instructions. The parental cells (12×10^4), resistant cells (17×10^4) were seeded into 6-well plates. 1 μL siRNA was mixed with 125 μL Opti-MEM (Invitrogen, 31985062) ; and 7.5 μL of Lipofectamine 3000 Reagent was mixed with 125 μL Opti-MEM in separate tubes. siRNA mixture was added onto Lipofectamine 3000 mixture and incubated for 15 min. Final mixture was added onto the cells dropwise and fresh media were given to the cells 8 h later. Next day, cells were trypsinized and seeded for cell viability or colony formation assays, RNA pellets were taken for subsequent mRNA expression assessment. siRNA silencing was monitored at the mRNA level. RT-PCR was used to determine the change in mRNA expression. siRNAs that were used for siRNA transfection are listed in the Table 2.1.

Table 2.1: Ambion Silencer Select siRNA IDs.

siRNA	ID
Negative control	4390844
BRPF1	s15422
BRPF2	s24390

2.4.3 qRT-PCR

Total RNA was extracted with RNA Isolation Kit (Zymo, R1055) and cDNA was synthesized from 1 µg total RNA using the M-MLV Reverse Transcriptase (Invitrogen, 28025013) Subsequently 10 ng cDNA template was amplified using LightCycler 480 SYBR Green I Master mix (Roche Diagnostics, 04707516001). The reaction mixture contained 0.15 µM specific primers for target genes that were listed in the table below and incubated at 95°C for 5 min, followed by 40 cycles of 95°C for 10 s, 60°C for 30 s, and 72°C for 1 s. β-Actin was used as reference control and qRT-PCR was run on the PikoReal Real-Time PCR System (Thermo Fisher Scientific). The relative fold change(FC) in gene expressions were measured with the $2^{(-\Delta\Delta CT)}$ method.

Table 2.2: The nucleotide sequences of the PCR primers used to determine gene expressions by qRT-PCR.

Gene Name	Forward primer	Reverse Primer
β-ACTIN	TCACCATGGATGATGATATCGC	ATAGGAATCCTTCTGACCCATGC
GAPDH	AGCCACATCGCTCAGACAC	GCCCAATACGACCAAATCC
BRPF1	CGTGGAATTGATCCGCAAGC	GCTCCAAGGTTTTGCGAAGG
BRPF2	CAGCGGAAGAAGCAGTTTGTG	TCTTTGGCAGCCTTCATCTCC
BRPF3	AGAACATCGGCTATGACCCC	CACCTCTGGGGACAAATGGG
ABCB1	ACAGAGGGGATGGTCAGTGT	TCACGGCCATAGCGAATGTT
PRMT5	TAAGCCAGAACCGTCCTCCA	AGATGGCCTGCTGGTACTGA
CCN2	GGTGTGGCTTTAGGAGCAGT	TGATGGCTGGAGAATGCACA
CXCL8	AACTTTCAGAGACAGCAGAGCA	TGGTTCCTTCCGGTGGTTTC
EGR1	TCCCATTTACTCAGCGGCAC	TGGAAACAGGTAGTCGGGGA
FOSL1	CTCTGGAGCCCTAACCCCTT	GTTGGGTGGATCACAGGAAGA
JUN	TAATCCAGTCCAGCAACGGG	GTGTTCTGGCTGTGCAGTTC
CR2	GTTTTCTTGGCTCTCGTCGC	CCAACAGCAATGGGGGTAGA
MYC	TTCCCCTACCCTCTCAACGA	CAGAGAATCCGAGGACGGAG
NFKB1	TAATGCCTTCCGGCTGAGTC	TGCTTCGGTGTAGCCCATTT
HERPUD1	GGAGGCTTTGACAGGAATGGA	ACGGCTTCACGTTTCTGCT

SEMA3C	CTGTGGATCGAGTGAACGCT	GCACAGTATGTTGTGCCGA
SERPINE1	AAGCCTAATCAGCCCACCAT	TAGCATTTGACACCACCCCT
GALNT3	AAAAGCGTTGGTCAGCCTCT	CCTTCTGGATGTTGTGCCGA
SIK1B	GGGTTCGTCGTGGTTGAGAT	CAGGAATGGAGAGCGTTGA
SLC7A2	CCTCGCGCTGTTTCTTGTTC	GATGCTGAACGCTGGCAAAA
DDX39A	CGGCGGAAAACCGAAGTTG	AGCTGTGGATGGAAACGTAGG
HEXIM1	CCAAGAAGAAGCGGCATTGG	ACTGCGTGGTGTTATAGGGC
MT1F	GACTGATGCCAGGACAACCT	AGCAAATGGGTCAAGGTGGTAT
NTN1	CACTTTCCCGGCCAGAGTTT	TGATGCGGGTAAATGTGGGG
TGFA	CCCTGTGTTTCCTTGCCCTT	TGAGCCATTGGAAACAGCGA
CEMIP2	GGGGTAGGGGAAGTAACATTGG	AGCCAGATGGGTGACGACTA
TNFRSF9	ACGGGGCAGAAAGAAACTCC	CAAGAAAGTCCCAACAGCCC
RUNX1	GCTTGTCCTTTTCCGAGCG	GAGGGTTAAAGGCAGTGGAGT
RAB3B	GAGTCCTTCAATGCTGTCCAAG	GAACAACCCTCTCTTCCTCCAT
CRIP1	AGCCGAGAGCCACACTTTC	GCATTAGGGGCAACAAGGGA
CRIP2	GTGCGACAAGACCGTGTACT	TCGCACTTGAGGCAGAACTT

2.4.4 H3K9, H3K18 and H3K27 Acetylation Levels upon BRPF Inhibition

H3K9, H3K18 and H3K27 acetylation protein levels were investigated upon treatment with BRPF inhibitors on Du145-DtxR cell lines after 1-3-6-9-12-24 h. 8×10^5 cells were seeded in 25T dishes and treated with 5 µM of indicated inhibitors; GSK5959 (Cayman, 901245-65-6), OF1 (Cayman, 919973-83-4) , PFI4, (Cayman, 900305-37-5)

2.4.5 Histone Extraction

Cells were centrifuged at 300 g for 5 min. Treated and untreated cells were lysed in Triton Extraction Buffer (TEB) containing 2 mM PMSF (Merck, 10837091001) on ice for 10 min at a final concentration of (1×10^6) cells/mL and centrifuged at 6.500 g for 10 min at 4°C. Supernatant (the cytoplasm) was discarded, and the pellet (the nuclei) was washed with TEB and centrifuged (6v.500 g, 10 min, 4°C). To acid extract the histones, nuclei were resuspended with 0.2N HCl (Sigma Aldrich, 320331) at 4°C overnight. Samples were centrifuged (6.500 g, 10 min, 4°C) and histone containing supernatant was neutralized with 2M NaOH (Sigma Aldrich, 221465) at 1/10 of the volume of the supernatant. Anti-Acetyl-Histone H3 (Lys9) (C5B11) Rabbit mAb, 9649 Cell Signaling Technologies; Anti-Acetyl-Histone H3 (Lys18) (D8Z5H) Rabbit mAb, 13998 Cell Signaling Technologies; Anti-Acetyl-Histone H3 (Lys27) Antibody, 4353; Anti-Histone H3 antibody (ab18521) Rabbit mAb Abcam antibodies were used for Western Blotting, 1:2000 diluted in TBST (tris-buffered saline with 0.1% Tween 20). To prepare 10X TBST (0.1% Tween 20), the following procedure is followed. First, 24.23 g of Tris base (Merck, 10708976001) and 80.06 g of NaCl (Merck, S9888) are weighed. These compounds are then dissolved in distilled water, bringing the volume up to 800 ml. Next, the pH of the

solution is adjusted to 7.6 using HCl. After that, 10 ml of Tween 20 is added to the solution. Finally, the volume is made up to 1 liter with distilled water.

2.4.6 SDS-PAGE and Western Blotting (WB)

Cells were harvested and centrifuged at 300 g for 5 min. Proteins were extracted by RIPA lysis buffer (EcoTech Biotechnology, R0278) containing protease inhibitor cocktail (Merck, 11697498001), 1mM PMSF (Merck, 10837091001) and phosSTOP phosphatase inhibitor (Merck, 4906845001) at 4°C for 30 min. The cell lysate was centrifuged at 15.000 g for 15 min at 4°C to separate proteins from other cellular particles. The resulting supernatant was quantified using a BCA assay. Protein containing supernatant kept on ice during experiments. PierceTM BCA Protein Assay Kit (Thermo Fischer Scientific, 23225) was used to measure protein concentrations. 2 mg/mL Bovine Serum Albumin standard diluted at different concentrations (0, 0.4, 0.8, 1.2, 1.6, 2 mg/mL) with ddH_2O. Working solution mix, containing Reagent A and Reagent B (50:1 ratio) were prepared. BSA standards and proteins were added into 96 well plates (10 µL/well) and mixed with BCA working solution (190 µL/well). The plate incubated at 37°C for 30 min. Absorbance was measured at 562 nm with Bio-Tek H1 Synergy microplate reader. Blank values were subtracted from all measurements. Protein concentrations were normalized to the standard curve. The Laemmli sample buffer (Bio-Rad Laboratories, 1610747) was added to the proteins and boiled at 95°C for 10 min. 30 µg of protein for each sample was loaded on 4-15% SDS-PAGE gel (Mini- PROTEAN® TGXTM Precast Gels, BIORAD, 161-0317). After electrophoresis (100 V and 60 min) proteins were transferred onto the PVDF membrane (Bio-Rad, 1620177) at 200 mA for 120 min at 4°C. The membranes were blocked with 5% NFDM (Bio-Rad Laboratories, 1706404) at room temperature for 1 h and immunoblotted with the primary antibodies against the protein of interest at 4°C overnight. The antibodies used for Western blotting are as given: β-Actin (Boster Bio, M01263-3), GAPDH (Abcam, ab9485), ABCB1 (Cell Signaling, E1Y7S), HA (Biolegend, 901502) BRPF1 (Abcam, ab259840; Invitrogen, 703489; Novus, NBP1-88369; Sigma Aldrich, SAB1401408; LSBIO, LS-C306572-50) and BRD1 (Abcam, ab181069). Next day the membranes were washed with TBST, and then incubated with the HRP-conjugated secondary antibodies (1:5.000 dilution in TBST for Goat anti-Rabbit (ab205718) , and Goat anti-Mouse IgG (ab97023) for 1 h at room temperature. The membranes were washed again with TBST. Chemiluminescent signal was detected with Immobilon Forte Western HRP substrate (Millipore, WBKLS0500) and imaged by LI-COR Odyssey FC Imaging system (LI-COR Biosciences).

2.4.7 CRISPR/Cas9 Knockouts

We utilized CRISPR/Cas9 technology to specifically disrupt the BRPF gene. Guide RNAs (gRNAs) targeting the BRPF gene were designed and validated, followed by transfection of cells with BRPF-specific gRNA/Cas9 constructs, as well as non-targeting controls. To clone the gRNA oligonucleotides (given in table 2.3), lentiviral CRISPR

plasmid was digested with BsmBI enzyme (NEB, R0580), followed by the dephosphorylation of backbone with Antarctic Phosphatase enzyme (NEB, M0289). The phosphorylation and annealing of gRNA oligos were achieved using T4 PNK enzyme (Thermo Fischer, M0201S). Ligation reaction was performed by using T4 Ligase (Thermo Fischer, M0202S). Ligation products were transformed into competent E. coli DH5-alpha cells. Subsequently, plasmid extraction was performed on bacterial colonies harboring the cloned gRNA, and the presence of the correct gRNA sequence was verified through diagnostic PCR analysis. Later, successfully cloned plasmids were used for virus production. The gRNA-containing plasmid, along with packaging plasmids such as psPAX2 and VSV-G, was co-transfected into HEK293T cells using the Fugene 6 (Promega, E2311) transfection method. For lentiviral packaging, (2×10^6) HEK293T cells were seeded to 10-cm plates. Next day, 2500 ng target plasmid, 2250 ng psPAX2 (Addgene Plasmid, 12260) and 225 ng VSV-G (Addgene Plasmid, 8454) plasmids were mixed in 200 µL serum-free DMEM. DNA mixture was then added to 200 µL serum-free DMEM containing 15 µL Fugene 6 (Promega, E2311). DNA-Fugene mixture was distributed to 10 cm plates as 400 µL dropwise. Next day, the fresh media was given. Supernatant containing viral particles was collected 48-72 h post-transfection and filtered through 45-µm filters (Invitrogen, F2502-3) to eliminate cell debris. Supernatants were mixed with PEG8000 in 10% final concentration (Sigma Aldrich, P2139, dissolved in PBS as 50% (w/v)). Supernatants were centrifuged at 2500 rpm for 20 min and pellets were resuspended with PBS as 100x concentrated. Viruses were stored at -80ºC until use. 8×10^4 cells were seeded in a 6-well plate and were transduced with 5 µL virus in the presence of 8 µg/mL protamine sulphate (Merck, P3369). After the fresh media was given, cells in each well were transferred to 10 cm plates in the presence of puromycin (Merck, P7130). Once the puromycin selection of uninfected cells was complete, the cells were separated into single colonies, allowing for the isolation and characterization of individual cell lines with BRPF1 and BRPF2 knockouts. CRISPR/Cas9-mediated knockout of BRPF2 cells were identified via western blotting, performed as described in Chapter 2.5.3.

Table 2.3: Oligonucleotide Sequences for CRISPR/Cas9 systems.

Guide	Oligonucleotide Sequence
BRPF1_g1-F	AAA CCT TGC GGA TCA ATT CCA CGA C
BRPF1_g1-R	CAC CGT CGT GGA ATT GAT CCG CAA G
BRPF1_g2-F	AAA CTG GCG TTA TAC TTG AGG CAG C
BRPF1_g2-R	CAC CGC TGC CTC AAG TAT AAC GCC A
BRPF1_g3-F	AAA CAC GGA GTA GGC CTC ATT CTC
BRPF1_g3-R	CAC CGA GAA TGA GGC CTA CTC CGT
BRPF2_g1-F	AAA CCC TGA TTC GCA ATC CTA TTT C
BRPF2_g1-R	CAC CGA AAT AGG ATT GCG AAT CAG G
BRPF2_g2-F	CAC CGA TCG AGC TGC TGC GCA AGC
BRPF2_g2-R	AAA CGC TTG CGC AGC AGC TCG ATC
BRPF2_g3-F	AAA CCG GCT CTA TAG AAC ACG GTG C
BRPF2_g3-R	CAC CGC ACC GTG TTC TAT AGA GCC G

NT_guide_-F	CAC CGT ATT ACT GAT ATT GGT GGG
NT_guide_-R	AAA CCC CAC CAA TAT CAG TAA TAC

2.5 Transcriptomic Changes in the Reversion of Taxane Resistance

2.5.1 ABCB1 mRNA Expression after BRPF Inhibition

Following siRNA transfection performed as described in Chapter 2.4.2, we assessed the mRNA levels of *ABCB1* by performing RNA extraction, cDNA Synthesis and qPCR as described in Chapter 2.4.3.

2.5.2 Calcein AM Retention Assay

To detect the ABCB1 efflux activity using calcein-AM, Du145 parental (4×10^3) and resistant (7.5×10^4) cells were seeded on 96-well plates. Cells were then incubated with 125 nM calcein-AM (Invitrogen, C1430) for 30 min at 37°C. The calcein fluorescence signal was detected by using a luminometer (Synergy H1 Hybrid microplate reader, BioTek). Signal was normalized to CTG viability signals. Images were taken by an inverted fluorescence microscope (Leica DMI8).

2.5.3 CellTiter-Glo® (CTG) Luminescent Cell Viability Assay

Cell viability was measured with Cell Titer-Glo® (Promega, G7570) Luminescent Cell Viability Assay. Cell Titer-Glo Substrate (G755A) and Cell Titer-Glo Buffer (G756A) mixed in 1:1 ratio and added (20 µL/well) to the wells. Plates were incubated at 37℃ for 10 min. Luminescence signal was detected with Bio-Tek H1 Hybrid Synergy microplate reader.

2.5.4 RNA sequencing and Analysis

Du145-DtxR cells were seeded in 6-well plates and treated with siRNAs. After treatment with BRPF siRNA and non-targeting control siRNA cells were harvested by trypsinization and centrifuged at 400 g for 4 min. RNA isolation was performed using the Quick-RNA MicroPrep Kit (Zymo Research, R1051) according to the manufacturer's protocol. RNA quantity and quality determination was done using Nanodrop 2000 (Thermo Fisher Scientific). Analysis was performed to identify differentially expressed genes; between Du145-DtxR i) siCtrl ii) siBRPF1 and iii) siBRPF2 treated cells. The comparisons were made with 3 biological replicates per treated cell line. Each paired-end sample FASTQ file was assessed for adapter contamination using FastQC. All samples had at least a mean quality score of 36 across base-pair positions. The sequencing data was aligned using STAR (transcriptome mapping) (Dobin et al. 2013), to the GENCODE GRCH38 (Frankish et al. 2019) Human reference transcriptome. Salmon (Patro et al. 2017) was used to quantify the STAR transcriptome BAM files based on the transcripts per million methods. To aggregate the transcript-level abundance to the gene-

level the R package tximport (Soneson et al. 2015) was used. The package DESeq2 (Love et al. 2014) was used to analyze the gene-level count data, identifying differentially expressed genes for each of the two contrasts. Significant differentially expressed genes (DEGs) were defined as genes with a log-FC > 1 (up-regulated) or log-FC < -1 (down-regulated) and a false-discovery rate (FDR) adjusted P-value < 0.05. The significant results from the gene expression analysis were annotated using the Biomart database (Durinck et al. 2009), to provide descriptions of gene function. Volcano, MA (base-2 log fold-change versus normalized mean counts), and log-FC comparison plots generated using ggplot2 were used to visualize the gene expression analysis results. Gene Set Enrichment Analysis (Subramanian et al. 2007) computed overlaps analysis in the Hallmark Collection of GSEA (MSigDB) database was performed using the fgsea R package (Korotkevich et al. 2019) and GSEA website (http://software.broadinstitute.org/gsea) to identify pathways and gene networks the differentially expressed genes are implicated in.

2.5.5 siRNA Silencing of RNA-seq Hits

siRNA transfections of Du145 taxane sensitive and resistant cells with Lipofectamine 3000 (Invitrogen, L3000015) were carried out as described in Chapter 2.4.2. The siRNA's are given in table 2.4.

Table 2.4 Ambion Silencer Select siRNA IDs for the RNA-seq hits.

siRNA	ID
MYC	s9129
JUN	s7660
EGR1	s4538
RUNX1	s229351
NFKB1	s9505
FOSL1	s15583

2.6 Chromatin Immunoprecipitation

2.6.1 Transfection with Overexpression Constructs

Cloning of BRPF1 into dTAG construct pLEX-305-C- dTAG plasmid (Addgene, 91798) was done by Özlem Yedier Bayram, PhD. Coding sequence of BRPF1 was amplified from GFP-BRPF1 plasmid (Addgene, 65382). The plasmid was used for lentivirus production and transduction as decribed in Chapter 2.5.5. Transfections of HEK293T cells with Lipofectamine 3000 (Invitrogen, L3000015) were carried out according to manufacturer's instructions. The cells (1×10^5) were seeded into 6-well plates. 2 µg plasmid DNA and 4 µL of P3000 reagent was diluted in 125 µL Opti- MEM. In a separate tube, 7.5 µL of Lipofectamine 3000 Reagent was mixed with 125 µL Opti- MEM. The mixture was mixed gently and incubated for 15 min at room temperature and then

introduced to the media. The cells were transfected with GFP-BRPF-V5 Overexpression plasmids: GFP-BRPF1 (Addgene Plasmid, 65382) GFP-BRD1 (Addgene Plasmid, 65375) 48 h after transfection.

2.6.2 Immunoprecipitation

Cells were lysed in ice-cold IP lysis buffer (150 mM NaCl, 10 mM Tris-HCl (pH 7.4), 1 mM EDTA, 1 mM EGTA (pH 8.0), 0.2 mM sodium ortho-vanadate, 0.2 mM PMSF, 1% Triton X-100, 0.5% NP-40) on ice for 30 min. The lysate was centrifuged for 10 min at 10.000g at 4°C, and the supernatant was transferred to a new tube. Protein concetration was determined using BCA assay. The lysates were pre-cleared and incubated with the specific immunoprecipitation antibody overnight at 4°C. Dynabeads® (Thermo Fisher protein A and G magnetic beads, 10001D-10004D) were added to capture the antibody-antigen complexes, followed by washing to remove non-specifically bound proteins. Laemmli buffer was used to dissociate the immunocomplexes from the beads. After the denaturation of proteins at 95°C for 5 min, the eluted proteins were subjected to SDS-PAGE and transferred onto a membrane. After blocking, the membrane was probed with primary antibodies overnight at 4°C, followed by incubation with appropriate secondary antibodies. The bands were imaged by LI-COR Odyssey FC Imaging system (LI-COR Biosciences).

2.6.3 ChIP-qPCR

Du145-DtxR cells were crosslinked with %1 formaldehyde (Sigma Aldrich, 818708) at room temperature for 10 min. Cross-linking was terminated by the addition of glycine (125 mM, 5 min) and cell suspension was centrifuged at 1000 g for 5 min at 4°C. Pellet was washed with cold PBS twice and resuspended in ChIP Lysis Buffer (10 mM Tris; 1 mM EDTA; 140 mM NaCl; 1% Triton X-100; 0.1% Na-deoxycholate; 1% SDS; 1 mM PMSF; Protease inhibitor cocktail) and incubated on ice for 10 min. The released chromatin was sonicated (power setting high) with Bioruptor Plus sonication device (Diagenode) and was centrifuged at 10.000 g for 10 min at 4°C. The supernatant containing the sheared chromatin (fragment sizes of 100-500bp) was collected. The chromatin preparation was incubated with prewashed Dynabeads® (Thermo Fisher protein A and G magnetic beads, 10001D-10004D) at 4°C for 30 min to avoid non-specific binding (preclearing). Antibodies were incubated with magnetic beads in PBS-T for 1 h at room temperature. Magnetic beads to which antibodies are bound were washed with PBS-T and ChIP lysis buffer, respectively. The magnetic bead-antibody complex and pre-cleared chromatin preparation was incubated overnight. The magnetic beads were washed with ChIP lysis buffer, low-salt buffer (0.1% SDS, 1% Triton-X 100, 2 mM EDTA, 20 mM Tris-HCl, 140 mM NaCl, pH 8.1), high salt buffer (0.1% SDS, 1% Triton-X 100, 2 mM EDTA, 20 mM Tris-HCl, 500 mM NaCl, pH 8.1), LiCl-containing buffer (0.25 M LiCl, 1% IGEPAL-CA 630, 1% deoxycholic acid, 1 mM EDTA, 10 mM Tris, pH 8.1), Tris-EDTA solution twice for 5 min, respectively. ChIP'ed DNA was eluted

using an elution buffer containing 1% SDS and 0.1M $NaHCO_3$ and reverse cross linked by incubating with Rnase A (0.3 mg/ml) (Thermo Fisher Scientific, 12091039) and NaCl (Merck, S9888) (5 M) for 30 min, followed by addition of proteinase K (0.3 mg/ml) (Thermo Fisher Scientific, EO0492) for 1 h. DNA was purified by using the ChIP DNA Clean & Concentrator kit (Zymo Research, D5205). Primers were designed by using UCSC Genome (https://genome.ucsc.edu/) and Ensembl Genome Browser (https://www.ensembl.org/index.html) and primer sequences are listed in Table 2.5. For the quantitative and simultaneous analysis of immunoprecipitated DNA, qPCR was run on the LightCycler 480 (Roche). ChIP qPCR results were calculated by % input method. The antibodies used for ChIP are as given: Acetyl-Histone H3 (Lys27) (D5E4) (CST, 8173S), BRPF1 antibody (Abcam, ab259840), Anti-HA antibody (Biolegend, 901502), PRMT5 (D5P2T) (Cell signaling, 79998S) and a non-specific IgG antibody (normal Rabbit IgG Sigma Aldrich, PP64B; normal mouse IgG Antibody sc-2025) for negative control).

Table 2.5: The nucleotide sequences of the PCR primers used to determine enrichment of ChIP'ed samples by qPCR.

Gene Name	**Forward primer**	**Reverse primer**
Chr 12 Gene Desert	TGTACAGGGCCTGGTTACCCACA	AGGAGGGCCTAGCTGGTGTCAT
Chr 4 Gene Desert	GAGTGTTGAAGCCCTAGCCA	GTTTGTGGCGATGTGTCCAG
ABCB1-primer pair 1 (-658)	GGTCTTCCCAGTAACCTACCA	ACATGGCTTAGGGATTGGGG
ABCB1-primer pair 2 (-234)	TTCTCTCTGTGACAGCTCAGT	AGCACAAATTGAAGGAAGGAGT
ABCB1-primer pair 3 (-130)	CCCTAAGCCATGTAACTCTTCG	TGACTATGGCTCCAAAGCAT
RUNX2	GGAAACGGAGGGGTCTGAAC	TAAGAGCTGGTTTCGCCGTC
RUNX3	TAAGCTCTTGCTGGTGGCTC	ATCGTCTGCTTTGGGACAGG
ANKRD1	AATGCGGGTTTACCATGCAG	GGCCGAGAGCCATAAAGACA
MYC 1	AGGCATAAGGACTGGGGAGT	CCCCATCAACTGGGCAGAAT
MYC 2	GCTCACTCCAAACCCAGGAA	GTTGTGAAGGCAGCAGAAGC

MYC 3	GATGCCAACTTCCTTCCCGA	AGGTTGCACAATGGCAGAGA
HSPA6	CTGCCCTTCAGAGATGAACTTTCC	CAGAAGAGGATGAACCGCCCT
CCN2	AAACAGGGACATTCCTCGCA	GGTCAGGATCAATCCGGTGT
NEK6	CTAAGTGCTCAGAAAGCCGC	TGGAATGTGCCTGACACGAC
FOSL1	GGCAGCGTCTGTTTGGTACT	CCAGGCTCGAAGTAATGGGG
MFSD14A	TGCGGTGTATCCCTATCCCT	CCTTTGTGGCCCTCTACGTT
HSPA1B	GAGGGTCCGCTTCGTCTTTC	GAACGCCGGAAACTCAACAC

2.6.4 Analysis of ChIP sequencing

For the ChIP-sequencing data analysis, initially, FastQC was used to assess the quality of the CHIP-sequencing fastq files for all samples. The genome mapping was then performed using bowtie2 (Langmead & Salzberg, 2012), aligning the reads to the latest human genome reference (GENCODE GRCh38). To ensure uniquely mapped reads, unmapped and duplicate reads were filtered out. Next, MACS2 was employed for peak calling, specifically identifying H3K27ac binding sites. The R package CHIPQC was utilized for quality control, evaluating read characteristics, enrichment of reads in peaks, peak signal strength, and peak profiles. (Carroll, Liang, Salama, Stark, & de Santiago, 2014) Read count frequency around TSS and other visualizations were generated using ChIPseeker (Q. Wang et al., 2022) and Genomic Regions Enrichment of Annotations Tool (GREAT) (McLean et al., 2010). For motif analysis, STREME (Bailey, 2021) within the MEME-Suite of software was utilized to analyze and identify specific sequence motifs associated with the identified peaks.

2.6.5 Statistical Analysis

All data were analyzed in Prism 8 (GraphPad) and statistical tests were applied as described in the figure legends. A value of $p < 0.05$ was considered statistically significant.

Chapter 3:
RESULTS

3.1 Generation of Taxane Resistant Cell Models

Investigating drug resistance is essential to understand the mechanisms underlying the survival and persistence of resistant cells, which can lead to the development of more effective treatment strategies and the identification of novel therapeutic targets. With the purpose of creating an *in vitro* model for taxane resistance in CRPCa, a subpopulation of cells that displayed resistance to taxane treatment was successfully generated by subjecting a population of CRPCa cells to exposure to increasing concentrations of taxanes. DtxR (Docetaxel-resistant) and CbzR (Cabazitaxel-resistant) cell lines, which are resistant to Dtx and Cbz respectively, were established from the CRPCa cell lines Du145 and 22Rv1 by Buse Cevatemre, PhD, and İpek Bulut, MSc. To establish taxane resistant PCa cells, over a span of 8 to 12 months, the taxane-sensitive cells (Du145-P and 22Rv1-P) underwent a cycle where they were allowed to grow for 24 h, followed by treatment with increasing doses of Docetaxel/Cabazitaxel (Dtx/Cbz) for a duration of 72 h as depicted in Figure 3.1A. Cell viability assays were performed to evaluate the acquired resistance levels of Dtx/Cbz compared to the parental and resistant cells as depicted in Figure 3.1B. The resistance profile was further confirmed using a clonogenic assay, which measured the number of remaining colonies after exposure to taxane in the taxane sensitive and resistant compartments as depicted in Figure 3.1C.

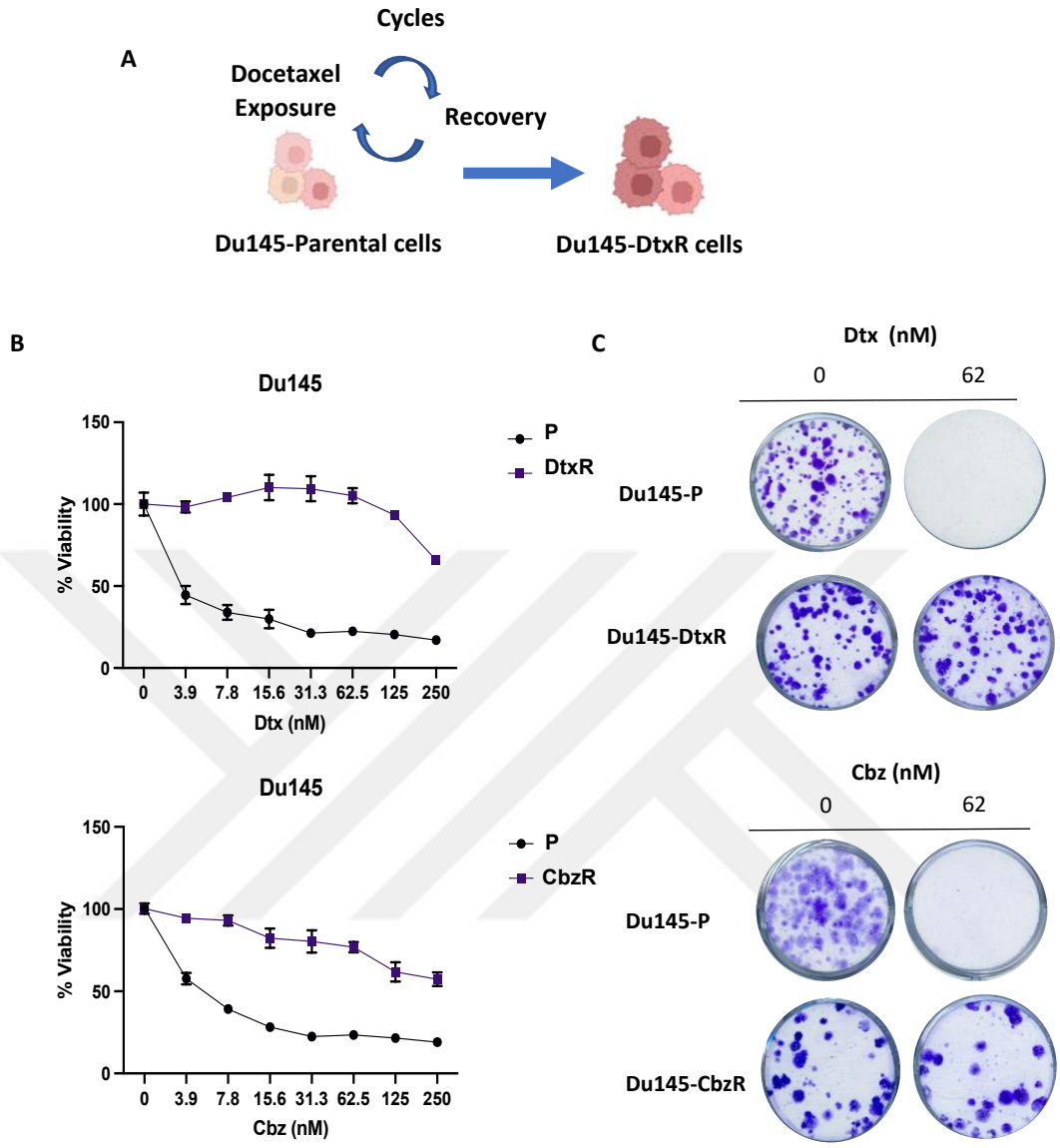

Figure 3.1: Generation and characterization of taxane resistant cells.

(A) Schema for establishing taxane resistant cell models. (B) The dose dependent effects of Dtx or Cbz on the cell viability of parental and resistant cell lines. The results were obtained by using SRB assay (72 h) and expressed as the mean ± standard deviation (SD) from 2 biological replicates. (C) Clonogenic images were obtained by treating cells with Dtx or Cbz for 72 h and the relative colony formation ability was analyzed 10 days after drug exposure.

Table 3.1 demonstrates relative levels of resistance to Dtx/Cbz in resistant lines compared to their parental compartment. The IC_{50} values of resistant cells were significantly higher

than those of parental cells exhibiting ~920-fold increase for DtxR and ~240 fold for CbzR.

Table 3.1: IC50 values and relative resistances of Dtx/Cbz resistant Du145 cells compared to parental cells.

The IC50 values were calculated using GraphPad Prism software.

Cell Lines	**IC50 to Dtx (nM)**	**Relative Resistance**
Du145-P	0.42	1
Du-145-DtxR	385	916.66
	IC50 to Cbz (nM)	**Relative Resistance**
Du145-P	1.07	1
Du-145-CbzR	257.6	240.74

Immunofluorescence staining in Figure 3.2, which was performed by PhD. Buse Cevatemre, shows the changes in α-tubulin cytoskeleton upon Docetaxel treatment in both taxane sensitive and resistant cells. Taxanes inhibit the depolymerization of microtubules by binding to the β-tubulin subunit in the cytoplasm and stabilizes the microtubules in taxane sensitive cells as it is depicted in Figure 3.2A but not in taxane resistant cells. In taxane resistant cells, microtubules remain intact according to immunofluorescence images in Figure 3.2B.

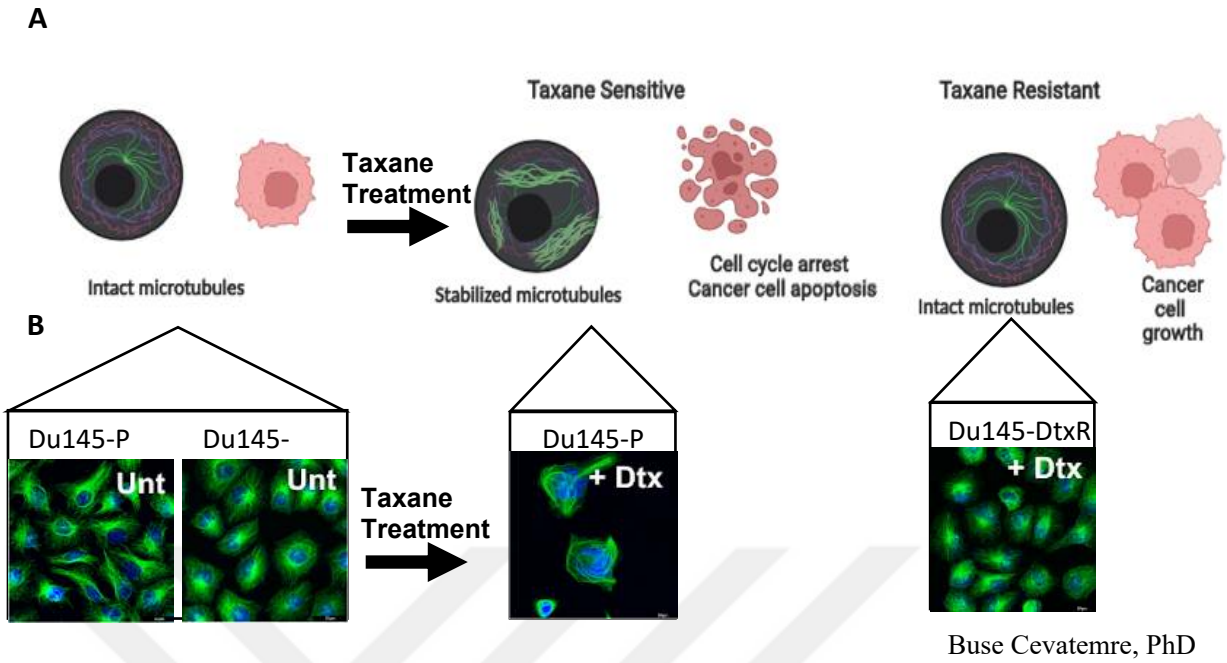

Figure 3.2: Taxane responses of taxane-sensitive and taxane-resistant cells.
(A) The model shows the microtubule cytoskeleton and taxane response in taxane sensitive and resistant cells. (B) Immunofluorescence staining was performed by PhD. Buse Cevatemre to visualize α-tubulin in both untreated and 30nM Docetaxel (for 24 h) treated Du145 taxane sensitive and resistant cells. The merged images depict the staining patterns obtained using DAPI (blue) and α-tubulin-specific antibody (green).

3.2 Understanding The Phenotypic Characteristics of Resistant Cells

Understanding the phenotypic characteristics of resistant cells is crucial for unraveling the mechanisms underlying their survival and persistence. In our study, we aimed to investigate the phenotypic features exhibited by cells that developed taxane resistance. These resistant cells exhibited distinct phenotypic alterations compared to their drug-sensitive counterparts. Exploring the phenotypic changes in these resistant cells is essential for elucidating the adaptive strategies employed by these cells and potentially identifying novel therapeutic targets to overcome drug resistance.

The scratch assay in Figure 3.3 demonstrates the migration and closure of a simulated wound by the cultured cells over time in the absence of fetal bovine serum (FBS), which was done to minimize the impact of cell proliferation on the closure process. The images capture the progression of wound closure, and the quantification analysis provides a measurement of the extent of wound closure, indicating the efficiency of cell migration. We observed a progressive reduction in the gap width between the wound edges in Du145-P cells, indicating active cell migration and wound closure. Notably, Du145-DtxR cells exhibited a decreased closure rate compared to the Du145-P cells. Du145-P cells

migrated faster than the resistant cells. Du145-P cells displayed a faster migration rate than the resistant cells. This disparity in migration rates could have been attributed to the high proliferation rate observed in the Du145-P cells. However, to exclude the influence of cell proliferation on the closure process, the experiment was specifically conducted without FBS, as FBS is a rich source of growth factors that stimulate cell proliferation. These findings suggest that resistant cells have decreased wound healing process.

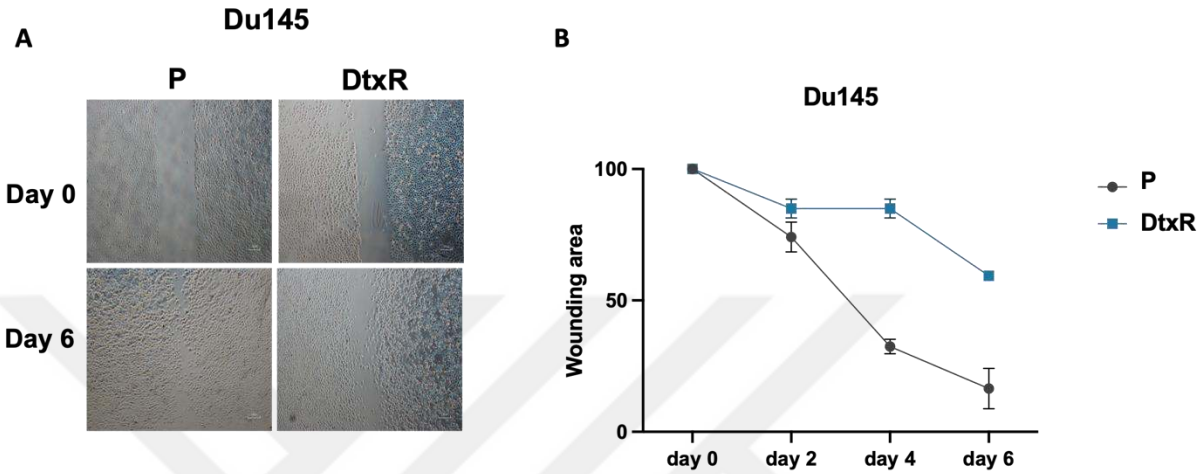

Figure 3.3: Wound healing scratch assay.
(A) Images of wound healing scratch assay performed on a monolayer of Du145 cells. Day 0 shows the initial scratch made on the cell monolayer. Subsequent images were taken at 2-day intervals until Day 6. (B) Quantification of wound closure over time is was achieved by using ImageJ software. The distance between the wound edges was measured at each time point and expressed as a percentage of the initial wound width. Data are presented as mean ± SD of two independent experiments.

We performed doubling time assay to assess the proliferation rates of taxane sensitive and resistant cells. The results of the doubling time assay revealed insights into the growth dynamics of the Du145-P and Du145-DtxR cell populations. In Figure 3.4A, progressively increased cell number with time is depicted, reflecting the overall expansion of the parental cells compared to the resistant counterparts. Figure 3.4B further confirmed this proliferation trend, the plot of the number of cell divisions (Ln(n)) against time demonstrated a delayed exponential pattern of resistant cells proliferation compared to the parental cells. This exponential growth suggests that the parental cells are actively dividing and increasing in number over time. Overall, the results demonstrate the active cell division and progressive growth of the Du145 cells, as evidenced by the exponential increase in cell divisions over time, the continuous rise in cell numbers, and the variations in doubling time at different passages. These findings contribute to our understanding of the growth behavior and dynamics of the Dtx resistant and sensitive cells, providing valuable information for further investigations.

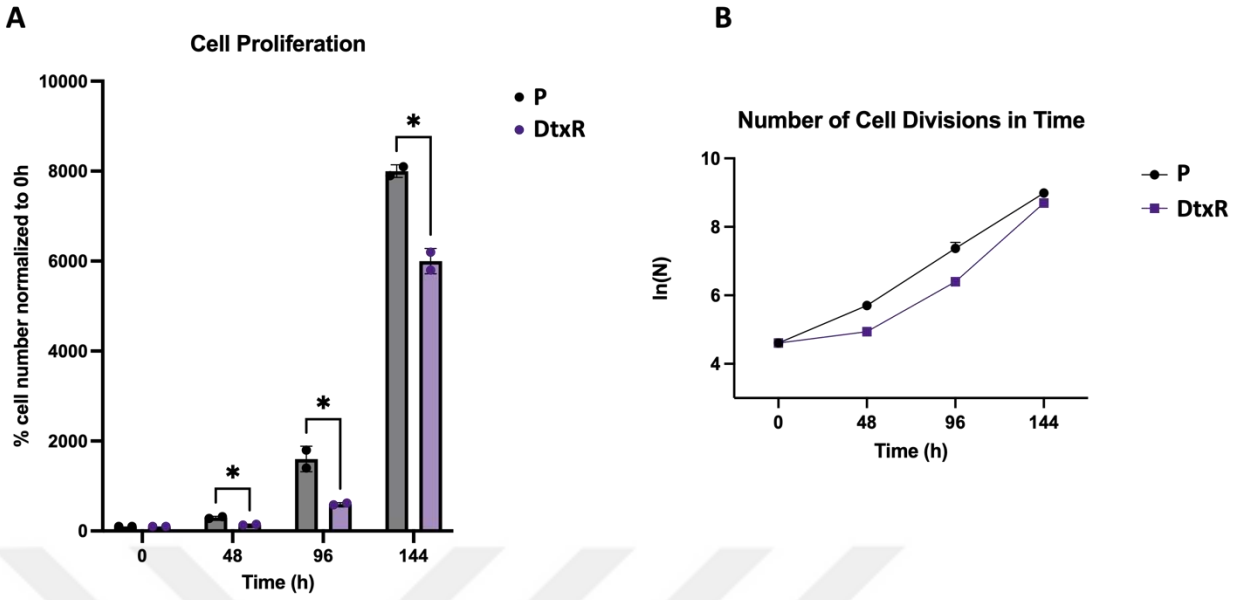

Figure 3.4: Analysis of cell doubling time for Du145-P and Du145-DtxR cells.
(A) Cell proliferation is depicted, with the number of cells (y-axis) increasing over time (x-axis), indicating the progressive growth of the cell population. 2-way ANOVA statistical analysis was performed. (*) indicates significant difference (P value <0.01). (B) The number of cell divisions (ln(n)) is plotted against time, demonstrating the exponential growth pattern of cell proliferation. Data are presented as mean ± SD of duplicate experiments.

The adhesion assay provides a visual and quantitative assessment of cell adhesion of taxane resistant and sensitive cells. Images in Figure 3.5 illustrate the adherence of Du145 and 22Rv1 cells with stained cells indicating successful adhesion. In Figure 3.5B, the quantification of cell adhesion demonstrates the percentage of cells that have adhered compared to the total cells attached at the last time point. These results offer insights into the less adhesive properties of resistant cells in comparison to their parental counterparts, facilitating further investigation into cellular adhesion mechanisms.

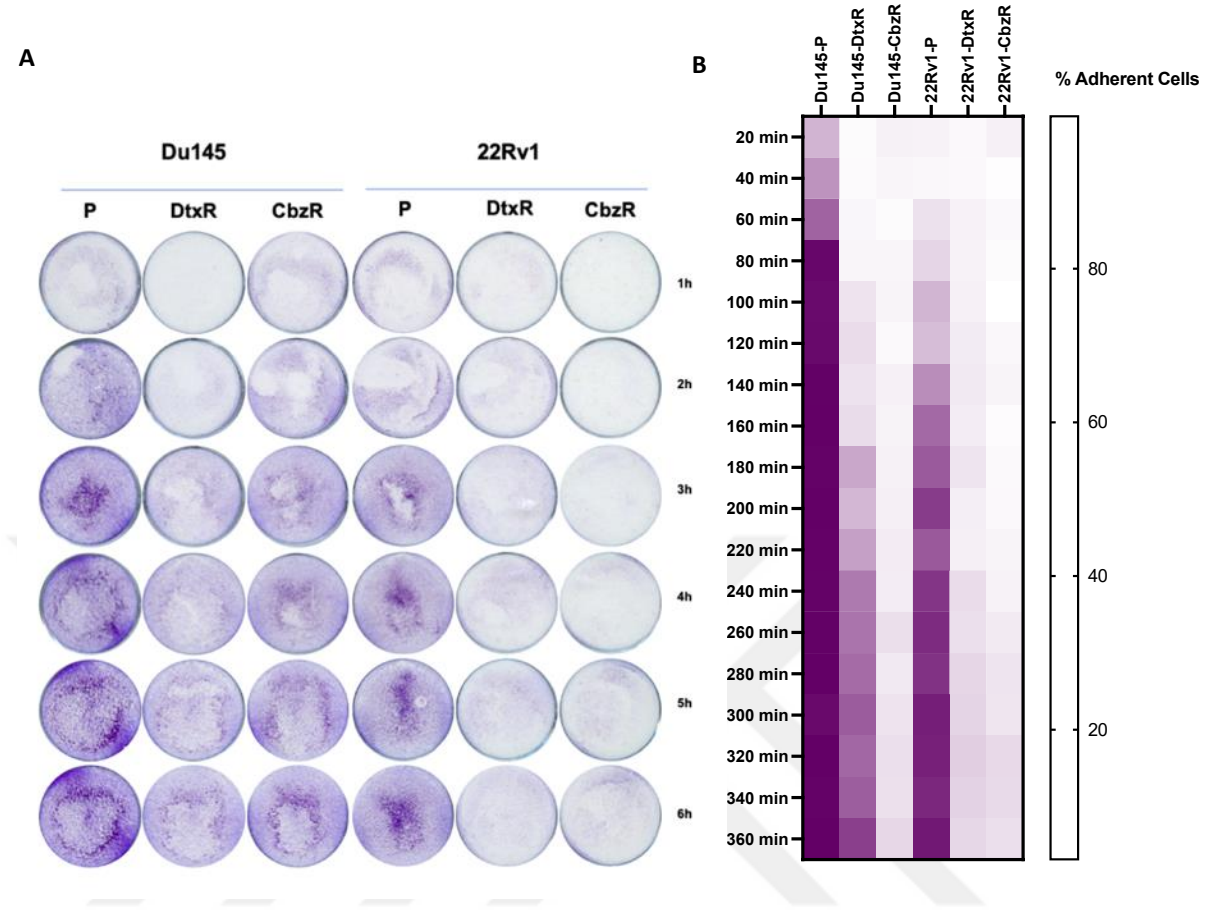

Figure 3.5: Adhesion Assay in taxane sensitive and resistant cells.
(A) Du145 and 22Rv1 taxane parental and resistant cells were seeded and allowed to adhere. Attached cells were fixed at the indicated time points (at 20 min intervals up to 6 h) after seeding. Attached cells were stained with crystal violet (Merck, 1.09218). (B) Quantification of cell adhesion was achieved by using ImageJ software and expressed as a percentage of the total attached cells.

3.3 BRPF Inhibition Reverses Taxane Resistance in PCa

3.3.1 Epigenetic Screens Identified BRPF as a re-sensitizer to taxanes

Buse Cevatemre, PhD. and İpek Bulut, MSc. assessed the role of epigenetic modifiers for their efficacy to revert taxane resistance in CRPCa and conducted an epi-drug screen to uncover the resensitizing factors. As depicted in Figure 3.6A this screen revealed five different groups of modulators (CBP/p300, Menin-MLL, SIRT, PRMT5 and BRPF) that were able to effectively revert resistance. As depicted in Figure 3.6B, Özlem Yedier Bayram, PhD. and Bengül Gökbayrak, PhD also identified BRPF as an essential gene for the taxane resistant 22Rv1 cells while not essential for the sensitive parental cells via Epi-targeted CRISPR Library Screening.

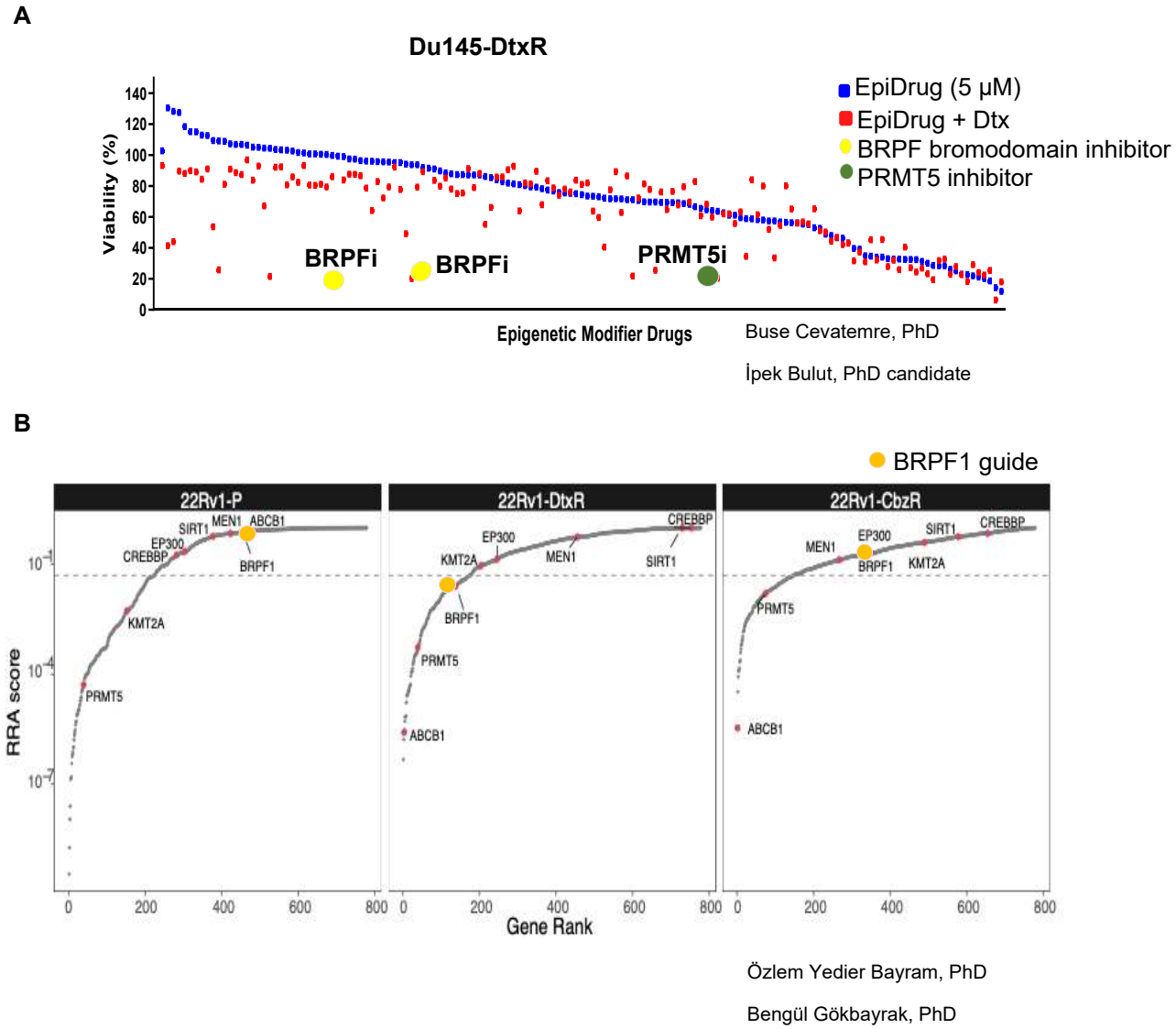

Figure 3.6: Epigenetic Drug Screen and Epi-targeted CRISPR Screen identified BRPF as a re-sensitizer to taxane.
Previous studies using (A) an epigenetic drug library using taxane resistant Du145 cells and (B) epi-targeted CRISPR screen using taxane resistant 22Rv1 cells has shown that inhibition of BRPF proteins efficiently reverses taxane resistance.

In Figure 3.7A, the combination treatment of the BRPF inhibitor, GSK5959, with Docetaxel was assessed for its impact on the viability of taxane-resistant CRPCa cells. Inhibition of BRPF1 via GSK5959 effectively reversed taxane resistance in Du145-DtxR cells Figure 3.7A.

SRB viability assay was performed after siRNA (small interfering RNA) mediated knockdown of BRPFs were achieved with the knockdown efficiency in Figure 3.7B. In Figure 3.7C, both Du145 and 22Rv1-DtxR cells were not re-sensitized to Dtx after BRPF

inhibition via siRNAs. Silencing BRPF proteins using siRNA in 22Rv1 cells didn't affect the cell viability in Figure 3.7C. Du145-DtxR cells seem to be vulnerable to siRNA treatment alone. Their viability reduced at 0 nM Dtx compared to siCtrl (Figure 3.7C), which might explain the absence of re-sensitization to Dtx in Du145-DtxR cells. There might be genetic differences that might contribute to the differential response to BRPF inhibition. This implies that the genetic makeup of the 22Rv1 cells might have certain variations or mutations that render them resistant to the effects of BRPF protein silencing via siRNA.

We aimed to investigate the effects of CRISPR/Cas9 knockout of BRPFs on the reversion of taxane resistance. Despite our efforts, we couldn't obtain a CRISPR/Cas9 knockout of BRPF1 in Du145-DtxR cells. The SRB viability assays were performed to confirm the effectiveness of BRPF inhibition in reverting taxane resistance in CRPCa. Figure 3.7D involved the Western blot confirmation of the knockouts of BRPF2 using CRISPR/Cas9 systems. Du145-non targeting guide and BRPF2 guide receiving cells were established and the viability of both taxane-sensitive and resistant cells was assessed following treatment with Docetaxel in Figure 3.7E. BRPF2 knockout in Du145-DtxR cells decreased their IC50 values against Dtx and re-sensitized resistant cells to Dtx while BRPF2 knockout in Du145-P cells didn't affect their response to Dtx. Silencing BRPF proteins in Du145-DtxR cells showed a similar phenotype to the result of the epigenetic drug library screen, supporting the importance of BRPFs for resistance.

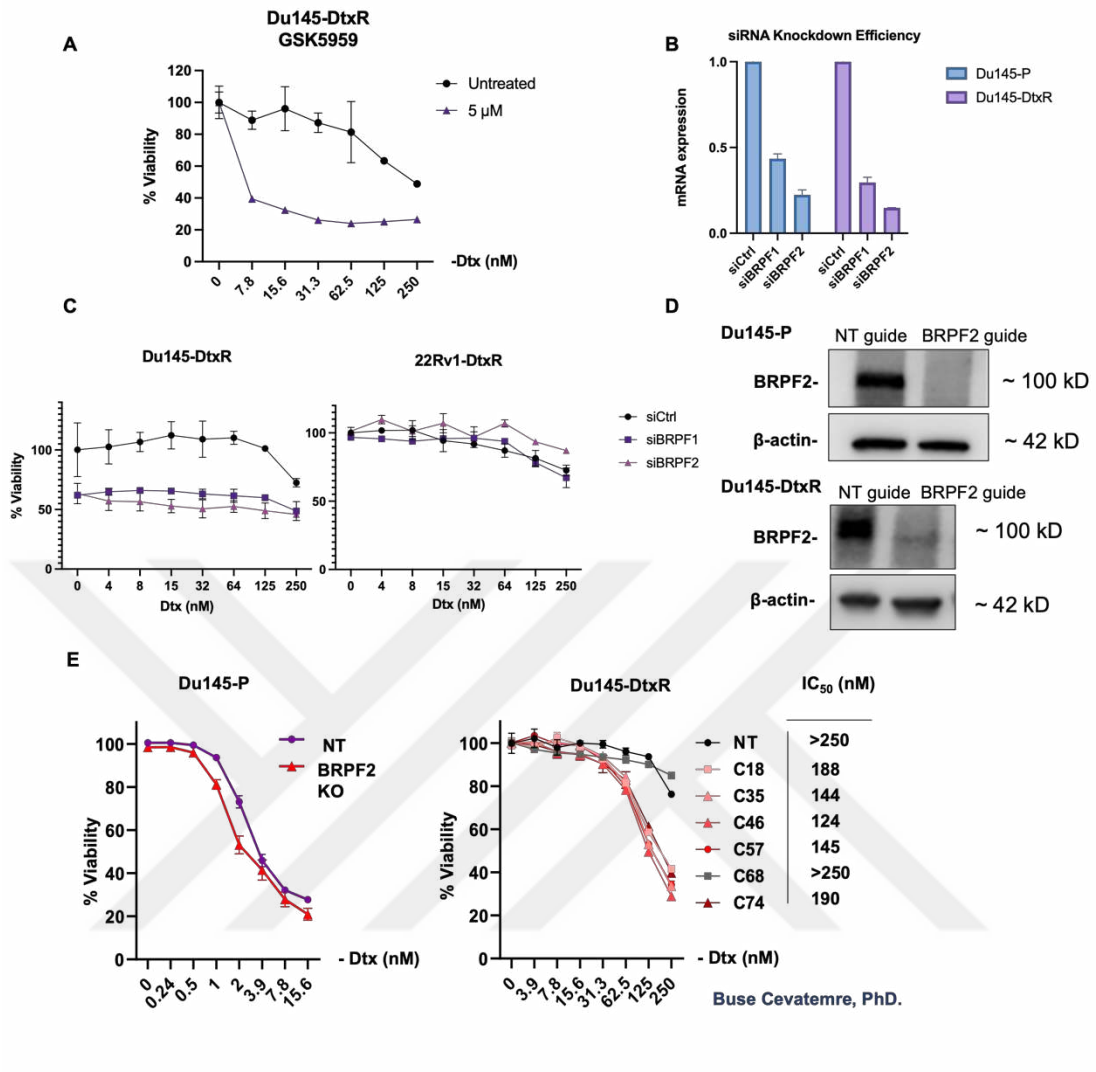

Figure 3.7: Confirmation of reversion of taxane resistance via BRPF inhibition.
(A) SRB viability assay showing the combination treatment of the BRPF inhibitor, GSK5959 (5 μM), and Dtx with increasing doses to confirm the reversion of taxane resistance in Du145-DtxR. (B) qPCR analysis was performed to investigate siBRPF1-2 knockdown efficiency in Du145 and 22Rv1-DtxR cells. (C) SRB viability assay was conducted to assess the impact of increasing doses of Dtx treatment on siRNA-mediated knockdown of BRPF1 and BRPF2. (D) Western blot analysis was performed to investigate BRPF2 knockout efficiency in Du145 cells. β-actin was used as loading control. (E) SRB viability assay showing treatment of Dtx with increasing doses in NT and BRPF2 guide receiving Du145 cells.

The clonogenic experiments after siRNA (small interfering RNA) mediated knockdown of BRPFs in Figures 3.8 and 3.9 provided evidence supporting the role of BRPF proteins in taxane resistance and further validated their potential as therapeutic targets for overcoming drug resistance in CRPCa cells. The inhibition of BRPF reduced the ability

of taxane resistant cells to form colonies while the colony formation capacity of parental cells was unaffected by BRPF inhibition as it was depicted in the graphs in Figure 3.10.

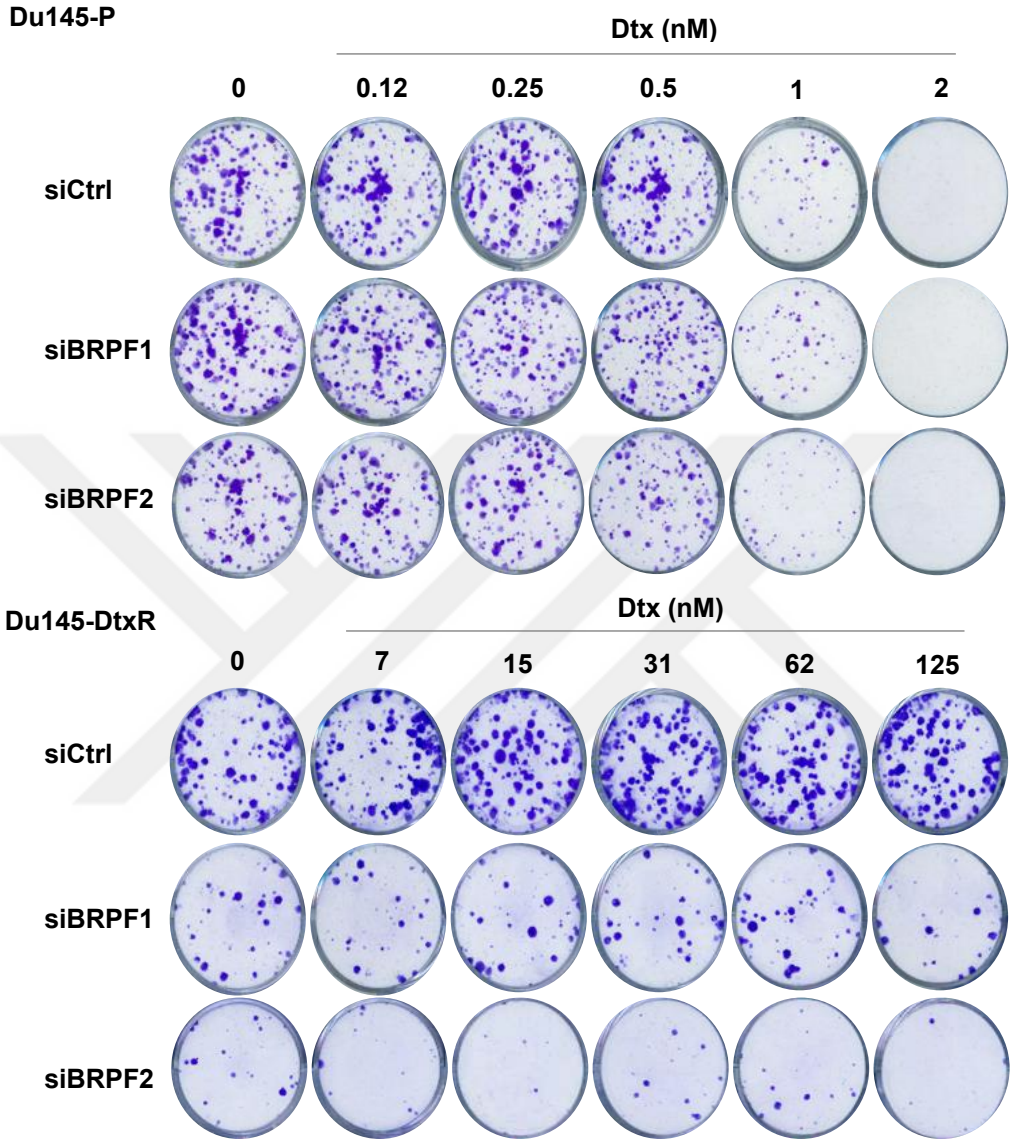

Figure 3.8: Colony Formation Assay after siRNA mediated BRPF1 and BRPF2 knockdown and Dtx treatment in Du145-P and Du145-DtxR cells.

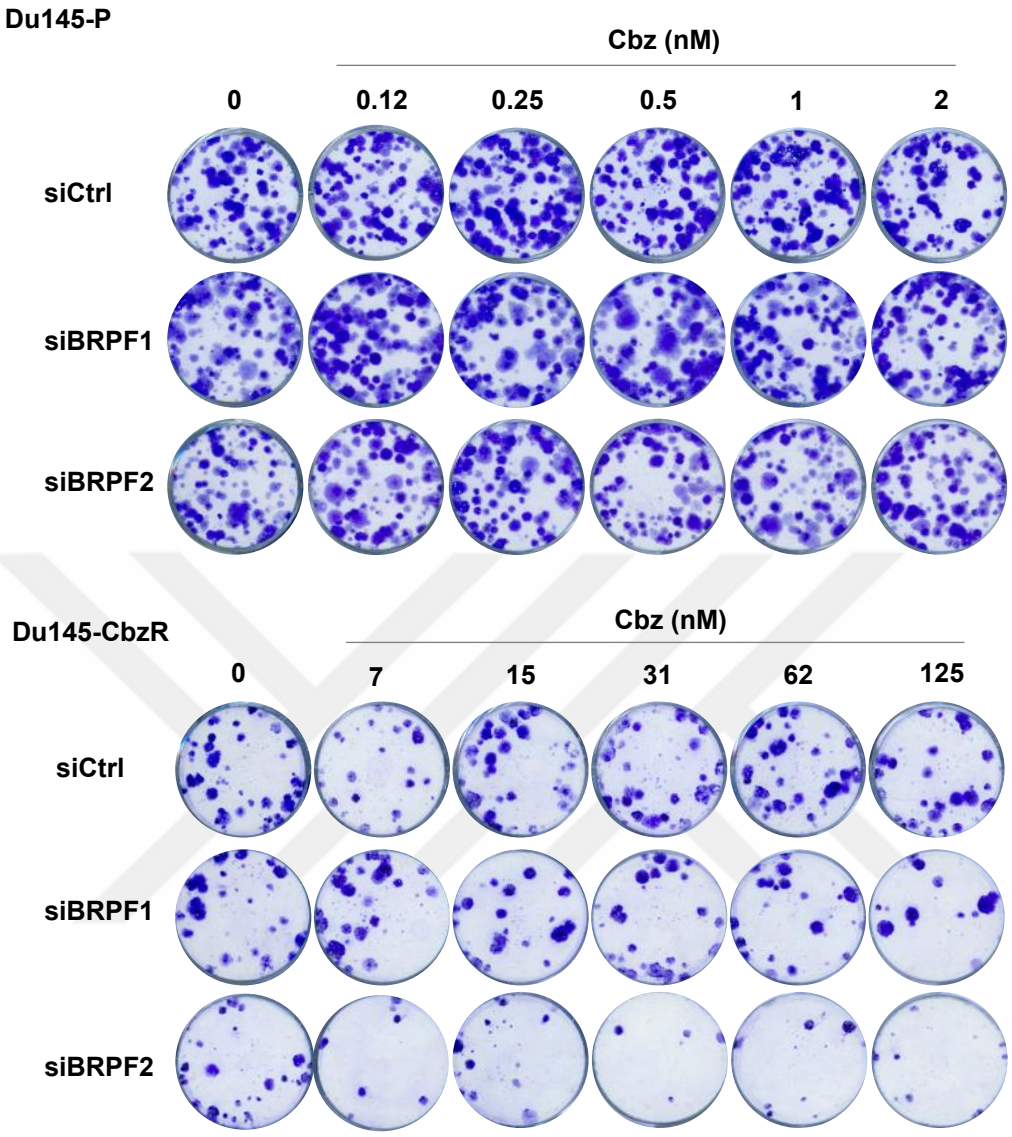

Figure 3.9: Colony Formation Assay after siRNA mediated BRPF1 and BRPF2 knockdown and Cbz treatment in Du145-P and Du145-CbzR cells.

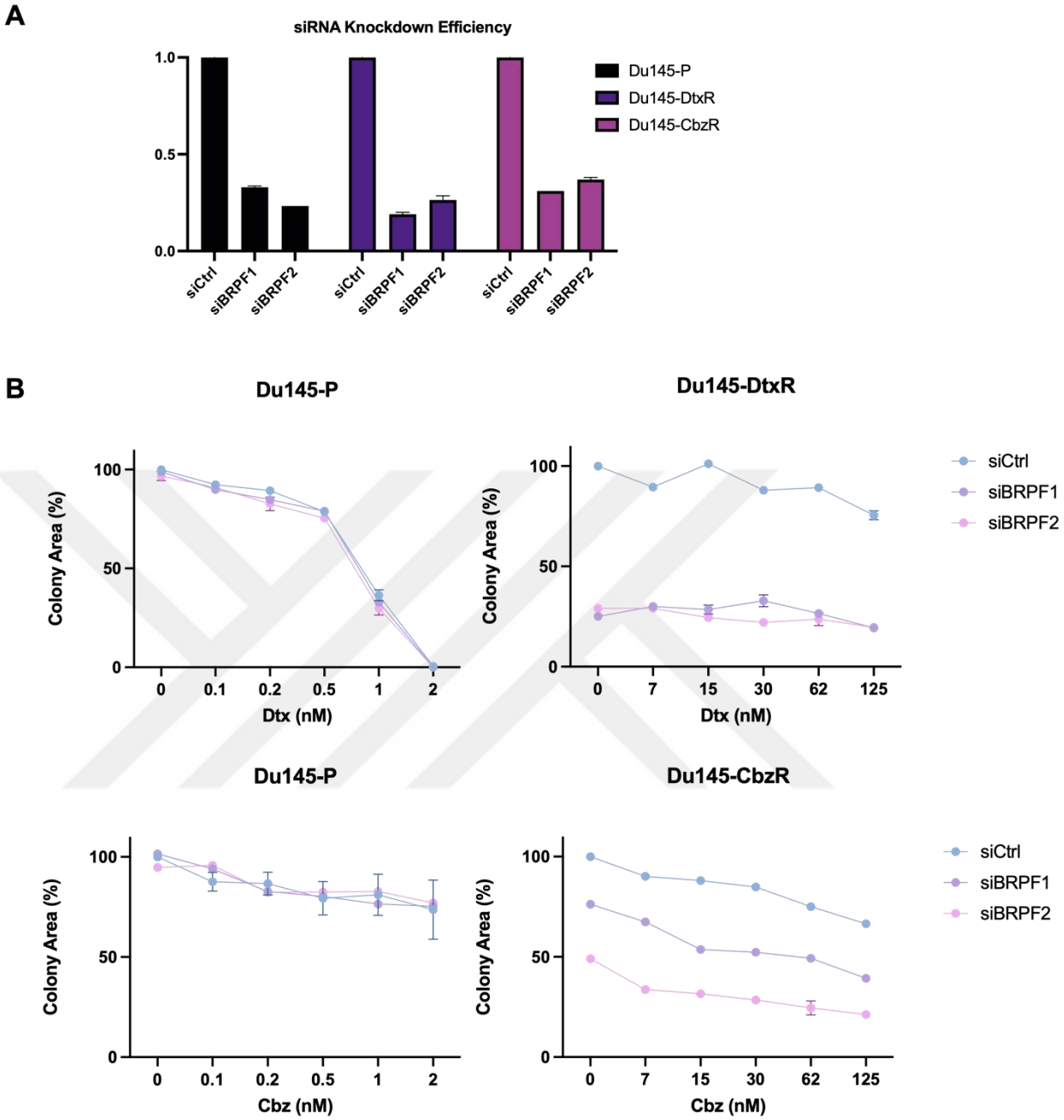

Figure 3.10: Quantification of Colony Formation Assays.
The cells were treated with siRNAs. The siRNA-treated cells, were re-seeded after 2 days, and then they were treated with taxane for 72 h. The cells were allowed to grow for an additional 10 days after the drug exposure before clonogenic images were obtained. (A) qPCR results showing siRNA knockdown efficiency for siBRPF1-2. Data are presented as mean ± SD of two independent experiments. (B) Quantification of colony area was achieved by using ImageJ software and expressed as a percentage of the siCtrl cells. Du145-P cells and Du145-DtxR cells after siCtrl, siBRPF1 and siBRPF2 Treatment, followed by 72 h taxane Treatment. Data are presented as mean ± SD of two independent experiments.

Gaining insights into the impact of BRPF expression on cellular characteristics is crucial for understanding the survival mechanisms of taxane-resistant cells. Therefore, our objective was to explore the cellular behaviors associated with BRPF inhibition.

We performed wound healing scratch assay to study cell migration and wound closure upon BRPF inhibition in vitro in taxane sensitive and resistant cells. Both in Du145-P and Du145-DtxR cells siBRPF2 treated cells migrated slower than the siCtrl treated cells in Figure 3.11. We observed increased closure rate between the wound edges in Du145-DtxR siBRPF1 treated cells, indicating active cell migration and wound closure. Notably, Du145-DtxR cells treated with siBRPF2 exhibited a decreased closure rate compared to the siCtrl treated cells as shown in Figure 3.11. The data obtained from our study reveals that the knockdown of BRPF in resistant cells has an impact on the wound healing process in both directions as depicted in Figure 3.11. The observed changes in wound healing, where BRPF1 knockdown results in an increase while the BRPF2 knockdown demonstrates a decrease, suggest that BRPF knockdown influences this process in a complex and non-linear manner. The wound healing assay was performed without FBS with the intention of specifically evaluating the migratory capacity of the cells. However, it is important to note that the time points selected for the assay, which extended up to day 6, could potentially influence the closure rate due to the combined effects of both migration and proliferation. Considering the impact of BRPF inhibition on cellular proliferation, it is plausible to consider that the reduced closure rate observed in the siBRPF2 treated cells could be attributed to a combination of impaired migration and decreased proliferation. These findings highlight the nature of the relationship between BRPF expression and cellular proliferation and wound healing, indicating that further investigations are required to fully comprehend the underlying mechanisms and clarify the precise roles of BRPFs in this context.

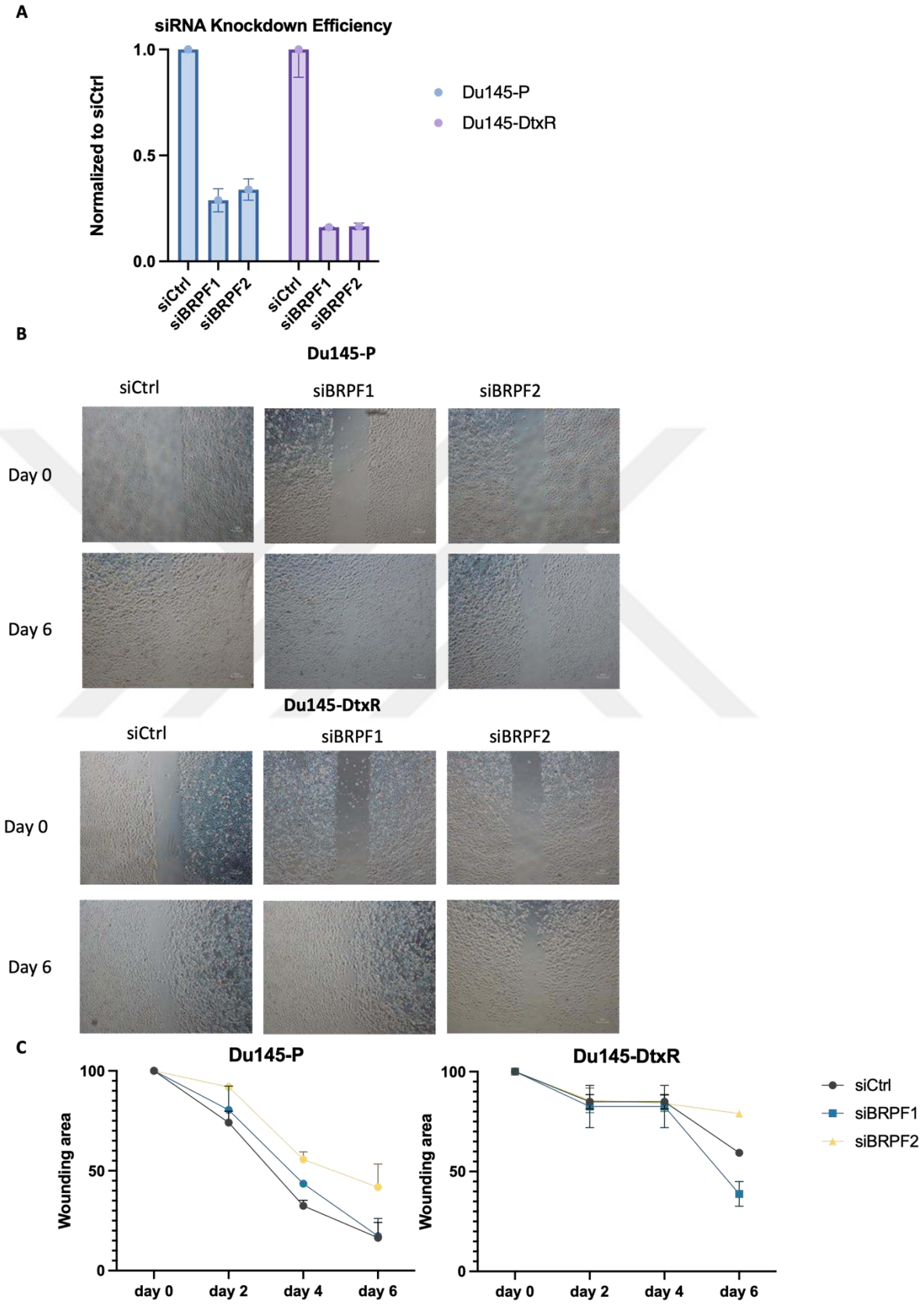

Figure 3.11: Wound healing scratch assay upon BRPF inhibition.

(A) qPCR results showing siRNA knockdown efficiency for siBRPF1-2. Data are presented as mean ± SD of two independent experiments. (B) Images of wound healing scratch assay performed on a monolayer of Du145 parental and Dtx resistant cells treated with siRNA. Day 0 shows the initial scratch made on the cell monolayer. Subsequent images were taken at 2-day intervals until Day 6. (C) Quantification of wound closure over time. The distance between the wound edges was measured at each time point and expressed as a percentage of the initial wound width. Data are presented as mean ± SD of two independent experiments.

To understand the growth kinetics and proliferation rates of taxane sensitive and resistant cell populations upon BRPF inhibition, we performed doubling time assay with siRNA treated cells. siRNA knockdown efficiency for the doubling time assay and adhesion assay were given in Figure 3.12A. The results of the doubling time assay revealed insights into the effects of BRPF inhibition on the growth dynamics of Du145-P and Du145-DtxR cells. In Figure 3.12B, we observe a decrease in the proliferation in siBRPF treated cells in both resistant-sensitive Du145 compartment. Figure 3.12C further confirmed this proliferation trend, the plot of the number of cell divisions (Ln(n)) against time demonstrated a delayed exponential pattern of siBRPF treated cells proliferation compared to the siCtrl treated cells. Cells with shorter doubling times show a faster proliferation rates, indicating their ability to divide more rapidly. In Figure 3.12D, the analysis of the doubling time values at each passage indicated that the variations in cell growth dynamics halts after the first cell passaging. Interestingly, siBRPF2 treated cells have a longer doubling time compared to the siCtrl treated cells at the initial passage. Overall, the results demonstrate the slowed cell division and growth of the Du145 parental and resistant cells upon siBRPF treatment, as evidenced by the decrease in cell divisions over time, and the long doubling time.

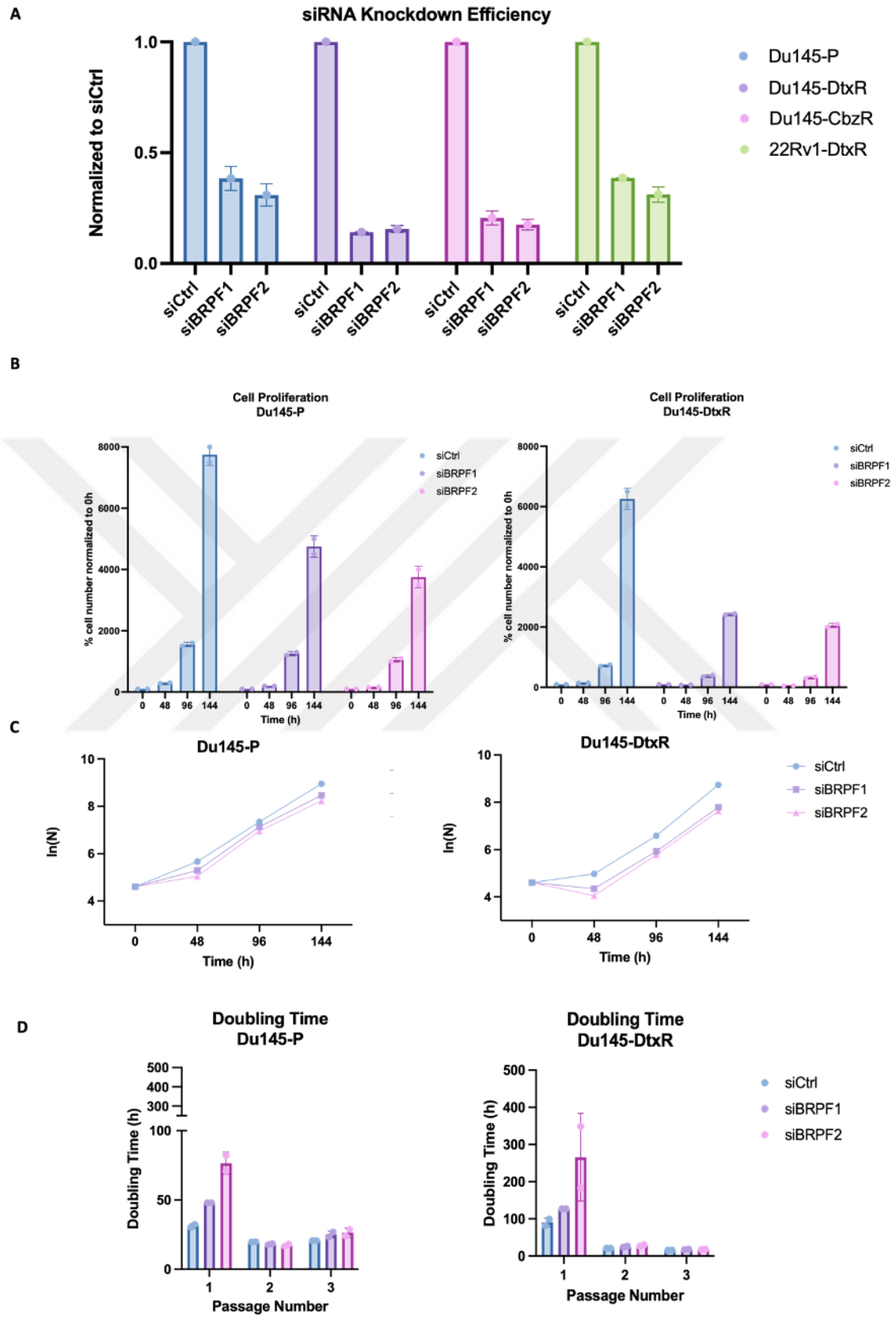

Figure 3.12: Analysis of cell doubling time for Du145-P and Du145-DtxR cells treated with siRNA.

(A) qPCR results showing siRNA knockdown efficiency in Du145 and 22Rv1 cells for siBRPF1-2. Data are presented as mean ± SD of two independent experiments. (B) Cell proliferation is depicted, with the number of cells (y-axis) increasing over time (x-axis), indicating the progressive growth of the cell population. (B) The number of cell divisions (Ln(n)) is plotted against time, demonstrating the exponential growth pattern of cell proliferation. (C) Doubling time is calculated for each passage, representing the time taken for the cell population to double in size. Data are presented as mean ± SD of duplicate experiments.

The representative images in the Figure 3.13 demonstrate the adhesion of Du145 both taxane sensitive and resistant cells and 22Rv1-DtxR cells treated with siBRPFs, where the stained cells indicate successful adhesion. These findings suggest that inhibiting BRPF has no impact on the adhesive properties of both taxane-resistant and sensitive cells. Similar to our previous findings in Figure 3.5, the difference in adhesive properties of taxane resistant and sensitive cells are observed in Figure 3.13.

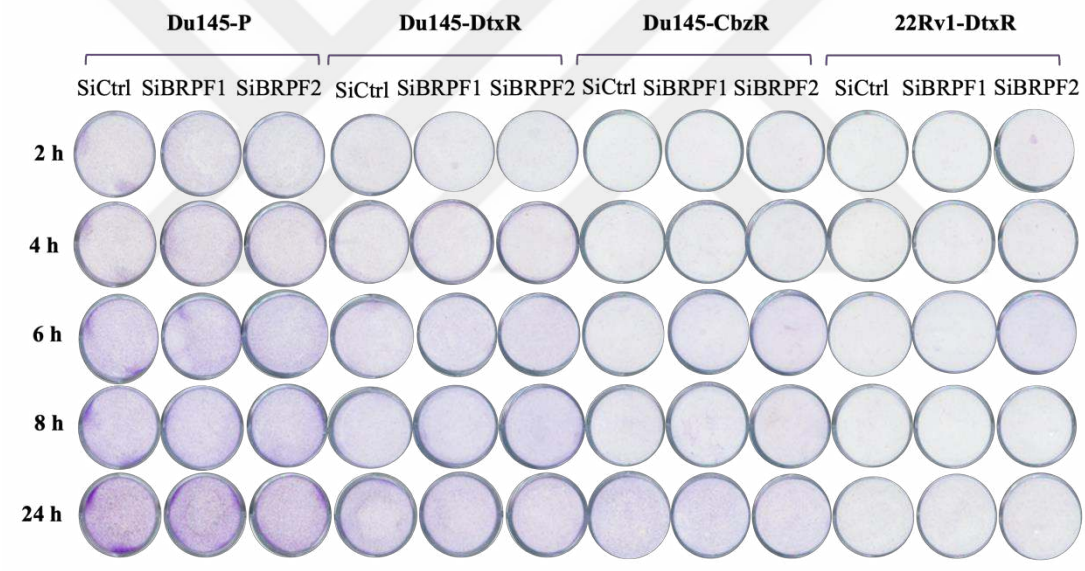

Figure 3.13: Adhesion Assay Du145-P/DtxR/CbzR and 22Rv1-DtxR following siRNA treatment.
Du145-P/DtxR/CbzR and 22Rv1-DtxR cells were seeded after siRNA treatment and allowed to adhere. Attached cells were fixed at the indicated time points (at 2 h intervals up to 24 h) after seeding. Attached cells were stained with crystal violet (Merck, 1.09218).

We performed immunofluorescence staining to understand cellular localization of BRPFs in Du145 cells. DAPI selectively binds to DNA, highlighting the nuclei of the cells. The blue fluorescence indicates the localization of cellular DNA within the nucleus. Actin-specific Texas Red™-X Phalloidin was used to label the actin cytoskeleton, which comprises a network of filamentous structures throughout the cell. The red fluorescence indicates the presence and distribution of actin filaments. The merged image in Figure 3.14 demonstrates the co-localization of the blue DAPI signal representing the nuclei and

the green BRPF signal representing the BRPFs. The co-localization can be observed as areas where blue and green signals overlap, indicating the presence of BRPFs within the cellular nuclei. These immunofluorescence images provide valuable insights into the cellular localization and distribution of BRPF proteins within the nuclei.

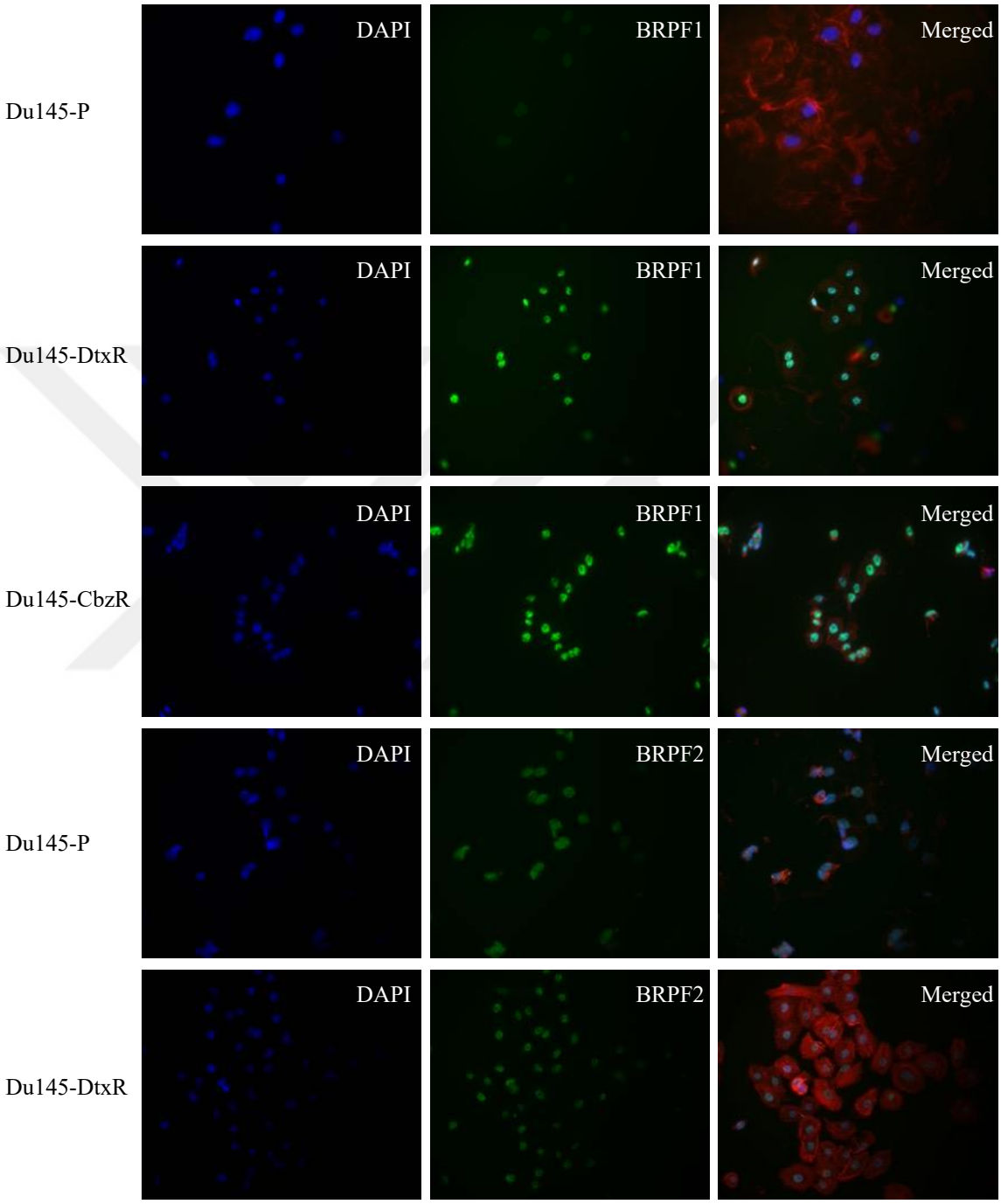

Figure 3.14: Immunofluorescence Images Showing BRPF1 and BRPF2 subcellular localization, DAPI and Actin Staining.
Immunofluorescence staining was performed to visualize the intracellular location of BRPFs, cellular nuclei and actin cytoskeleton. The images depict the staining patterns obtained using DAPI (blue) and BRPF1 and BRPF2 specific antibodies (green), Texas

Red™-X Phalloidin (red). Merged image of BRPF, DAPI and actin staining. (A) Representative immunofluorescence image showing BRPF1 staining in Du145-P/DtxR cells.

3.3.2 BRPF Inhibition Changes Histone Acetylation at H3K27.

BRPFs are known to regulate histone modifications H3K9, H3K14, and H3K23 acetylation for gene activation due to their epigenetic reader activity (Cheng et al., 2021). We investigated different acetylation marks in Du145-DtxR cells after BRPF inhibition. The Western blot results revealed a decrease in the levels of H3K27ac and H3K9ac 1h after GSK5959 treatment as depicted in Figure 3.15. This decrease suggests that BRPF plays a critical role in regulating the acetylation status of H3K27 and K3K9 and its inhibition leads to a global decrease in H3K27ac and H3K9AC levels. These findings strongly argue for the involvement of BRPF in the regulation of gene expression through modulation of histone acetylation. The restoration of acetylated histone expression was observed within a 24 h time frame, suggesting that these alterations in epigenetic modifications take place rapidly.

These results from the Western blot analysis in Figure 3.15 provide strong evidence that BRPF is a key regulator of histone acetylation dynamics, with potential implications for gene transcription and cellular processes influenced by H3K27ac. This finding also supports the epigenetic impact of BRPF inhibition via small molecule inhibitiors. Further studies are warranted to elucidate the transcriptomic changes that occur when BRPF modulates H3K27ac and to explore its functional significance in taxane resistance.

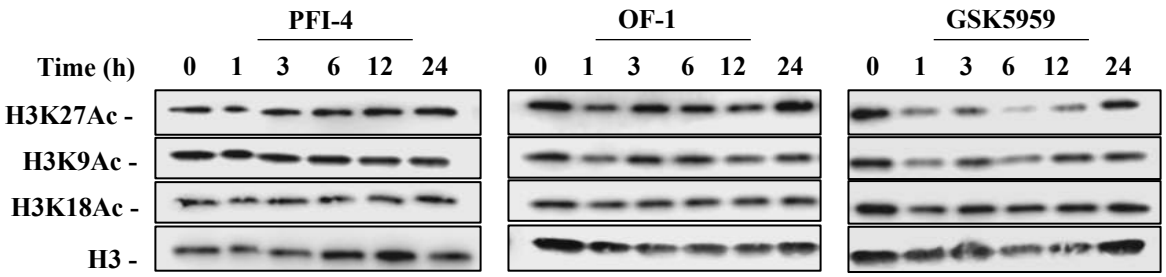

Figure 3.15: Changes in Acetylated Histones upon BRPF inhibition.
Western blot analysis was performed to investigate the changes in acetylated histone levels in DU145-DtxR cells following BRPF inhibition via small molecule inhibitors of BRPF (PFI4, OF1, GSK5959) Total H3 was used as loading control.

3.4 Transcriptomic Changes Upon BRPF Inhibition in Taxane Resistant Cells

3.4.1 ABCB1 Is Upregulated in Taxane Resistant Cells.

In previous studies, differentially expressed genes in Docetaxel-resistant (Du145-DtxR) and Cabazitaxel-resistant (Du145-CbzR) cells compared to Du145 parental cells (Du145-

P) were analyzed using RNA sequencing by Buse Cevatemre, Ph.D. *ABCB1* was one of the top hits, whose expression was greatly increased in taxane resistant cells as shown in the Figure 3.16A. In Figure 3.16C, we employed Western blotting to validate the observed overexpression. The objective of our study was to identify the specific genes, gene sets, and pathways that exhibit differential regulation in resistant cells when compared to their parental counterparts. Additionally, we aimed to identify common genes and pathways among these that display differential regulation mediated through BRPFs, that might revert resistant cells back to the parental state. In our investigation, we sought to identify and analyze DEGs between resistant cells and parental cells, allowing us to understand the specific epigenetic alterations associated with the development of resistance.

The Gene Set Enrichment Analysis (GSEA) revealed the most positively enriched gene sets as the following: Myc targets, Unfolded Protein Response, TNFA signaling via NFKB, E2F targets, inflammatory response, G2/M checkpoint, IL6-JAK-STAT3 signaling as depicted in Figure 3.16B. IL6-JAK-STAT3 pathway is associated with chemoresistance in TNBC (K. Wang et al., 2018). We aimed to identify the pathways that may be involved in the development of resistance and the reversion of the resistance mediated through the inhibition of BRPFs.

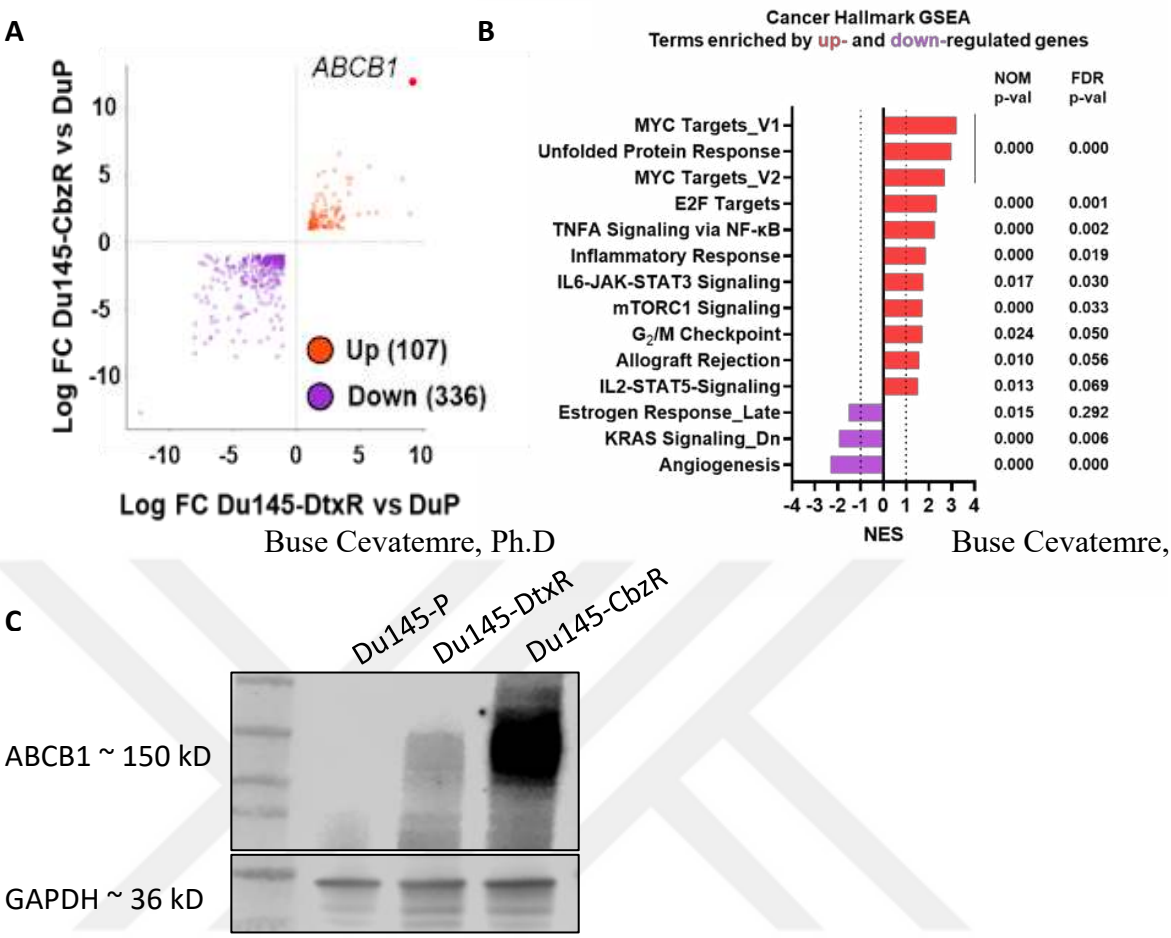

Figure 3.16: Transcriptomic Changes in the Emergence of Taxane Resistance.
(A) Differentially expressed genes (FDR < 0.05, and $Log_2FC \geq 1$ or ≤ -1) from Dtx and Cbz resistant cells were distributed based on their expression changes in the same direction (up or down). The red and blue scatters indicate up- and down-regulated DEGs, respectively. (B) Gene set enrichment (GSEA) analysis using Hallmark Gene Sets, h.all.v2023.1.Hs.symbols.gmt dataset from the MSigDB revealed the upregulation of genes involved in MYC signaling, unfolded protein response (UPR), NFKB and E2F signaling. (C) Expression levels of ABCB1 protein in parental and taxane resistant cell lines, determined by western blotting, GAPDH was used as loading control.

According to the RNA sequencing performed on taxane resistant and sensitive cells, in Figure 3.16, there were 3 common DEGs in both taxane resistant cells, Du145-DtxR and CbzR: *CRIP1, CRIP2* and *RAB3B*. Cysteine-rich intestinal protein 1 (CRIP1) is a member of the LIM zinc finger protein family, believed to play a role in cellular growth and differentiation (Y. Gao et al., 2022). Gene expression profile from t (8;21) AML patients showed that the CRIP1-high group exhibited an enrichment of immune-related pathways, including TNFA signaling via NFκB pathways. Upregulation of CRIP1 has been detected in a variety of tumors, including breast cancer, colorectal tumors, and thyroid cancer (Y. Gao et al., 2022). A study has shown that knockdown of CRIP1 augmented breast cancer cell invasion in vitro (Ludyga et al., 2013). CRIP1 is downregulated in pancreatic

carcinoma (Terris et al., 2002). As evident from the literature, the functions and roles of CRIP1 and CRIP2 in cancer are still being elucidated. According to RNA-seq, we have observed expressions of *CRIP1* and *CRIP2* were significantly low (CRIP1 log_2FC: -3.07, FDR=6.475E-73 and CRIP2 log_2FC: -3.97, FDR= 3.44337E-75) in Du145-DtxR and (CRIP1 log_2FC:-2.43, FDR= 1.0037E-49 and CRIP2 log_2FC:-1.50, FDR= 3.3927E-18) in Du145-CbzR compared to parental cells.

RAB3B, a member of the Rab family of small GTP-binding proteins, is a key regulator of vesicular traffic (Lledo, et al., 1993). Despite limited understanding of its role in cancer, studies have indicated that RAB3B is present in high levels in urinary exosomes of PCa patients (L. Wang et al., 2017). Additionally, increased expression of RAB3B has been associated with chemoresistance and enhanced metastatic capabilities in hepatoma cells (Tsunedomi et al., 2022). According to RNA-seq, we have observed expression of *RAB3B* was high (log_2FC: 1.59, FDR=4.1938E-55) in Du145-DtxR and (log_2FC: 1.58, FDR= 2.24495E-54) in Du145-CbzR compared to parental cells.

We showed increased expression of *CRIP1, CRIP2* and *RAB3B* in the BRPF2 knockout cell as shown in Figure 3.17. Despite our initial expectations of *RAB3B* being downregulated upon BRPF inhibition, the results showed a different trend. Therefore, the reversion of taxane resistance via BRPF inhibiton might not involve the regulation of these 3 DEGs (*CRIP1, CRIP2* and *RAB3B)* expression.

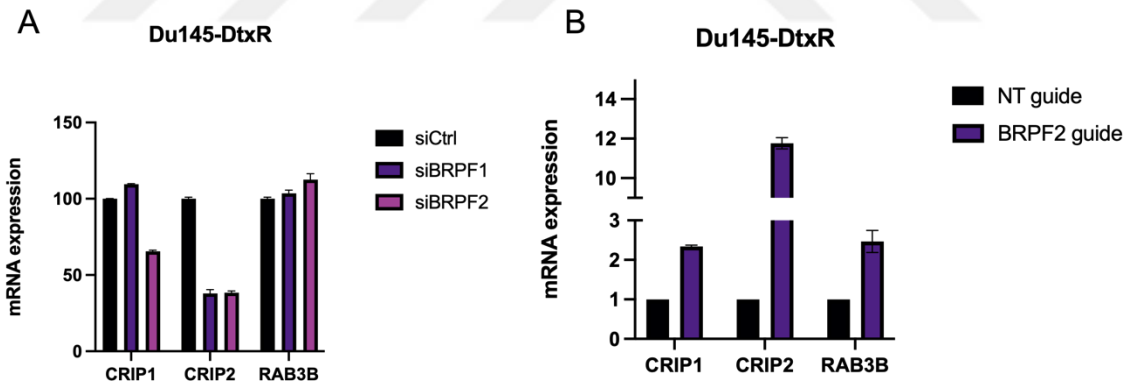

Figure 3.17: mRNA expression of *CRIP1, CRIP2,* and *RAB3B* upon BRPF inhibition. (A) qPCR results showing mRNA expression of candidate genes in siBRPF1 and siBRPF2 treated Du145-DtxR cells. BRPF knockdown efficiency is achieved by 80%. (B) qPCR results showing mRNA expression of candidate genes in BRPF2 knockout Du145-DtxR cells.

3.4.2 BRPF Inhibition Reduced ABCB1 mRNA Expression.

We aimed to investigate the effects of siRNA knockdown of BRPF1 and BRPF2 and CRISPR/Cas9 knockout of BRPF2 on the expression of *ABCB1*. Our results demonstrate that targeting BRPF1 and BRPF2 using siRNA leads to a significant decrease in ABCB1

expression, while CRISPR/Cas9 knockout of BRPF2 completely eliminates the mRNA expression of *ABCB1* (as depicted in Figure 3.18).

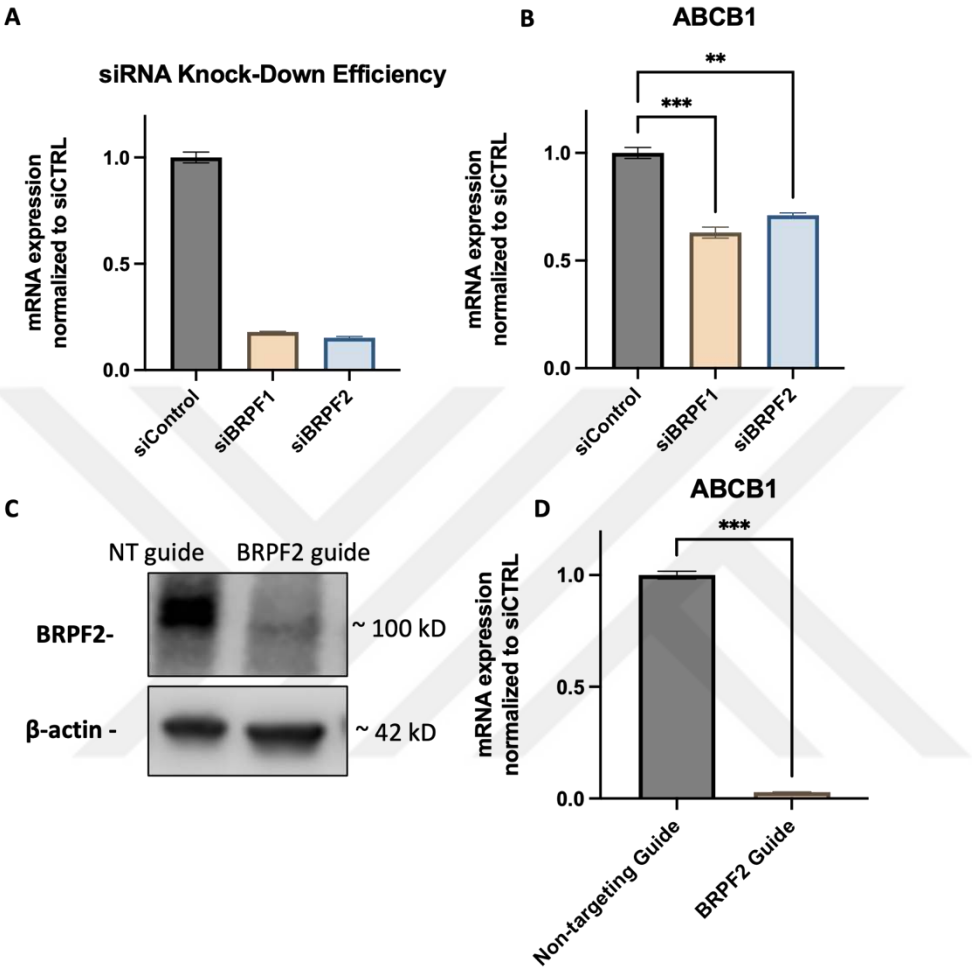

Figure 3.18: BRPF inhibition decreases ABCB1 expression.
(A) qPCR results showing siRNA knockdown efficiency for siBRPF1-2. Data are presented as mean ± SD of two independent experiments. (B) qPCR results showing *ABCB1* mRNA expression in Du145-DtxR cells after siBRPF1 and siBRPF2 normalized to siCtrl. (C) Western blot showing BRPF2 expression in Du145-DtxR cells that received non-targeting guide and single colony of BRPF2 knockout. (D) qPCR results showing *ABCB1* mRNA expression in single colony of Du145-DtxR cells that received BRPF2 guide normalized to non-targeting guide. Data are presented as mean ± SD of two independent experiments. 2-way ANOVA statistical analysis was performed. (**) indicates significant difference (P value <0.01), (***) indicates P value <0.001.

The intracellular accumulation of calcein-AM was examined to confirm the functional activity of the ABCB1 in Dtx sensitive and resistant Du145 cells. Calcein-AM, a substrate of the efflux transporter ABCB1, undergoes transformation into fluorescent calcein (green) by intracellular esterases, enabling the assessment of ABCB1-mediated drug

efflux and drug resistance mechanisms (Zahra et al., 2020). The efflux of calcein-AM is enhanced in the presence of ABCB1, leading to a decrease in the production of fluorescent calcein. Consistent with the expression of ABCB1, the majority of Du145 cells that were exposed to calcein-AM retained the dye, while only a small number of Du145-DtxR cells exhibited green fluorescence from calcein, indicating its efflux from the cells.

siBRPF1 and siBRPF2 treatment resulted in a slight increase in calcein fluorescence signal in the calcein retention assay as shown in Figure 3.19, but this increase was not statistically significant, suggesting that siBRPF treatment does not have a substantial effect on calcein retention. Further experiments indicating that BRPF may directly alter MDR efflux mechanisms are needed.

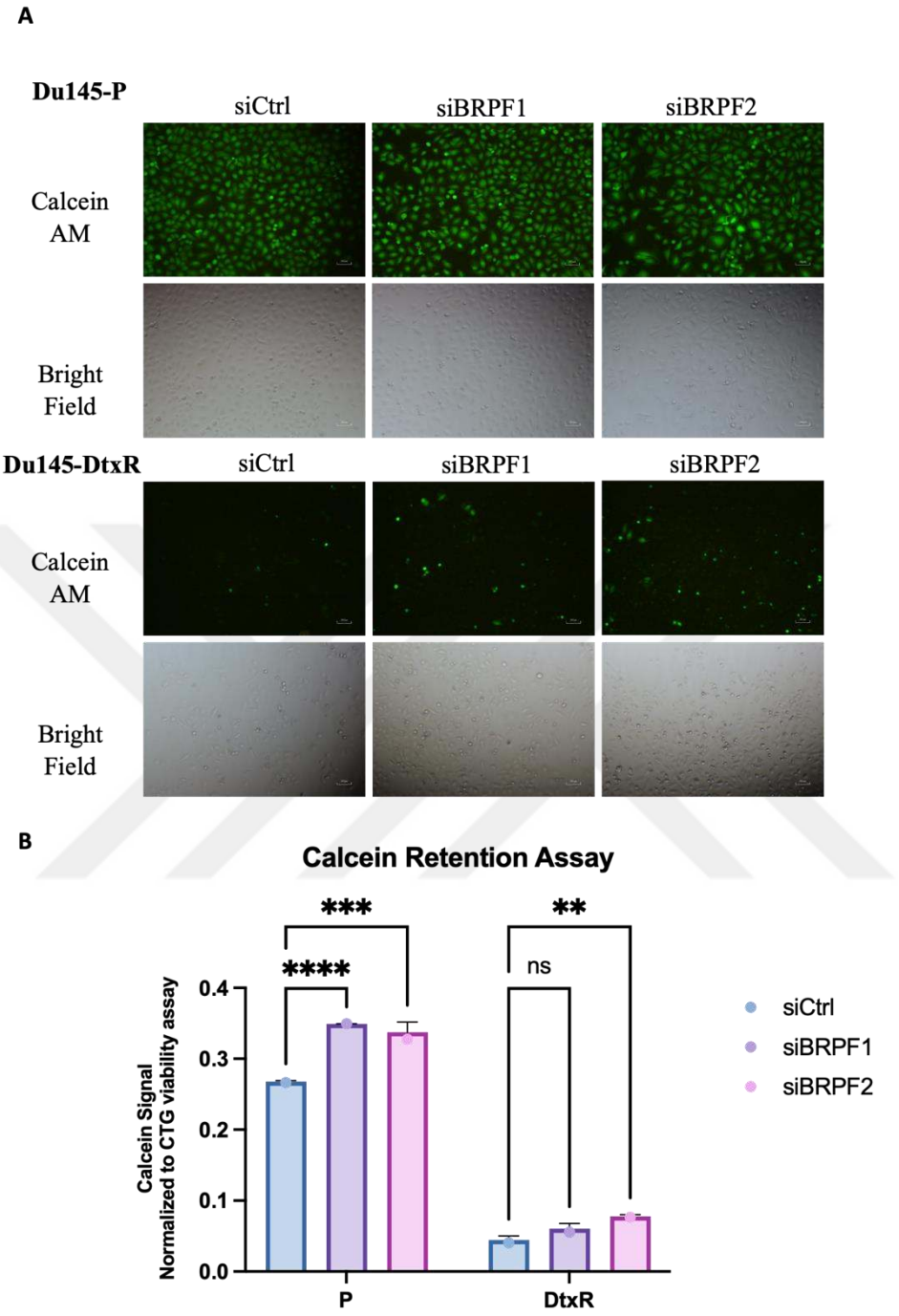

Figure 3.19: Calcein Retention Assay.
(A) Parental and resistant Du145 cells were treated with siBRPFs and then incubated with calcein-AM and calcein signal, cells were visualized under a fluorescence microscope. (B) Calcein signal normalized to CTG viability assay. Data are presented as mean ± SD of two independent experiments. 2-way ANOVA statistical analysis was performed. (**) indicates significant difference (P value <0.01), (***) indicates P value <0.001, (****) indicates P value <0.0001.

3.4.3 RNA Sequencing Upon BRPF inhibition

To elucidate the mechanisms of effects of BRPF inhibition in the reversal of taxane resistance in CRPCa cells, we conducted RNA sequencing analysis subsequent to silencing BRPF1 or BRPF2 using siRNA technology. We were unable to generate CRISPR/Cas9 knockouts specifically targeting BRPF1. Consequently, we excluded this option from our study. We chose RNA silencing as our preferred approach instead of direct drug inhibition to minimize the risk of off-target effects. Furthermore, while BRPF inhibitors have the ability to inhibit all BRPFs, their effectiveness may vary across different BRPF subtypes.

Identifying genes that are differentially expressed in Du145-DtxR cells after BRPF inhibition provide guidance in determining important genes involved in drug resistance. To understand how BRPF inhibition reverses taxane resistance, we decided to investigate the genes that were both upregulated in resistant cells and downregulated in siBRPF treated cells. Du145-DtxR cells were treated with siBRPF1 and siBRPF2. Their knockdown efficiency was confirmed by qPCR as shown in Figure 3.20A. The RNA sequencing revealed changes in the transcriptome level upon downregulation of BRPF1 and BRPF2 gene expression using siRNA in Du145-DtxR cells are presented. The RNA-seq analysis plots provide a visual representation of gene expression patterns in siRNA treatment groups, aiding in the identification of differentially expressed genes, and the overall understanding of the downstream targets of BRPFs. The PCA (Principal Component Analysis) plot in Figure 3.20B displays the gene expression profiles of siRNA treatment groups in a multidimensional space. Each point represents an RNA sequencing sample, and the position distinguishes its gene expression pattern. The plot provided an overview of the similarity or dissimilarity between samples based on their gene expression profiles. PCA plot demonstrated that the replicates from each group of siCtrl and siBRPF1, siBRPF2 treated cells were clustered together within each group and clearly separated from each other based on global transcriptome profiles. The MA plot in Figure 3.20C and D displays differential gene expression between siRNA treatment groups. The log-FC (M) of gene expression levels is plotted against the log-mean expression (A) of the genes. Genes exhibiting significant differential expression in siBRPF treatment groups are highlighted in Figure 3.20C and D. The volcano plots in Figure 3.20E and F visualizes differential gene expression between siRNA treatment groups, like MA plot. The log-FC is plotted against the statistical significance (represented as -log10 FDR). Genes with a logFC (FC) > 1 (upregulated) or < -1 (downregulated) and a false discovery rate (FDR) adjusted p-value < 0.05 were classified as differentially expressed genes (DEGs). Genes exhibiting both substantial FCs and statistical significance are highlighted, which offer valuable information regarding biologically significant distinctions.

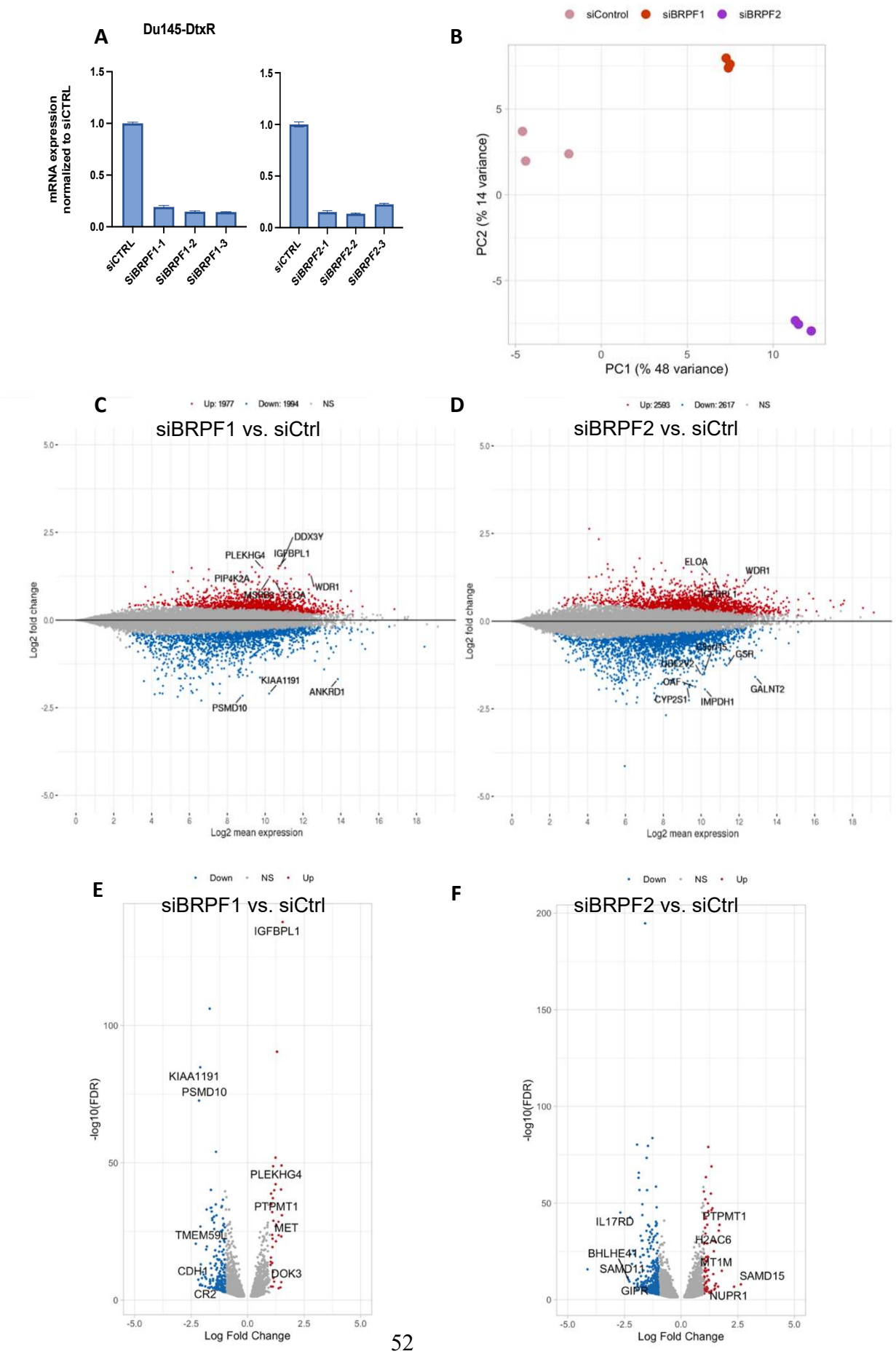
A
Du145-DtxR
mRNA expression normalized to siCTRL
siCTRL
siBRPF1-1
siBRPF1-2
siBRPF1-3
siCTRL
siBRPF2-1
siBRPF2-2
siBRPF2-3
B
siControl
siBRPF1
siBRPF2
PC2 (% 14 variance)
PC1 (% 48 variance)
C
Up: 1977
Down: 1994
NS
siBRPF1 vs. siCtrl
Log2 fold change
Log2 mean expression
DDX3Y
PLEKHG4
IGFBPL1
PIP4K2A
WDR1
ELOA
KIAA1191
ANKRD1
PSMD10
D
Up: 2583
Down: 2617
NS
siBRPF2 vs. siCtrl
Log2 fold change
Log2 mean expression
ELOA
WDR1
GSR
GALNT2
IMPDH1
CYP2S1
E
Down
NS
Up
siBRPF1 vs. siCtrl
-log10(FDR)
Log Fold Change
IGFBPL1
KIAA1191
PSMD10
PLEKHG4
PTPMT1
MET
TMEM59L
CDH1
DOK3
CR2
F
Down
NS
Up
siBRPF2 vs. siCtrl
-log10(FDR)
Log Fold Change
IL17RD
PTPMT1
H2AC6
BHLHE41
MT1M
SAMD11
SAMD15
GIPR
NUPR1

Figure 3.20: RNA sequencing analysis plots.
(A) BRPF1 and BRPF2 mRNA levels and (B) Principal Component Analysis (PCA) plot of RNA-seq samples from siCtrl, siBRPF1 and siBRPF2 in Du145-DtxR cells. (C) MA plot (B) MA plot for siBRPF1, (C) MA plot for siBRPF2, (D) Volcano plot showing the DEGs (Differentially Expressed Genes) (FDR < 0.05, and $Log_2FC \geq 1$ or ≤ -1) between siControl and siBRPF1 treated cells, (E) Volcano plot plot showing the DEGs (FDR < 0.05, and $Log_2FC \geq 1$ or ≤ -1) between siControl and siBRPF2 treated cells, the red, blue and gray scatters indicate upregulated, downregulated and no DEGs between the indicated groups, respectively.

A total of 218 genes were found to be expressed differently between siBRPF1 and siControl samples. IGFBPL1 (logFC = 1.54; FDR = 2.11e-138) was the most significantly upregulated gene, while TMEM59L (logFC = -2.29; FDR = 3.26e-21) was the most significantly downregulated gene. Between siBRPF2 and siControl, a total of 398 genes were found to be differently expressed. SAMD15 (logFC = 2.63; FDR = 1.20e-08) was identified as the most significantly upregulated gene, while BORCS8-MEF2B (logFC = -4.13; FDR = 1.88e-16) was identified as the most significantly downregulated gene. However, the expression of these genes was also downregulated in Dtx-resistant cells compared to parental cells. For instance, the expression of the TMEM59L gene in Dtx-resistant Du145 cells showed a logFC of -2.56 (FDR = 6.98e-16) compared to parental cells, indicating further reduction following siBRPF1 treatment. Based on this observation, we narrowed down our gene pool of interest to focus on genes whose expression, determined in resistant cells compared to parental cells, showed a reverse change following siBRPF treatments. Accordingly, among the genes that were upregulated in Dtx-resistant Du145 cells compared to parental cells, genes whose expression was downregulated (in the opposite direction) following siBRPF1 and siBRPF2 treatments were identified (Figure 3.21A). Similarly, among the genes that were downregulated in Dtx-resistant Du145 cells compared to parental cells, genes whose expression was upregulated following siBRPF1 and siBRPF2 treatments were identified (Figure 3.21C).

With the purpose of gaining knowledge about the molecular functions, cellular components, and biological processes involved in the reversion of taxane resistance, we conducted computed overlaps analysis. Computed overlaps in the Hallmark Collection of GSEA (Gene Set Enrichment Analysis) MsigDB database revealed the five most positively enriched gene sets among the intersecting 145 genes in the Figure 3.21A. These gene sets were identified as the complement, IL2 STAT5 signaling, inflammatory response, epithelial-mesenchymal transition (EMT), and TNFA signaling via NFKB in Figure 3.21B. The positive enrichment of these signaling pathways indicates their potential involvement in the taxane resistance.

Computed overlaps in the Hallmark Collection of GSEA MsigDB database also revealed four most positively enriched gene sets among the intersecting 141 genes in the Figure

3.21C. These gene sets were identified as the hallmark interpheron alpha response, interpheron gamma response, apical junction and mitotic spindle in Figure 3.21D. The positive enrichment of these signaling pathways indicates their potential involvement in the taxane resistance.

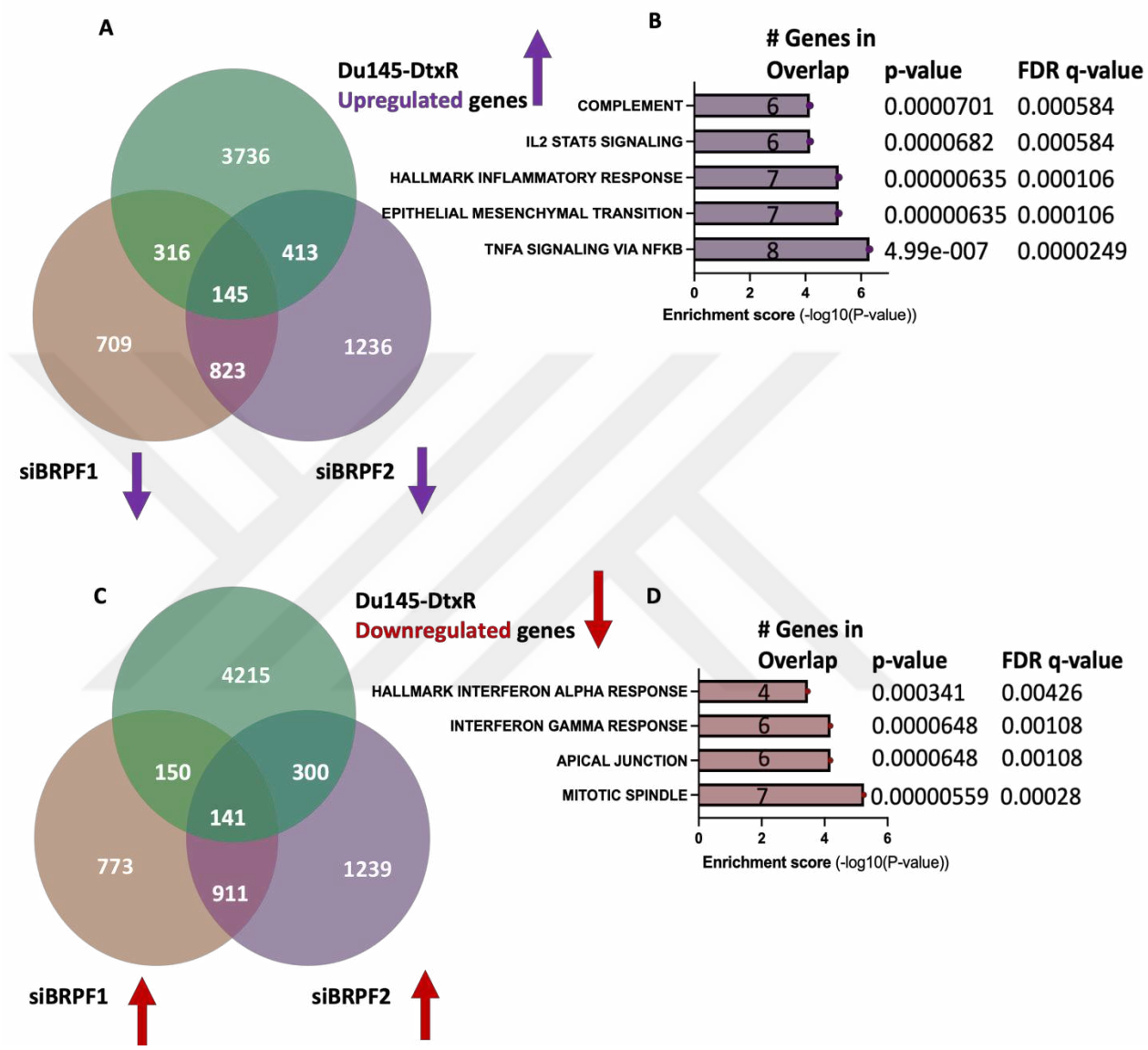

Figure 3.21: GSEA Computed Overlaps Analysis using Hallmarks that were inversely regulated in Dtx-resistant Du145 cells compared to BRPF inhibition.
(A) Venn diagram showing the number of DEGs that were upregulated in Dtx-resistant Du145 cells compared to parental cells (green region), the genes whose expression was downregulated (in the opposite direction) following siBRPF1 (orange region) and siBRPF2 (purple region) treatments. (B) Bar plot depicting Computed Overlaps in the Hallmark Collection of GSEA MsigDB database, with the enrichment scores (ES), number of Genes in Overlap, P-values and FDR q-values of the positively enriched gene sets among the 145 genes that intersect with the three regions in A (C) Venn diagram showing the genes that were downregulated in Dtx-resistant Du145 cells compared to

parental cells (green region), the genes whose expression was upregulated (in the opposite direction) following siBRPF1 (orange region) and siBRPF2 (purple region) treatments. (D) Bar plot depicting Computed Overlaps in the Hallmark Collection of GSEA MsigDB database, with the enrichment scores (ES), number of Genes in Overlap, P-values and FDR q-values of the positively enriched gene sets among the 141 genes that intersect with the three regions in C.

Overall, these findings shed light on the specific biological processes and molecular functions that are activated in response to the BRPF inhibition, providing valuable insights into the potential mechanisms underlying the reversion of taxane resistance. Further investigation of these pathways and their associated genes may contribute to the development of targeted therapeutic strategies for enhancing taxane efficacy in cancer treatment.

3.4.4 Validation of Significantly Altered Genes Identified Through RNA Sequencing.

Following the identification of differentially expressed genes, genes that could be potentially associated with ABCB1/MDR1 or drug resistance were selected for validation. The genes with logFC value greater than 1 (upregulated) or less than -1 (downregulated), corresponding to at least a 2-FC, that were found to be commonly upregulated or downregulated in taxane-resistant cells (compared to parental cells) and exhibited an expression change in the opposite direction were selected for validation. The functions of the identified genes, which were found to be significantly altered, were examined in the literature to assess their potential role in overcoming drug resistance. This involved investigating if they have been associated with drug resistance in different cancers, their association with microtubules (the target of taxanes), or their demonstrated relationship with ABCB1/MDR1. As shown in Table3.2, differentially expressed genes identified through RNA sequencing were associated with drug resistance.

Table 3.2: DEGs identified through RNA-seq that could be associated with drug resistance.
The table includes gene names, their relationship with drug resistance, and corresponding references. The genes highlighted in red are those that showed downregulation in expression after siBRPF treatment in Dtx-resistant cells. The genes highlighted in blue are those that showed upregulation in expression after siBRPF treatment in Dtx-resistant cells.

Gene Name	Drug Resistance Relationship	Reference
GALNT3	Supports tumor formation, liver metastasis, and chemo resistance in colorectal cancer cell lines via the linc01296-GALNT3 axis.	(B. Liu et al., 2018)
SERPINE1	Reverses the paclitaxel resistance in triple-negative breast cancer through suppression of VEGFA.	(Q. Zhang, Lei, & Jing, 2020)
TGFA	Enhances resistance to EGFR blockade in colorectal cancer cells through the TGF-alpha and amphiregulin paracrine network.	(Hobor et al., 2014)
CXCL8	Upregulated in chemoresistant lines of colorectal cancer cells.	(Dabkeviciene et al., 2015)
TNFRSF9	Complete regression of large solid tumors observed using anti-CD137 (TNFRSF9) immunotherapy in drug-resistant hematopoietic cells.	(McMillin et al., 2006)
SLC7A2	Expression levels of SLC7A2 are associated with improved survival in breast cancer patients. SLC family members play important roles in ovarian cancer tumorigenesis, resistance development, and progression.	(Sun, Bi, Liu, & Yang, 2020)

CCN2	Increases drug resistance in osteosarcoma by enhancing ABCG2 expression.	(Tsai et al., 2019)
HERPUD1	Involved in chemotherapy resistance mediated by the UPR.	(Avril, Vauléon, & Chevet, 2017)
EGR1	Enhances drug resistance in breast cancer by modulating MDR1 expression independently of GGPPS.	(Tao et al., 2013)
SEMA3C	A therapeutic target in prostate and other cancers.	(Hui, Tam, Jiao, & Ong, 2019)
SIK1B	Suppresses tumor function and regulates drug resistance in breast cancer.	(Xin et al., 2021)
HEXIM1	Critical determinant of response to tamoxifen.	(Ketchart et al., 2011)
MT1F	Plays a significant role in tumor formation, progression, and drug resistance.	(Si & Lang, 2018)
NTN1	Combination therapy with chemotherapeutic agents and netrin-1 enhances cancer cell death.	(Paradisi et al., 2013)

The RNA sequencing hits that were found to be related to drug resistance were validated by qPCR as shown in Figure 3.22. Among these genes, *TGFA* and *EGR1* were upregulated in resistant cells. Other research shows that there have been findings of elevated levels of growth factors, including IGF-1, EGF, and TGFA/B in metastatic CRPCa (Hour et al., 2015). According to a study, the overexpression and activation of EGFR cause the overexpression of the AKT-dependent ABCB1 (MDR1) protein, which in turn mediates Dtx resistance in CRPCa (Hour et al., 2015). EGR1 is known to activate the gene transcription of *ABCB1* in paclitaxel resistant breast cancers (Tao et al., 2013).

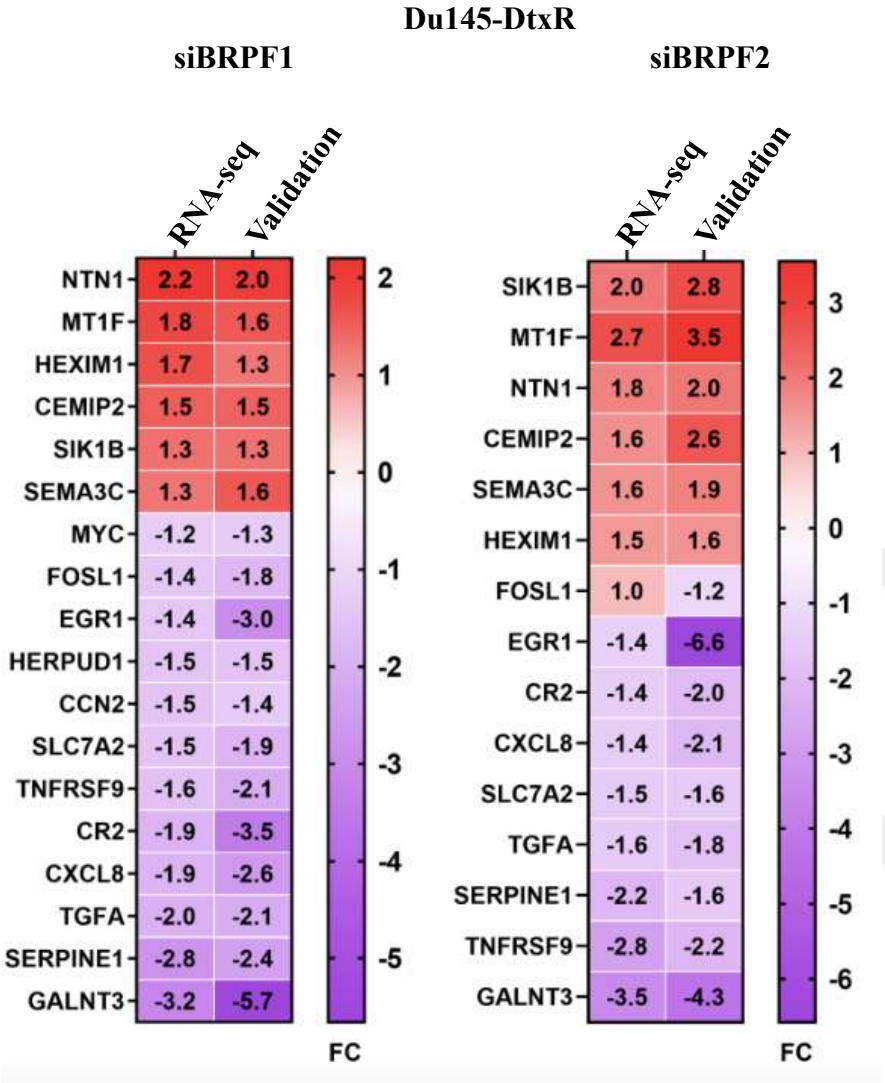

Figure 3.22: The heatmap showing the RNA sequencing results in FC relative to siCtrl treated samples and in house qPCR validation of RNA-seq hits that were found to be related to drug resistance.

The fact that siRNA-mediated targeting of BRPFs did not increase the taxane response as effectively as epi-drugs or that drug/siRNA applications caused a slight decrease in ABCB1 expression suggested that there may be a mediator regulator in the mechanism. Based on this, transcription factors known to regulate ABCB1, which are expressed more in our resistant cells compared to parental cells, were determined. Among these, the transcription factors that are also downregulated by siBRPF treatment were selected. The effects of targeting *MYC, JUN, EGR1, RUNX1, NFKB1,* and *FOSL1* genes with siRNA in Du145-DtxR cells were analyzed in terms of taxane resistance (clonogenic viability assays) and their effects on MDR1 (expression analysis) were determined.

We observed a decrease in colony formation ability when taxane-resistant CRPCa cells were treated with siRUNX1 and siNFKB1 compared to the control group in Figure 3.23.

Combining siRNA treatment with treatment with taxanes didn't further decrease the number of colonies.

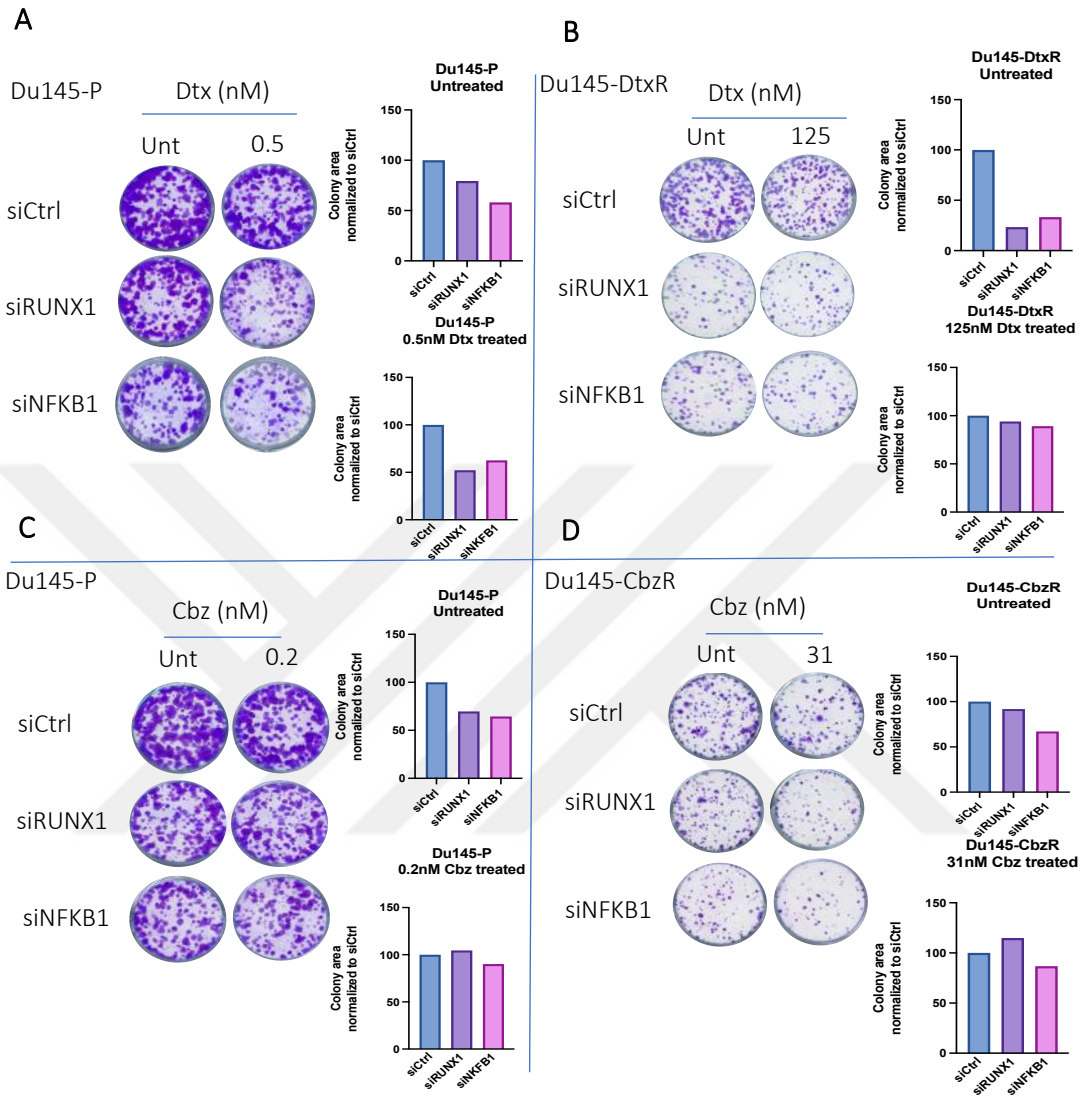

Figure 3.23: Colony Formation Assay after siRNA mediated *RUNX1* and *NFKB1* knockdown following Dtx and Cbz treatment.
Clonogenic images and the quantification of these images for siRUNX1 and siNFKB1 treated (A) Du145-P cells, (B) Du145-DtxR cells following Dtx treatment, (C) Du145-P cells following Cbz treatment, (D) Du145-DtxR cells following Cbz treatment.

The number of colonies formed in the *JUN* and *MYC* inhibition group was lower, indicating a dependance on these genes in the resistant cells as it can be seen in Figure 3.24.

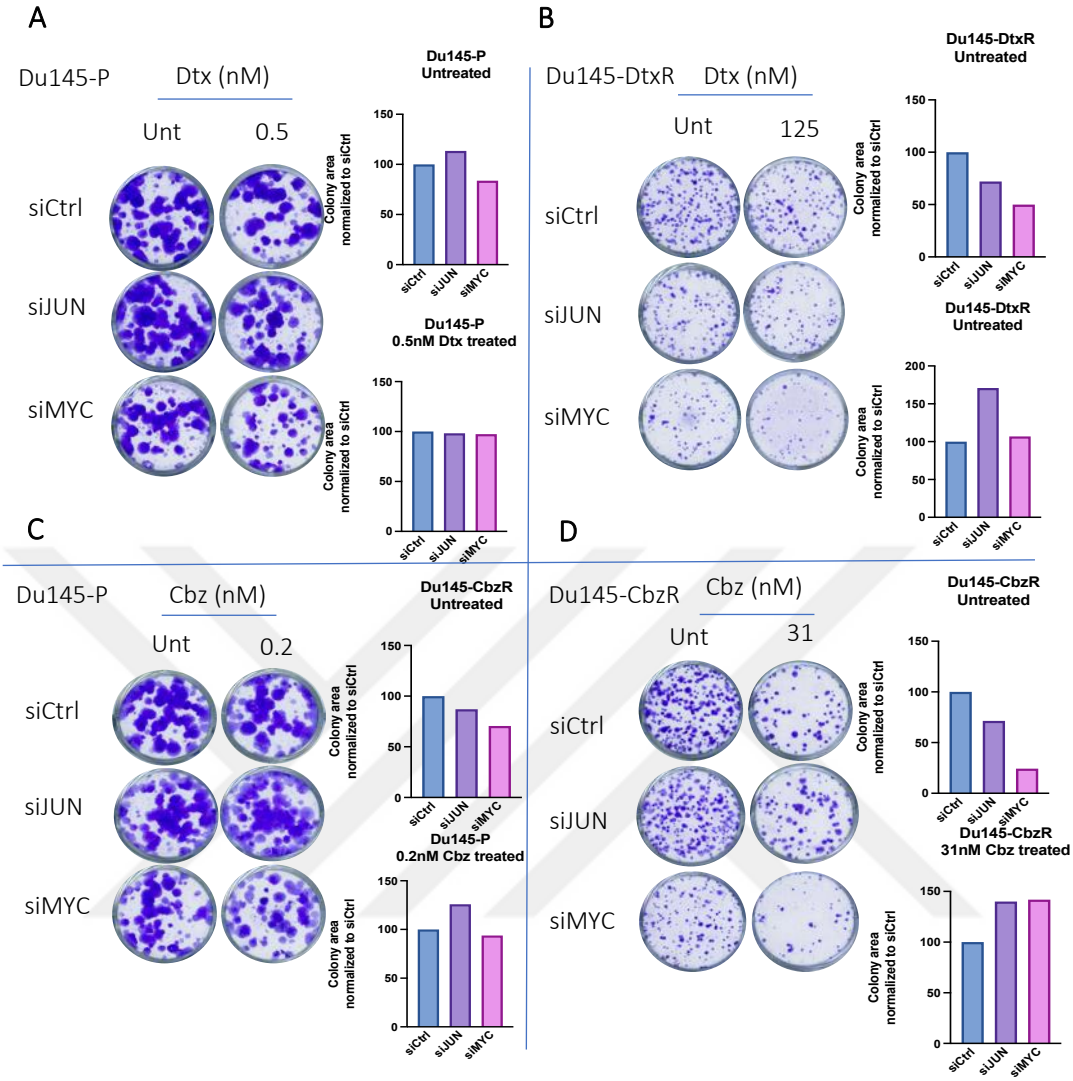

Figure 3.24: Colony Formation Assay after siRNA mediated *JUN* and *MYC* knockdown following Dtx and Cbz treatment.
Clonogenic images and the quantification of these images for siJUN and siMYC treated (A) Du145-P cells, (B) Du145-DtxR cells following Dtx treatment, (C) Du145-P cells following Cbz treatment, (D) Du145-DtxR cells following Cbz treatment.

The quantification of colony formation revealed a reduction in colony number in siFOSL1 treated Du145-DtxR cells. This finding supports the inhibitory effect *FOSL1* inhibition with the combination of taxanes on the colony forming capacity of taxane-resistant CRPCa cells. In Du145-CbzR cells the growth inhibitory effect of *FOSL1* and *EGR1* inhibition was not observed, as shown in Figure 3.25.

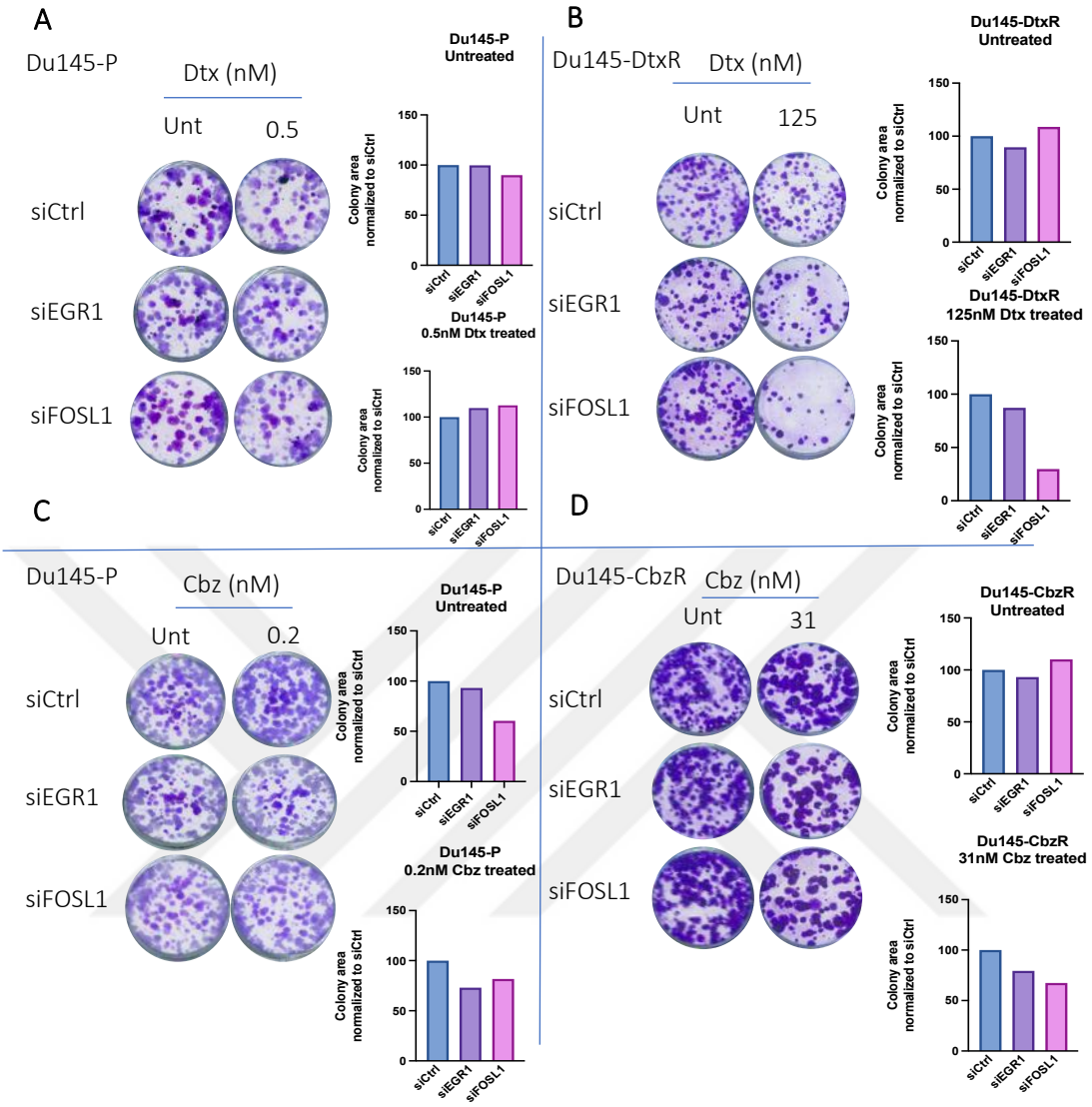

Figure 3.25: Colony Formation Assay after siRNA mediated *EGR1* and *FOSL1* knockdown following Dtx and Cbz treatment.
Clonogenic images and the quantification of these images for siEGR1 and siFOSL1 treated (A) Du145-P cells, (B) Du145-DtxR cells following Dtx treatment, (C) Du145-P cells following Cbz treatment, (D) Du145-CbzR cells following Cbz treatment.

The mRNA expression of *ABCB1* changed slightly upon siRNA mediated inhibition of *RUNX1* in Du145-DtxR cells. It is established that BRPF1 plays a role in the regulation of gene expression of *RUNX1* (Ullah et al., 2008). In our study, we hypothesized that BRPF1 may directly or indirectly regulate the expression of *ABCB1*. If the regulation is indirect, it is possible that BRPF1 exerts its influence on *ABCB1* through its modulation of *RUNX1*. *NFKB1* inhibition resulted in a decrease in *ABCB1* expression in Du145-CbzR cells, while the inhibition of *JUN, MYC, FOSL1* and *EGR1* slightly decrease *ABCB1* mRNA expression (Figure 3.26D). Our data showed that silencing these transcription factors or the pathways involving these genes revert resistance at least partially potentially explaining how BRPFs may be reverting taxane resistance.

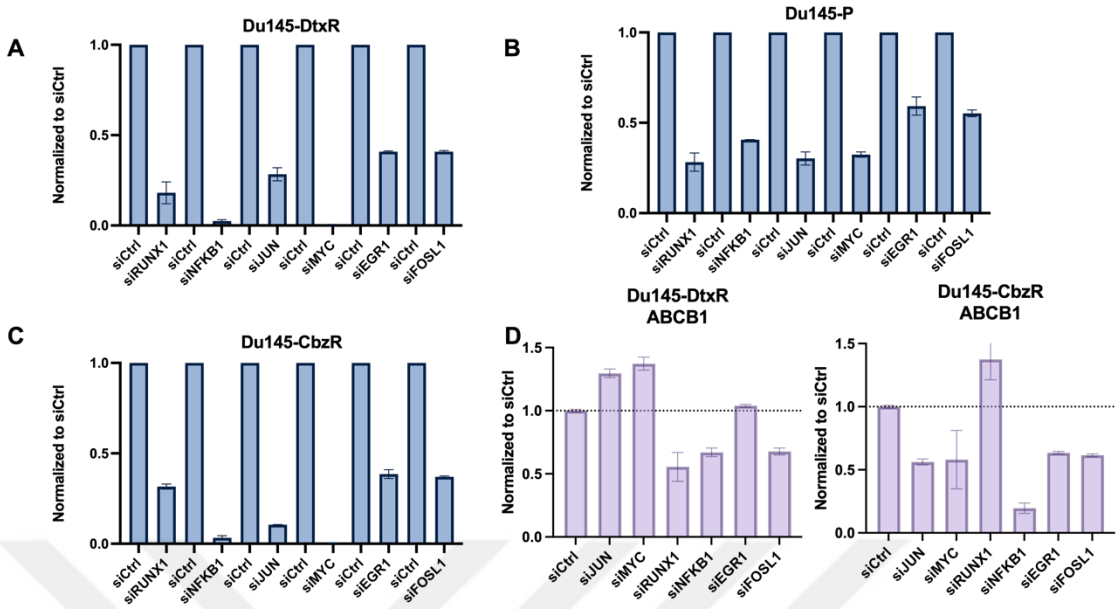

Figure 3.26: mRNA expression of *ABCB1* and selected genes after siRNA treatment. siRNA knockdown efficiency of (A) Du145-P cells, (B) Du145-DtxR cells, (C) Du145-CbzR cells, (D) *ABCB1* mRNA expression in siRNA mediated knockdown of *MYC, JUN, EGR1, RUNX1, NFKB1,* and *FOSL1.* Data are presented as mean ± SD of two independent experiments.

3.5 The effect of BRPF inhibition on Other Types Of Cancers

3.5.1 Measurement of BRPF Expression in Different Cells Lines

We wanted to investigate the mRNA expression profiles of our candidate genes in other types of cancers. To do so, we assessed the gene expression of *ABCB1, BRPF1, BRPF2, PRMT5, RAB3B, CRIP1* and *CRIP2* in other PCa, acute lymphocytic (ALL) and AML, hepatocellular carcinoma, non-small lung cancer and breast cancer via qPCR.

PRMT5 was included in this study due to its importance in taxane resistance. Inhibiting PRMT5, similar to inhibiting BRPF, could potentially overcome taxane resistance in CRPCa as shown in Figure 3.6A.

Our qPCR analysis of mRNA expression profiles in various types of cancers shed light on the differential expression patterns of candidate genes, including *ABCB1, BRPF1, BRPF2, PRMT5, RAB3B, CRIP1,* and *CRIP2* in Figure 3.27 and 3.28. The *BRPF* family genes, in particular, exhibited consistently high expression levels across most cancer types investigated. Our qPCR analysis showed the high expression of *ABCB1* in Jurkat, K562, Thp-1, HepG2, Huh7, H1299 and U2OS cell lines. Therefore, we aimed to investigate the relationship between *ABCB1* expression and taxane resistance in these *ABCB1* expressing cell lines.

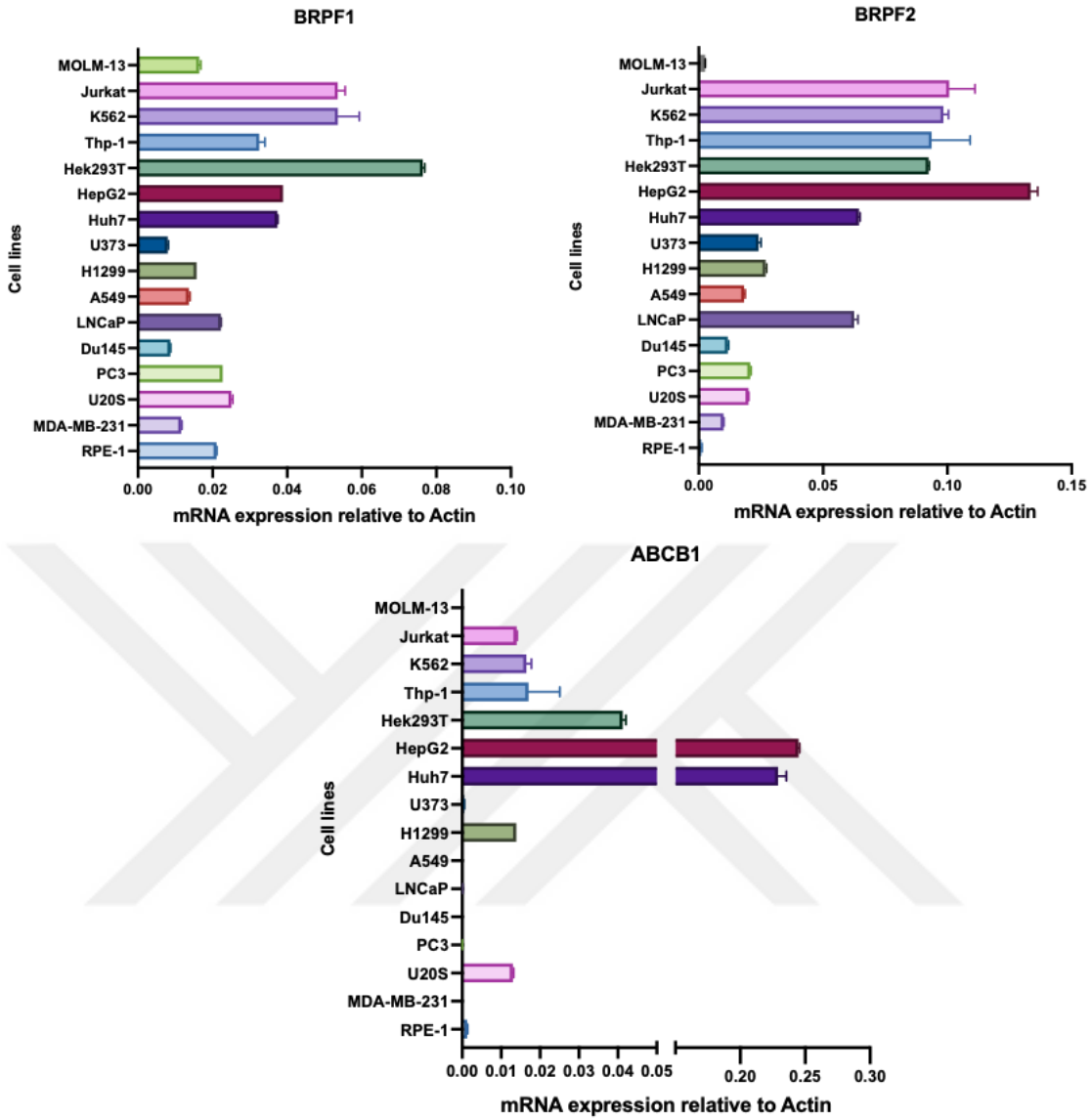

Figure 3.27: qPCR results showing *BRPF1-2* and *ABCB1* gene expressions in different cell lines. Data are calculated using 2^-Delta Ct (ΔCt) method and presented as mean ± SD of two independent experiments.

Our investigation showed that *PRMT5* and *RAB3B* were consistently expressed in the majority of the cell lines examined. The continuous expression of *PRMT5*, an arginine methyltransferase involved in a variety of cellular functions including the control of gene expression, points to its potential importance in these cell lines (Kim & Ronai, 2020). The expression levels of *RAB3B*, a Ras-related GTPase family member involved in vesicle trafficking, were similarly consistent among the cell lines examined (Tsunedomi et al., 2022) On the other hand, there were notable differences in the expression of *CRIP1* and *CRIP2* between the various cell lines. *CRIP1* and *CRIP2* have been linked to a number of biological processes, including signal transduction and controlling cell development (Ludyga et al., 2013; Y. Gao et al., 2022). The observed change in their expression levels shows that these genes are subject to context-dependent regulation. Additionally, it was

observed that leukemia cell lines (Jurkat, K562, and Thp-1) exhibited high expression levels of *BRPF1*, *BRPF2* along with *ABCB1* in Figure 3.27. This information provides insight into the potential association between the expression of these genes and the taxane response in these cell lines.

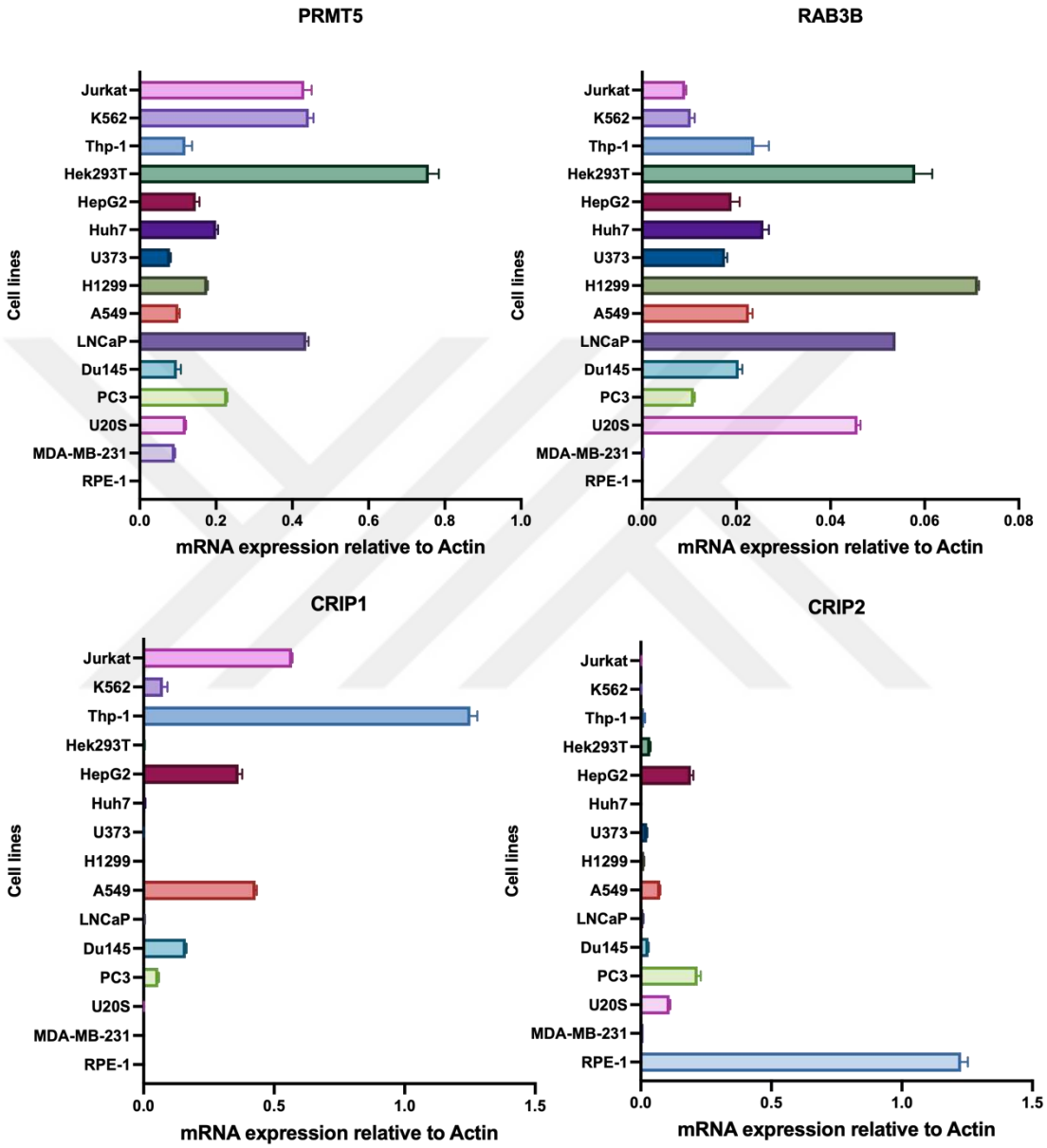

Figure 3.28: qPCR results showing other candidate genes; *PRMT5, CRIP1-2* and *RAB3B* expressions in different cell lines. Data are calculated using 2^-Delta Ct (ΔCt) method and presented as mean ± SD of two independent experiments.

To compare the expression profile of *ABCB1* with the taxane response of different cell lines, IC50 values were generated against Dtx. The IC50 values provide a measure of drug sensitivity and allow for the evaluation of the response to Dtx treatment. The table below presents the IC50 values for each cell line.

Table 3.3: *ABCB1* expression and IC50 values to Dtx in different cell lines.

IC50 values calculated using GraphPad Prism.

Cell line	ABCB1 mRNA expression	Dtx IC50 (nM)
U20S	0.013046682	19.93
PC3	0.0000367213	11.79
Du145	0.0000555659	0.42
LNCaP	0.0000926212	69.645
A549	0.0000255327	2.672
H1299	0.013936299	280.3
Huh7	0.229172575	4.37
HepG2	0.244855074	4.588
HEK293T	0.041215834	96.7
Thp-1	0.017054556	9.7
K562	0.016506532	5.613
Jurkat	0.013989188	4.347
MOLM-13	0.00	24.9

The cells were stratified into two distinct groups based on their expression levels of *ABCB1*: those with expression levels lower than 0.01 were classified as the "low" group, while those with expression levels higher than 0.01 were classified as the "high" group. Subsequently, a scatter plot was generated to visually represent the relationship between the expression levels of *ABCB1* and the corresponding Dtx IC50 values of the cells that were also listed in the Table 3.3 (Figure 3.29). The group of cells with high expression levels of *ABCB1* exhibited slightly higher IC50 values compared to the group of cells with low expression levels, although it was not statistically significant (Figure 3.29). One possible explanation for the lack of statistical significance could be the limited number of cells expressing *ABCB1*. Since the subset of cells expressing *ABCB1* is relatively small in size, these cells might have contributed to the observed non-significant results.

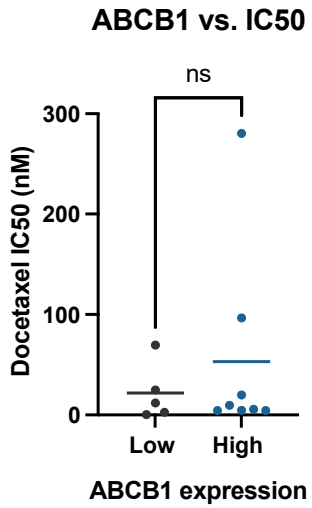

Figure 3.29: *ABCB1* expression high and low groups of cells and their Dtx IC50 values.

Further analysis and exploration of the relationship between *ABCB1* expression and taxane response, in conjunction with the expression of *BRPF1, BRPF2* can help uncover potential mechanisms and predictive markers for drug resistance in leukemia. We aimed to verify whether inhibiting BRPF could act as a sensitizer to taxane, or reverse taxane resistance in other types of cancers.

3.5.2 BRPF inhibitor GSK5959 and OF1 decreased cell viability in K562 cells.

The CTG viability assays were performed to investigate the effect of BRPF inhibition on the survival of AML cell lines. As seen in Figure 3.30, the combination treatment of the BRPF inhibitor, GSK5959 and OF1 with Dtx was not affecting K562 and MOLM-13 cells. Interestingly, inhibition of BRPFs alone caused a decrease in the cell survival in K562 cells, highlighting the potential importance of BRPF proteins in the survival of AML cells.

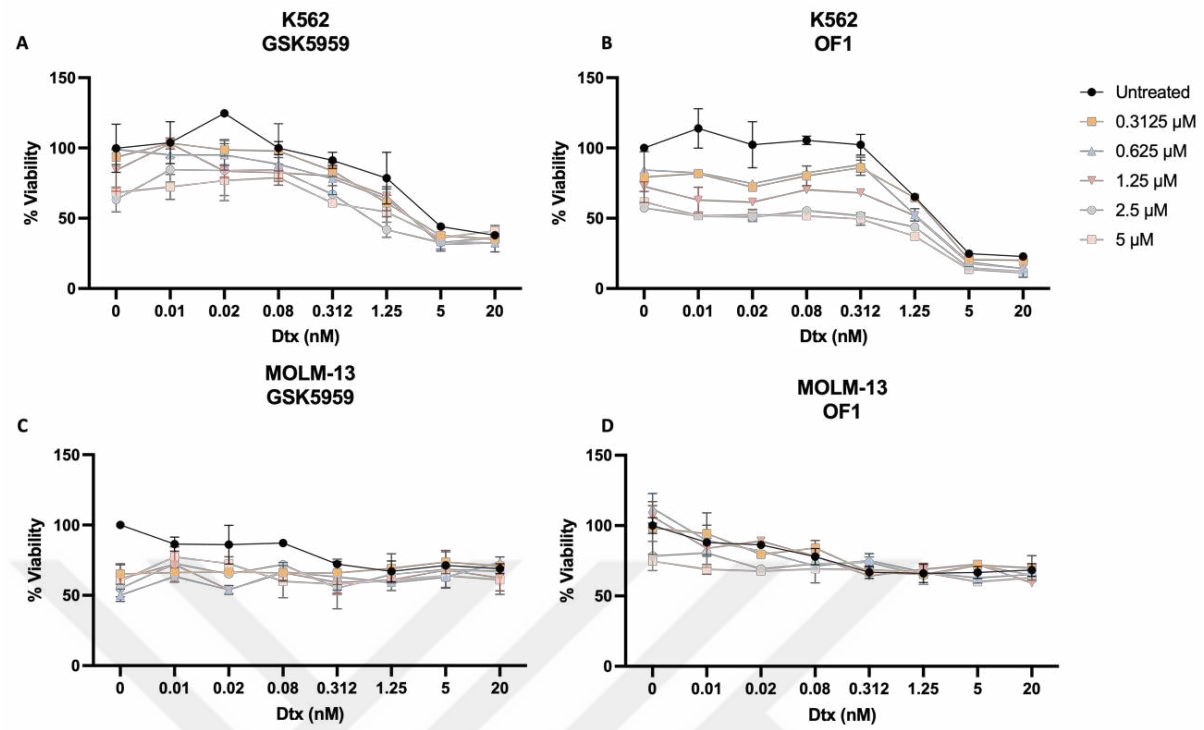

Figure 3.30: Dose-response of BRPF inhibitors (GSK5959 and OF1) on Leukemia cell lines MOLM-13 and K562.
Cells were co-treated with Dtx (0.01-20 nM) and indicated inhibitors (GSK5959 or OF1) (0.31-5 µM) and the results were obtained by CTG viability assay (72 h). The data is expressed as mean ± SD. (A) GSK5959 and Dtx treatment in K562 cells (B) OF1 and Dtx treatment in K562 cells (C) GSK5959 and Dtx treatment in MOLM-13 cells (D) OF1 and Dtx treatment in MOLM-13 cells.

In order to assess the impact of BRPF inhibition on the viability of different cell lines, SRB viability assays were conducted. Figure 3.31 illustrates the results obtained from these assays, focusing on the combination treatment of the BRPF inhibitors (GSK5959 and OF1) with Dtx in Huh7, HEPG2, H1299, U20S and A549 cells. The combination treatment of GSK5959 and Dtx did not exhibit additive effects on cell viability, as indicated by the SRB viability assay results (Figure 3.31) Similarly, the combination treatment of OF1 and Dtx in these cells did not affect the cell viability (Figure 3.31).

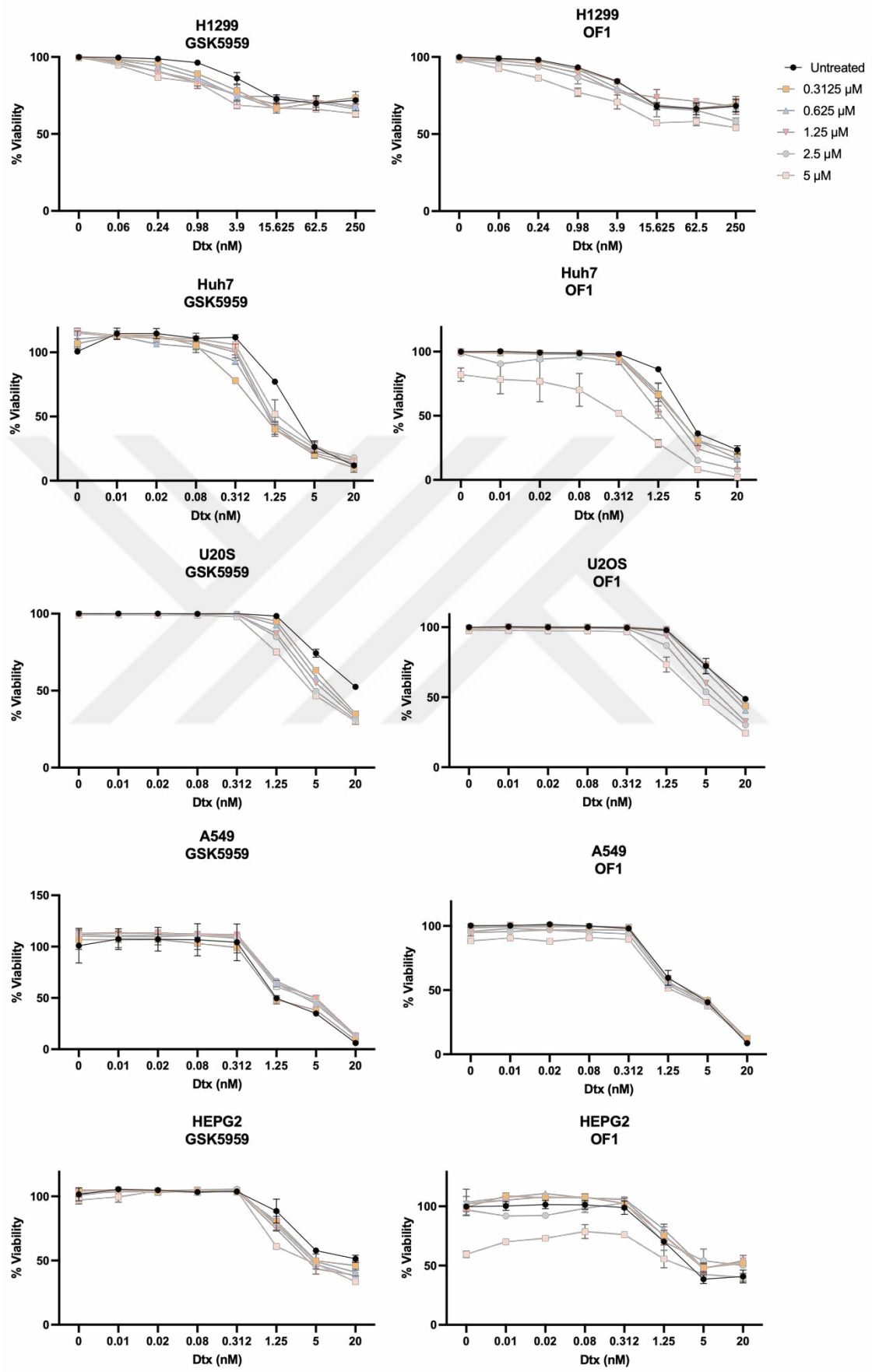
H1299
GSK5959
H1299
OF1
Huh7
GSK5959
Huh7
OF1
U20S
GSK5959
U2OS
OF1
A549
GSK5959
A549
OF1
HEPG2
GSK5959
HEPG2
OF1
% Viability
Dtx (nM)
0 0.06 0.24 0.98 3.9 15.625 62.5 250
0 0.01 0.02 0.08 0.312 1.25 5 20
Untreated
0.3125 µM
0.625 µM
1.25 µM
2.5 µM
5 µM

Figure 3.31: Dose-response of BRPF inhibitors (GSK5959 and OF1) on HepG2, Huh7, U20S, A549 and H1299 cells.
H1299 cells were co-treated with Dtx (0.06-250 nM), and indicated inhibitors (GSK5959 or OF1) (0.31-5 μM). HepG2, Huh7, U20S and A549 cells were co-treated with Dtx (0.01-20 nM), the results were obtained by SRB viability assay (72 h). The data is expressed as mean ± SD.

Overall, these findings suggest that the combination treatment of BRPF inhibitors with Dtx did not affect cell viability in the tested cell lines. However, the individual inhibition of BRPFs showed a notable impact on cell survival, indicating the potential significance of BRPF proteins in cell viability of AML.

3.6 Chromatin Immunoprecipitation

The chromatin immunoprecipitation (ChIP) was conducted to investigate the interaction of BRPF with chromatin.

Exogenous expression of BRPFs confirmed using Western blot analysis as shown in Figure 3.32. We validated the specificity of the anti-BRPF1 and anti-BRPF2 antibody. The bands at the molecular weight of BRPF1 and BRPF2 was detected in BRPF-V5 overexpression plasmid transfected cells, indicating that the antibody specifically recognizes BRPFs.

We obtained HA-tagged BRPF1 expressing Du145-DtxR cells by transducing cells with lentivirus containing HA-BRPF1 construct and confirmed HA-tagged BRPF1 expression with Western blot in Figure 3.32, in order to pull-down BRPFs via anti-HA antibody. We confirmed the exogenous expression of HA-tagged BRPF1 using Western blot analysis.

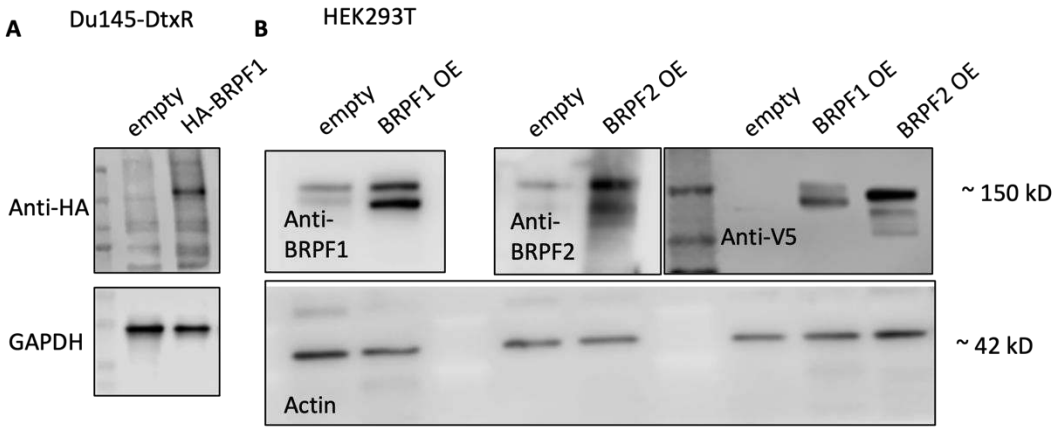

Figure 3.32: Exogenous expression of BRPF confirmed using Western blot analysis.
Western blotting was conducted to assess the presence of target proteins in the transduced or transfected cells. HA-BRPF1 stable expression in Du145-DtxR cells was detected with

(A) anti-HA antibody, (B) HEK293T cells were transiently transfected BRPF1 and BRPF2-V5 constructs and proteins were blotted with anti-BRPF1, BRPF2 and V5 antibody (from left to right), GAPDH and Actin were used as loading controls.

The Western blot analysis in Figure 3.33 revealed the successful immunoprecipitation of the target BRPF proteins, indicated by the detection of specific immunoreactive bands in the IP samples. These immunoprecipitation results highlighted the successful capture of target proteins, which led us to continue with ChIP eperiments using these antibodies. We optimized sonication conditions (Figure 3.34).

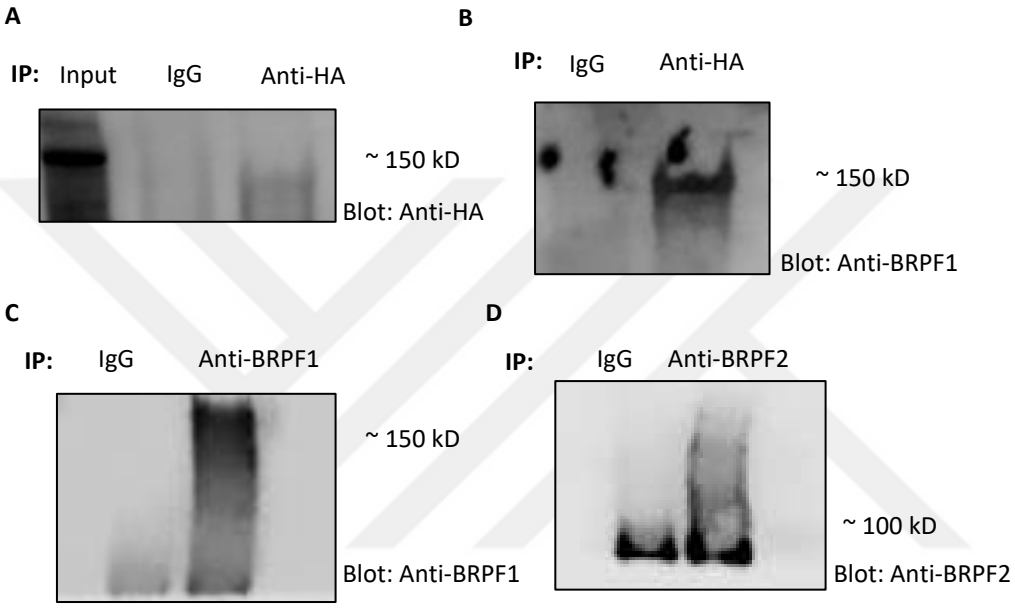

Figure 3.33: Immunoprecipitation (IP) experiment to assess the pull-down efficiency of HA and BRPF antibodies.
Western blotting was conducted to assess the presence of target proteins in the immunoprecipitated samples. The immunoprecipitates were obtained using anti-HA antibody, blotted with (A) anti-HA antibody, (B) BRPF1 antibody. The immunoprecipitates were obtained using (C) anti-BRPF1 antibody, (D) anti-BRPF2 antibody.

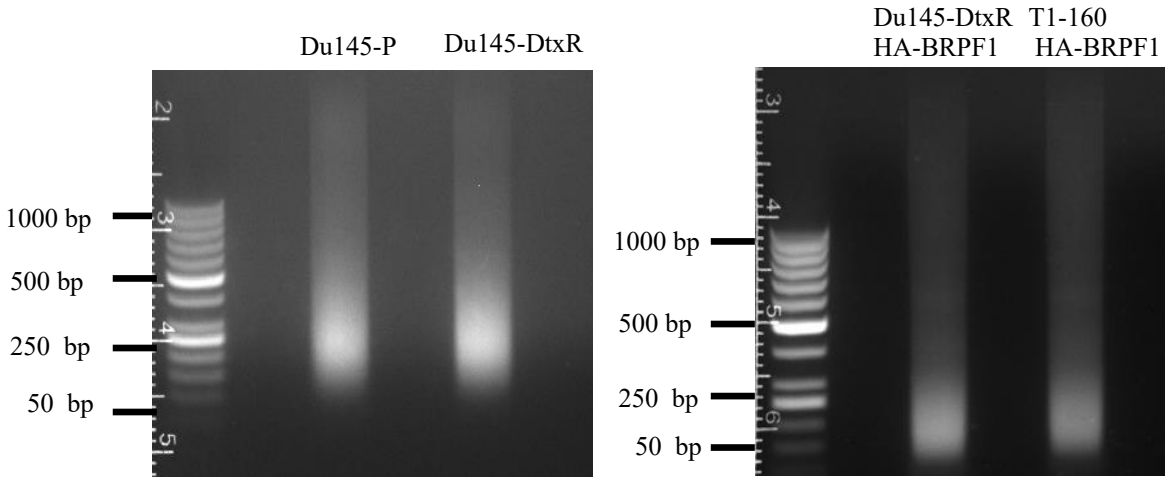

Figure 3.34: ChIP sonication optimized as 40 cycles 45 sec ON/15 sec OFF, with BioRuptor Sonicator.

To test whether BRPF1 directly regulates *ABCB1* expression, we analyzed the enrichment of BRPF1 on the promoter of *ABCB1* in Du145-DtxR cells using chromatin immunoprecipitation (ChIP) assays. We found that, in comparison with IgG and gene desert region controls, BRPF1 was indeed enriched at the promoter region of *ABCB1* and at the promoter of *RUNX2*, positive control in Figure 3.35.

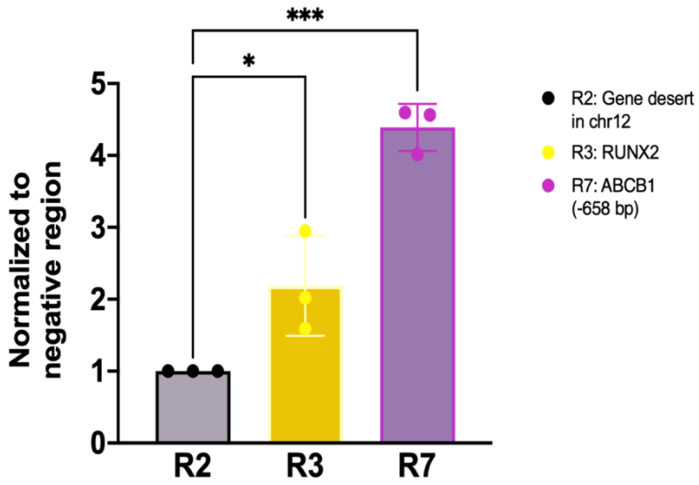

Figure 3.35: ChIP-qPCR showing normalized BRPF1 enrichment at positive control region (*RUNX2*) and *ABCB1* promoter region normalized to control region (*Chr12 gene desert*) in Du145-DtxR cells.
Data are shown as percentage of ChIP input; dots represent individual biological replicates, bars represent mean of replicates. Ordinary one-way ANOVA statistical analysis was performed. (*) indicates significant difference (P value <0.05), (***) indicates P value <0.001.

Both endogenous and exogeneous BRPF1 were pulled down using anti-BRPF1 and anti-HA antibodies. ChIP-qPCR results indicate the occupancy of the *ABCB1* promoter by BRPF1 in Du145-DtxR cells, strongly arguing for the direct regulation of the *ABCB1* gene via BRPF1 (Figure 3.36).

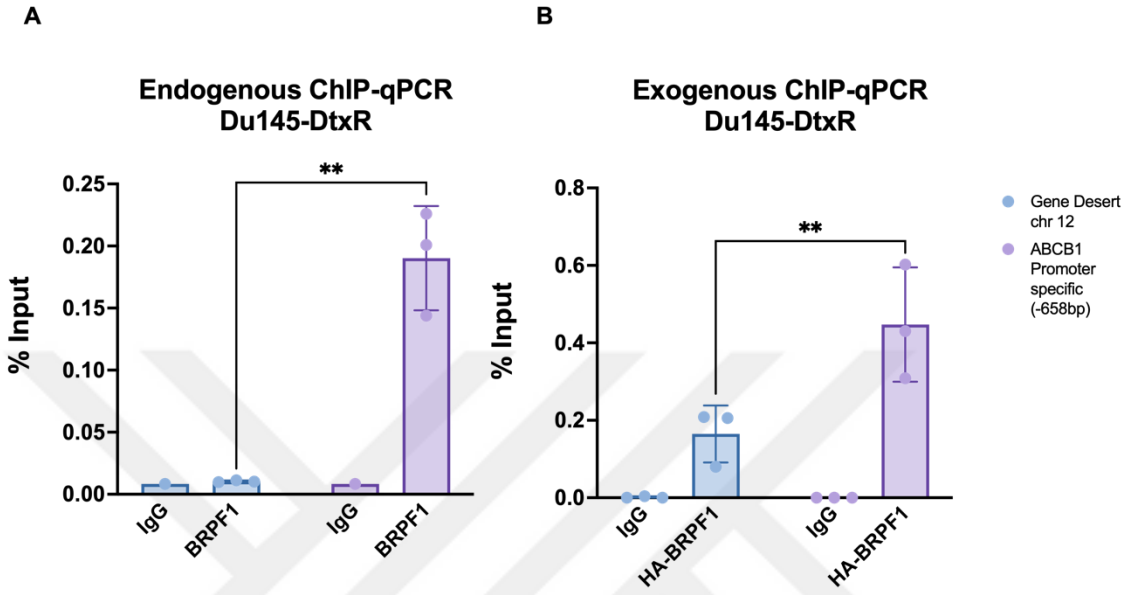

Figure 3.36: ChIP-qPCR showing both endogenous and exogenous BRPF1 enrichment at the *ABCB1* promoter in Du145-DtxR cells.
(A)ChIP-qPCR using anti-BRPF1 antibody to pulldown endogenous BRPF1 (B) ChIP-qPCR using anti-HA antibody to pulldown exogenous HA-tagged BRPF1 in Du145-DtxR cells. Data are shown as percentage of ChIP input; dots represent individual biological replicates, bars represent mean of replicates. 2-way ANOVA statistical analysis was performed. (**) indicates significant difference P value <0.01.

Triple-negative breast cancer (TNBC) is the most aggressive and recurrent type of breast cancer, known for its poor prognosis and limited treatment options (Wein & Loi, 2017). One potential factor contributing to the challenges in TNBC treatment is chemotherapy resistance, particularly in the metastasized population where brain and lung metastases frequently occur (Wein & Loi, 2017). In this context, investigating the role of BRPF1 through chromatin immunoprecipitation (ChIP) experiments in Taxol-resistant in TNBC could provide valuable evidence into its potential involvement in chemotherapy resistance via MDR efflux. By exploring *ABCB1* promoter binding of BRPF1 and its potential interactions with other transcriptional co-factors or chromatin modifiers, we can gain a better understanding of the underlying molecular mechanisms driving chemotherapy resistance in other types of cancers. Such knowledge could potentially pave the way for the development of targeted therapies and improved treatment strategies for patients with chemotherapy resistance.

Both endogenous and exogeneous BRPF1 were pulled down using anti-BRPF1 and anti-HA antibodies in Paclitaxel resistant TNBC, T1-160 cells, derived from SUM159 by Özlem Yedier Bayram, PhD. ChIP-qPCR results indicate the occupancy of the *ABCB1* promoter by BRPF1 via ChIP-qPCR, strongly arguing for the direct regulation of the *ABCB1* gene via BRPF1 (Figure 3.37).

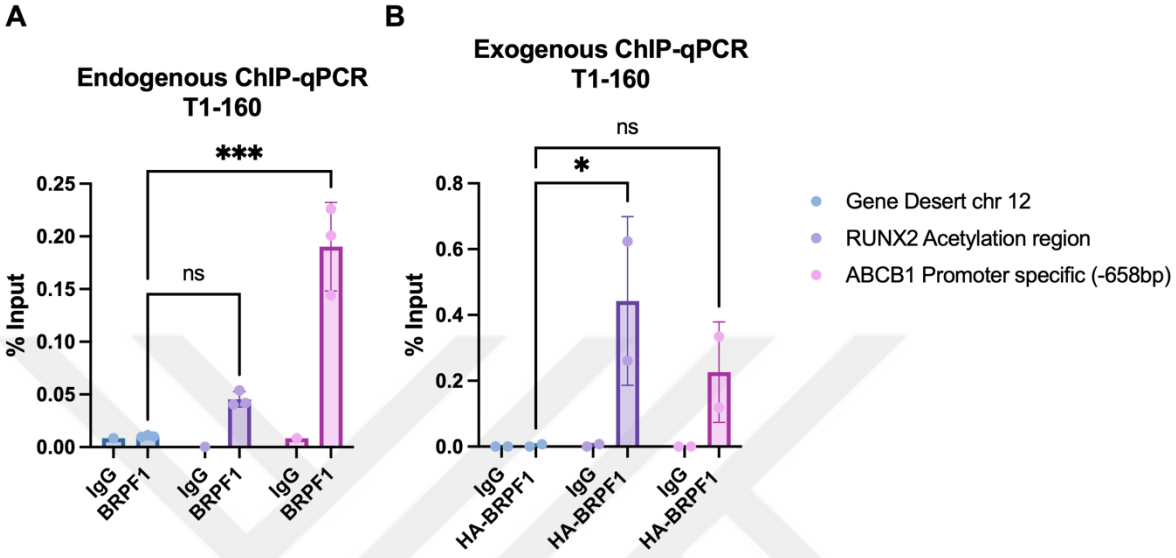

Figure 3.37: ChIP-qPCR showing both endogenous and exogenous BRPF1 enrichment at the *ABCB1* promoter in T1-160 cells which are Paclitaxel resistant TNBC cells derived from SUM159 by Özlem Yedier Bayram, PhD.
(A)ChIP-qPCR using anti-BRPF1 antibody to pulldown endogenous BRPF1 (B) ChIP-qPCR using anti-HA antibody to pulldown exogenous HA-tagged BRPF1 in T1-160 cells. Data are shown as percentage of ChIP input; dots represent individual biological replicates, bars represent mean of replicates. 2-way ANOVA statistical analysis was performed. (*) indicates significant difference P value <0.05, (***) indicates significant difference P value <0.001.

Next, we aimed to investigate how PRMT5, one of the hits obtained from the previous epigenetic drug screen, that reverses taxane resistance when inhibited as shown in Figure 3.6A. For this purpose, we conducted ChIP-qPCR experiments to examine the DNA binding regions of PRMT5. We designed primers specific to the regions that were known to be bound by PRMT5 listed in Table 3.4 (Rengasamy et al., 2017).

Table 3.4 PRMT5 ChIP-seq targets and scores in MDA-MB-231 cells obtained from Cistrome DB with ENCODE ID: GSM1964895) (Rengasamy et al., 2017)

Gene	**Score**	**Coordinate**
NEK6	2.072	chr9:124286414-124352441
ANKRD1	2.010	chr10:90912099-90921274
HSPA6	1.927	chr1:161524539-161526893
CCN2	1.774	chr6:131948175-131951371
FOSL1	1.695	chr11:65892048-65900387
MYC	0.658	chr8:127736230-127742950

PRMT5 ChIP-qPCR results indicate the occupancy of all putative targets of PRMT5 in MDA-MB-231 cells; *NEK6, ANKRD1, HSPA6, CCN2, FOSL1* and *MYC* by PRMT5 (Figure 3.38). PRMT5 was not enriched at the promoter of *ABCB1* (Figure 3.38).

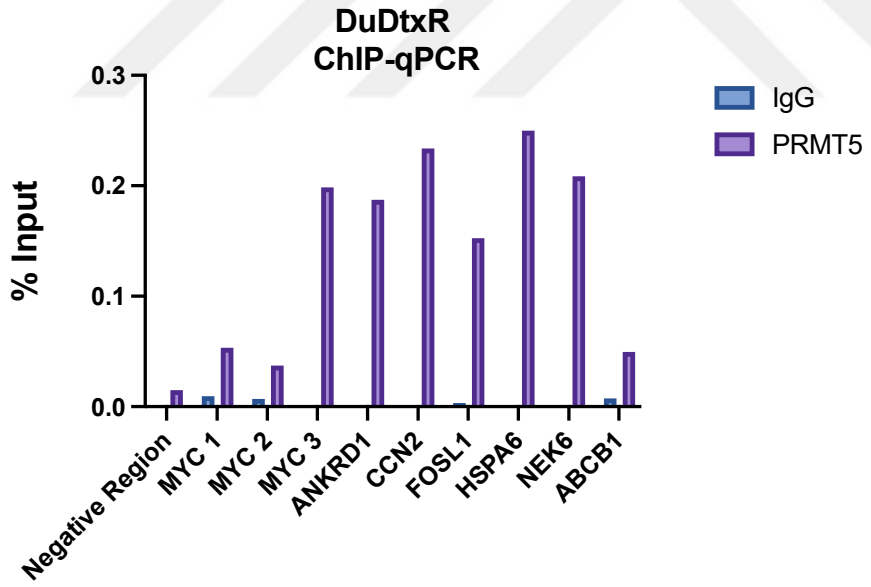

Figure 3.38: ChIP-qPCR showing endogenous PRMT5 enrichment at the promoters of *MYC, CCN2, FOSL1, NEK6, ANKRD1* and *HSPA6*.
ChIP-qPCR using anti-PRMT5 antibody to pulldown endogenous PRMT5. Data are shown as percentage of ChIP input coming from single experiment.

3.6.1 ChIP sequencing

We have shown that BRPF directly binds to *ABCB1* promoter region and regulates gene transcription. Additionally, we aimed to investigate H3K27ac occupancy within *ABCB1* promoter region in Du145-DtxR cells. ChIP-seq with H3K27ac provided valuable insights into the epigenetic differences of resistant cells. In this study, we focused on identifying the genomic loci bound by H3K27ac in Du145-DtxR cells. H3K27ac is a histone modification associated with active gene transcription and enhancer activity (Creyghton et al., 2010). It is primarily found in active enhancers and promoters (Creyghton et al., 2010).

To visualize the peak distribution within the genome, firstly, we assessed the H3K27ac enrichment around the TSS. To display the frequency and distribution of the distance to the nearest TSS or distribution of peak lengths, a histogram was used. As shown in Figure 3.39A, the x-axis for the histogram of distance to the nearest TSS is centered at 0. Average profile of H3K27ac ChIP peaks binding to TSS region, read count frequency around TSS was plotted in Figure 3.39B. In Figure 3.39C, the distribution of H3K27ac-binding loci relative to TSS was visualized. The percentage of region–gene associations according to genomic regions' distance to TSS was computed and visualized in Figure 3.39D, E and F by Genomic Regions Enrichment of Annotations Tool (GREAT). Then, we assessed the location distribution. The location represents where each peak located and the value includes the 3′UTR (untranslated region), 5′UTR, exon, intergenic region, intron, non-coding, promoter-TSS and transcription termination site (TTS), as depicted in the pie chart of genomic location distribution in Figure 3.39G. This pie chart reveals the percentage of peaks for each category.

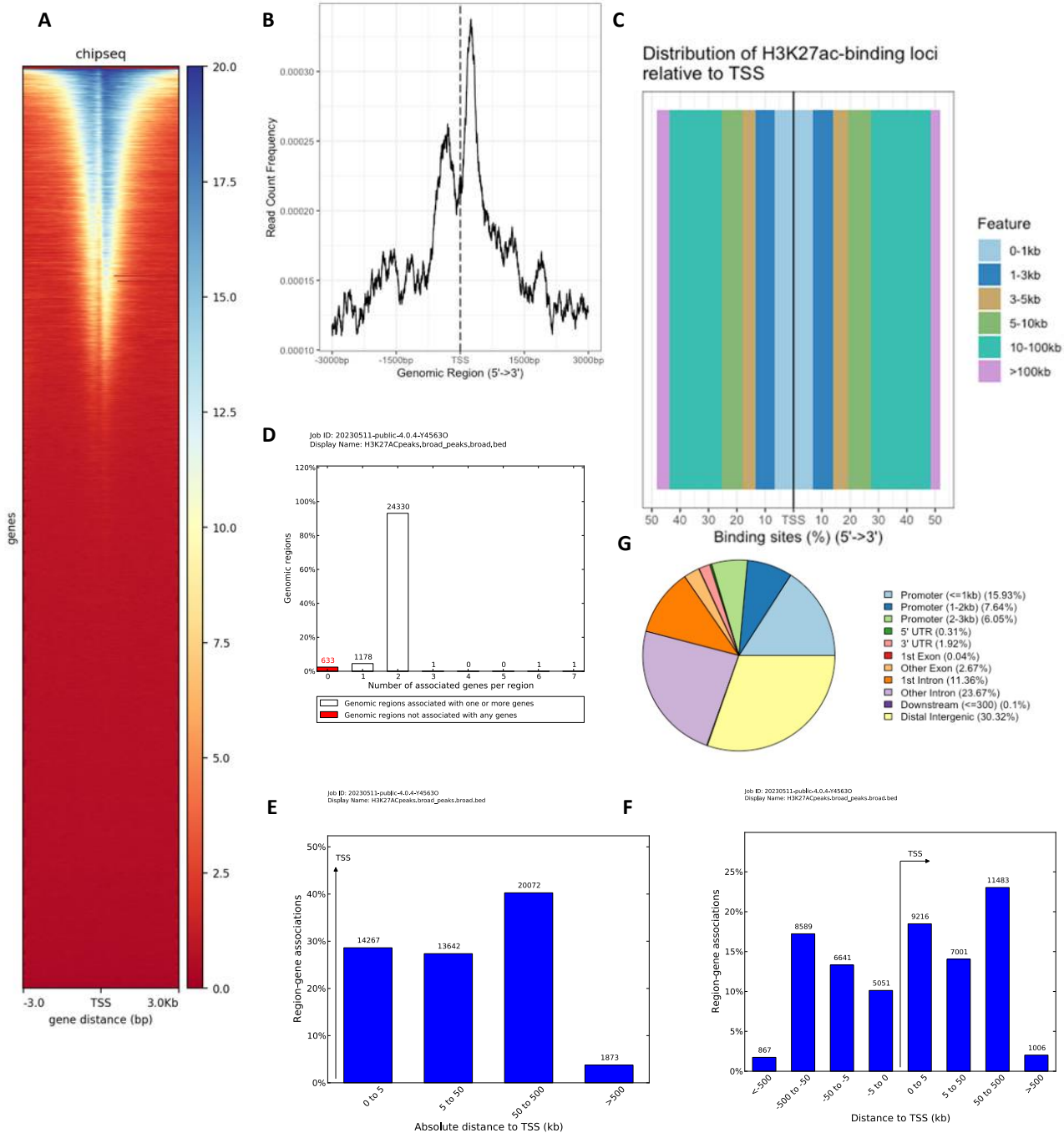

Figure 3.39: H3K27ac ChIP-seq Region-Gene Association Graphs.
(A)Heatmap showing the Profile of H3K27ac ChIP peaks binding to TSS (transcription start site) regions, flanking 3kb from TSS generated using deeptools (Ramírez et al., 2016) (B) Plot showing Average Profile of H3K27ac ChIP peaks binding to TSS region, read count frequency around TSS, generated using ChIPseeker. (Q. Wang et al., 2022) (C) Distribution of H3K27ac-binding loci relative to TSS generated using ChIPseeker. The percentage of binding sites upstream and downstream from the TSS of the nearest genes were calculated, and the distribution is visualized. (D) Number of associated genes

per region, (E) binned by orientation and distance to TSS, (F) binned by absolute distance to TSS computed by Genomic Regions Enrichment of Annotations Tool (GREAT) (McLean et al., 2010) (G) Pie chart of the genomic location distribution of H3K27ac. This plot shows the percentage for each genomic location category. The categories are sorted by descending percentage, generated using ChIPseeker.

Top 15 of H3K27ac enriched sites and physically annotated gene loci are listed in Table 3.5.

Table 3.5: Top 15 of H3K27ac enriched sites and physically annotated gene loci.
Binding peaks ordered by fold enrichment from high to low.
In this table, the genes that were occupied by H3K27ac in Du145-DtxR cells are given. The table includes peak number for each gene, RP scores, and adjusted RP values for each gene.

Gene	Coordinate	Peak number	RP score	Adjusted RP score
LNPEP	chr5:96935641-97029411	3	2.217	1
RUSC1-AS1	chr1:155316853-155323845	4	2.032	0.917
PKNOX1	chr21:42974509-43033582	3	2.02	0.911
AP4S1	chr14:31026642-31096450	3	2.001	0.903
USP22	chr17:20999592-21043039	3	1.978	0.892
RUSC1	chr1:155323936-155331118	4	1.972	0.889
UBQLN4	chr1:156035293-156053825	4	1.915	0.864
STRN3	chr14:30893798-31026401	3	1.894	0.854
LAMTOR2	chr1:156054725-156058510	4	1.886	0.851
SCAF11	chr12:45919130-45990618	3	1.738	0.784
SAP30BP	chr17:75667115-75708062	2	1.702	0.757
NUB1	chr7:151341811-151378461	2	1.678	0.757
RECQL5	chr17:75649713-75667189	2	1.697	0.755

ZNF790-AS1	chr19:36797562-36828111	2	1.662	0.749
MIEF1	chr22:39502229-39518134	2	1.661	0.749
MAP2K3	chr17:21288035-21315239	7	2.559	0.743

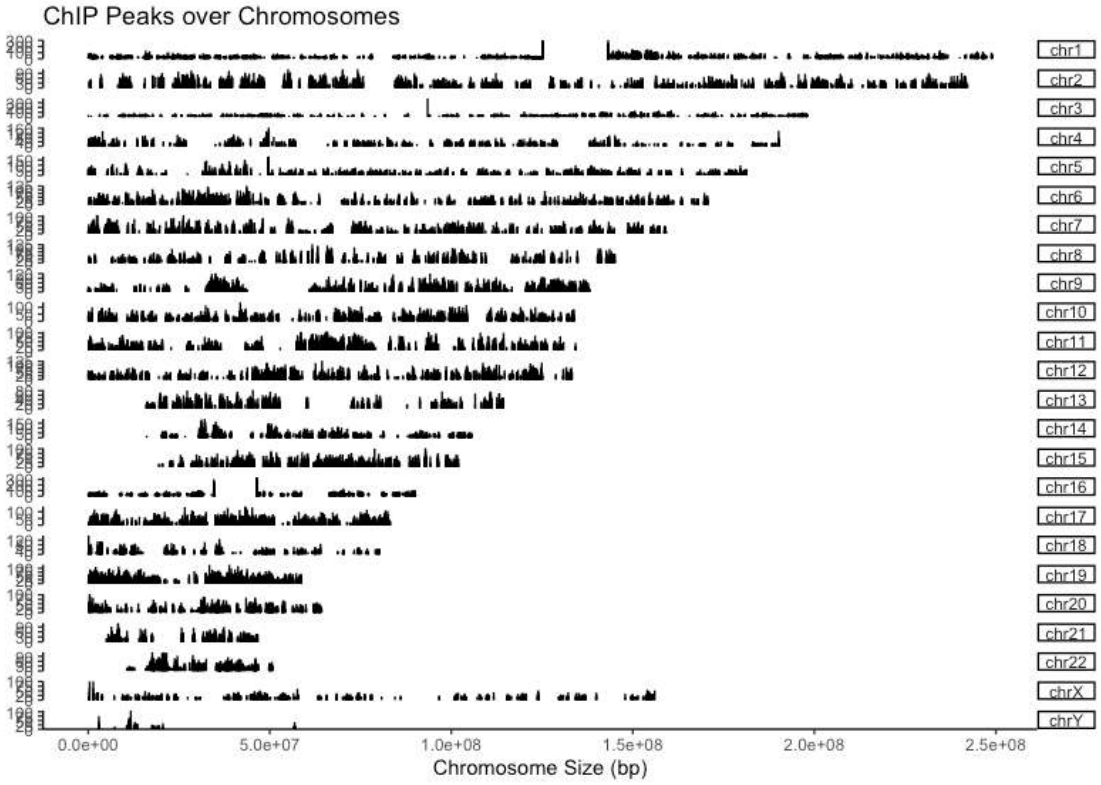

Figure 3.40: Genome wide distribution of H3K27ac ChIP-seq peaks in Du145-DtxR cells.

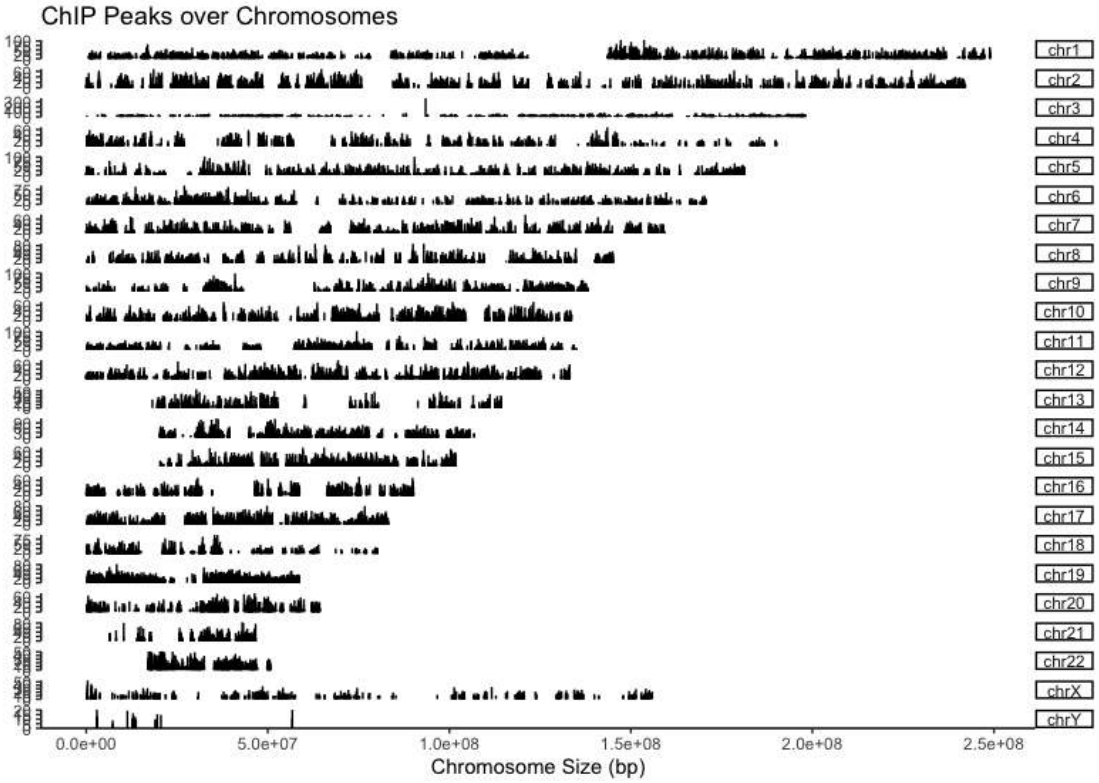

Figure 3.41: Genome wide distribution of H3K27ac ChIP-seq peaks in Du145-P cells. Data obtained from CistromeDB (Kalender Atak et al., 2017) (CistromeDB: 87561, ENCODE ID: GSM2702220).

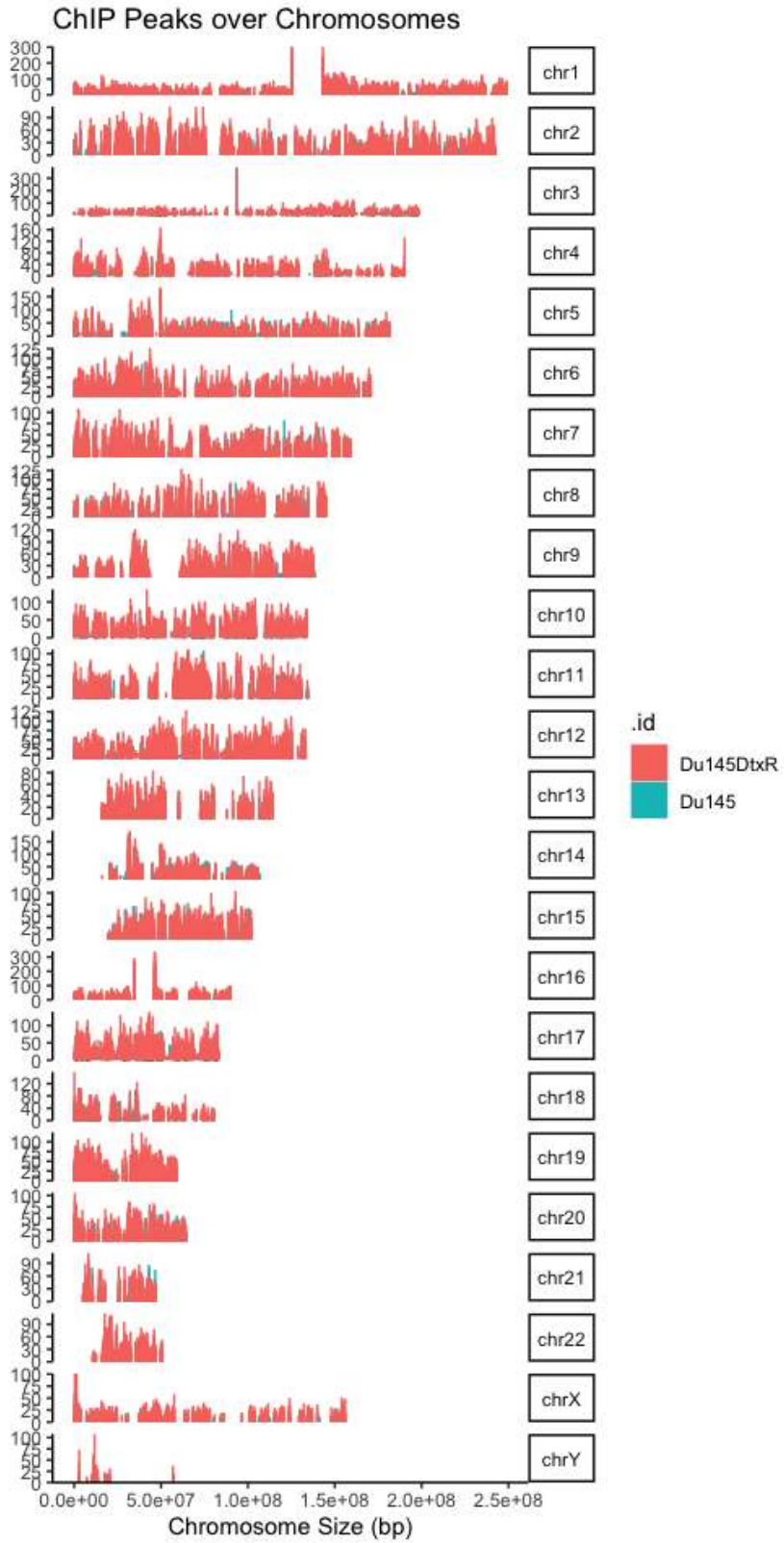

Figure 3.42: Genome wide distribution of H3K27ac ChIP-seq peaks in both Du145-DtxR and Du145-P cells. Data obtained from CistromeDB (Kalender Atak et al., 2017) (CistromeDB: 87561, ENCODE ID: GSM2702220).

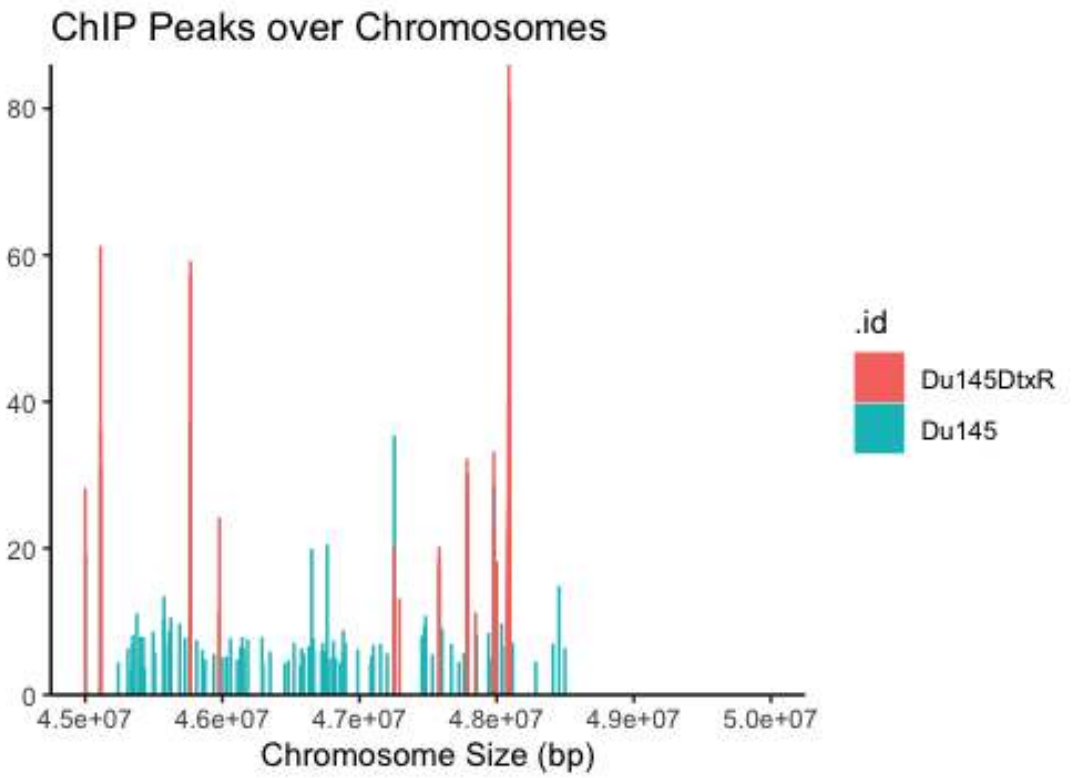

Figure 3.43: Locus wide distribution of H3K27ac ChIP-seq peaks in both Du145-DtxR and Du145-P cells in human genome (hg38) chromosome 7 (chr7) where *ABCB1* is located.
H3K27ac in Du145-DtxR ChIP peaks are in black. H3K27ac in Du145-P ChIP peaks are in red (Kalender Atak et al., 2017) (CistromeDB: 87561, ENCODE ID: GSM2702220).

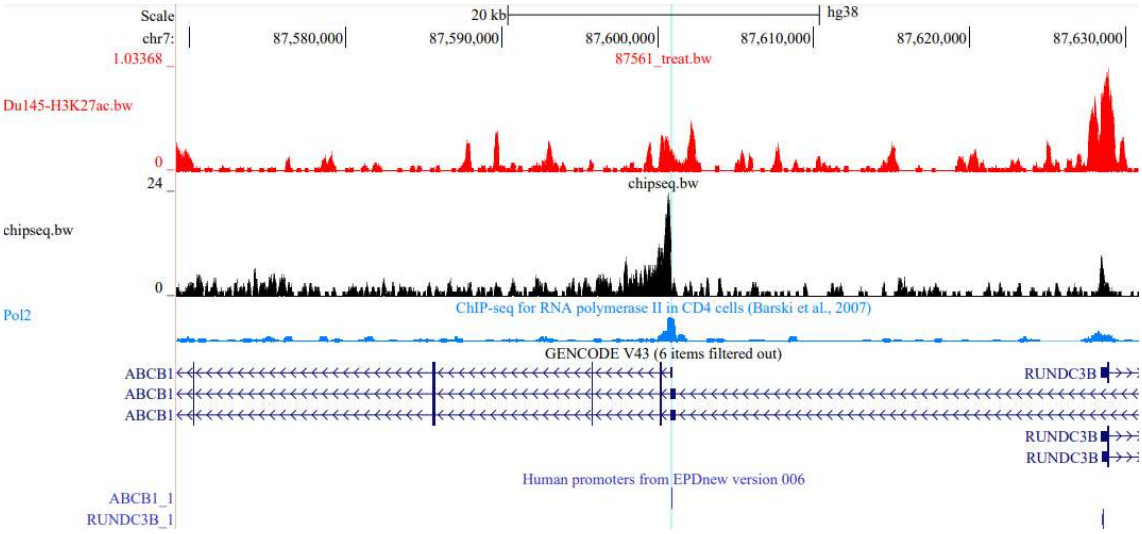

Figure 3.44: UCSC genome browser snapshot of ChIP-Seq normalized signal profiles for H3K27ac in Du145-DtxR cell line on human genome (hg38) chromosome 7 (chr7).

H3K27ac in Du145-DtxR ChIP peaks are in black. H3K27ac in Du145-P ChIP peaks are in red. *ABCB1* promoter is highlighted in blue. Data obtained from (Kalender Atak et al., 2017) (CistromeDB: 87561, ENCODE ID: GSM2702220).

In Table 3.6, the genes that were occupied by H3K27ac in Du145-Dtx cells are given. ChIP enrichment scores are used in conjunction with the RP score to predict the significance of differential gene expression. By utilizing the RP score, we can generate the receiver operating characteristic (ROC) curve and precision-recall (RP) curve, enabling us to calculate the area under the curve (AUC). These informative metrics assist users in determining the regulatory direction (activating, repressive, or both) of the transcription factor. These scores measure the binding affinity between H3K27ac and specific DNA regions, providing additional insights into the regulation of gene expression.

A comparative analysis was conducted between the genes listed in Table 3.6 and the H3K27ac ChIP data obtained from Du145 cells. Interestingly, the examination revealed that only two genes, namely *EGR1* and *RUNX1*, exhibited acetylation in Du145-P cells and they were given in the Table 3.7. In contrast, a significant peak near the *ABCB1* gene in Du145-P cells was not identified, unlike the presence of H3K27ac occupation near the *ABCB1* promoter region in Du145-DtxR cells. These findings suggest differential patterns of H3K27ac occupancy, highlighting the distinct regulatory landscape in the two cell populations under investigation.

Table 3.6: H3K27ac ChIP peaks in Du145-DtxR cells for the genes related to taxane resistance. The table includes peak number for each gene, RP scores, and adjusted RP values for each gene.

Gene	Coordinate	Peak number	RP score	Adjusted RP score
ABCB1	chr7:87503862-87600888	1	0.726	0.211
RUNX1	chr21:34787800-34888690	4	1.699	0.494
RUNX2	chr6:45422576-45551082	1	0.506	0.147
RUNX3	chr1:24899510-24930279	1	0.891	0.259
MYC	chr8:127735433-127742951	3	1.958	0.569
EGR1	chr5:138465491-138469315	2	0.982	0.285
FOSL1	chr11:65892135-65900526	7	0.556	0.161

Table 3.7: H3K27ac ChIP peaks in Du145-P cells for the genes related to taxane resistance. Data obtained from (Kalender Atak et al., 2017) (CistromeDB: 87561, ENCODE ID: GSM2702220).

Gene	Coordinate	Peak number	RP score	Adjusted RP score
EGR1	chr5:138465491-138469315	1	0.645	0.291
RUNX1	chr21:34787800-35049298	2	0.731	0.33

Additionally, we performed MEME analysis of sequences in H3K27ac peaks. We identified enriched sequence motifs. The results obtained from the MEME analysis revealed several significant motifs enriched in the H3K27ac peaks in Du145-DtxR cells. These motifs provide valuable insights into the regulatory elements and potential transcription factor binding sites associated with H3K27me3 modifications in the specific cellular context. The analysis identified motifs in Figure 3.47 with a significant E-value (≤ 0.05), indicating their statistical significance and potential functional relevance.

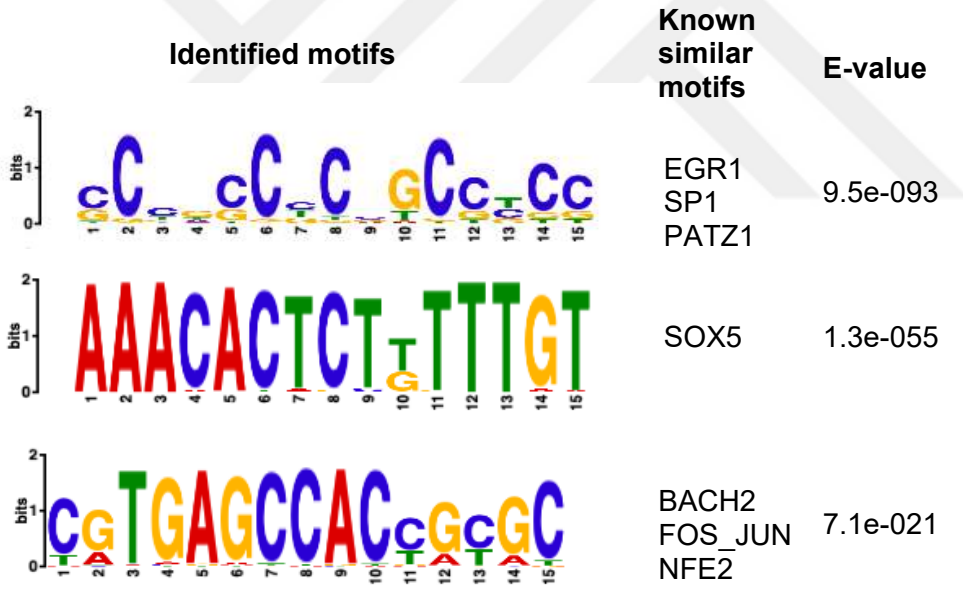

Figure 3.45: The significant motifs (E-value ≤ 0.05) found by the programs MEME, and STREME; and ordered by E-value.
Motifs enriched in the H3K27me3 peaks in Du145-DtxR cells determined by MEME analysis (Bailey, 2021).

Chapter 4: **DISCUSSION**

4.1 Summary of Key Findings

In this study, we aimed to investigate the molecular pathways involved in the reversion of taxane resistance through BRPF proteins in CRPCa cells. Our findings revealed several important insights. BRPF inhibition with small molecules resensitized taxane-resistant CRPCa cells to Dtx suggesting that targeting BRPF proteins could overcome taxane resistance. Efficient silencing of both BRPF1 and BRPF2 mildly reversed taxane resistance, while knockout of BRPF2 effectively reversed resistance (Figure 3.7). However, attempts to generate BRPF1 knockout in resistant cells were unsuccessful, indicating its essential role in cell viability. RNA sequencing analysis identified the genes differentially regulated in both Dtx resistant cells and in BRPF inhibited cells (Figure 3.22). Inhibition of BRPFs might result in the expression profile of these genes resembling the parental-like cells. RNA seq analysis following BRPF inhibition revealed pathways such as TNFA signaling via NFKB that might revert back to the sensitive transcriptomic profile (Figure 3.21). Data showed that silencing these pathways was able to mimic BRPF inhibition and revert resistance at least partially (Figure 3.23, 3.24 and 3.25), potentially explaining how BRPFs may be reverting taxane resistance.

Silencing BRPFs using siRNAs and knocking out of BRPFs led to the downregulation of *ABCB1*, which encodes a permeability glycoprotein (Pgp) involved in drug efflux (Figure 3.18). This suppression of *ABCB1* function may explain how cells can be resensitized to taxane treatment. The proposed mechanism for the reversion of taxane resistance involves the downregulation of *ABCB1* expression via BRPF inhibition in resistant cells as depicted in the Figure 4.1.

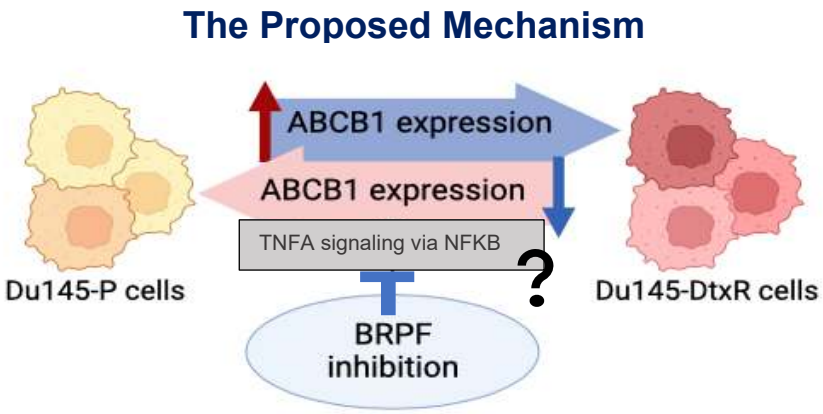

Figure 4.1: Schematic explanation for the taxane resistance mechanism via BRPFs. Figure created with biorender.com.

Chromatin immunoprecipitation followed by quantitative PCR (ChIP-qPCR) analysis demonstrated the direct binding of BRPF1 to the *ABCB1* promoter, indicating the direct regulation of the *ABCB1* gene by BRPF1 in Du145-DtxR cells. (Figure 3.36) To further validate the role of BRPF1 in chemotherapy resistance, ChIP-qPCR experiments were also conducted in Paclitaxel-resistant TNBC cells (Figure 3.37). The results demonstrated the occupancy of the *ABCB1* promoter by both endogenous and exogenous BRPF1, confirming its role in regulating *ABCB1* expression in Paclitaxel-resistant TNBC cells. This finding is significant as *ABCB1* is involved in multidrug resistance (MDR) and contributes to the poor response to chemotherapy in TNBC and CRPCa.

Additionally, we displayed that *ABCB1* promoter region was occupied by H3K27ac in taxane resistant CRPCa cells, but not in parental cells (Figure 3.44). As shown in the model in Figure 4.1, we have reached the conclusion that the transcriptional activation of *ABCB1* is attributed to BRPF1. This might be accomplished through the facilitation of acetylation at specific lysine residues of H3K27 as shown in the Figure 4.2. This process is more likely to be mediated by a BRPF complexes, which consists of MOZ/MORF, ING5 and EAF6. However, further investigation and clarification are necessary to gain a deeper understanding of the individual members of BRPF complexes and their interactions. Further studies are warranted to elucidate the potential clinical applications of these findings.

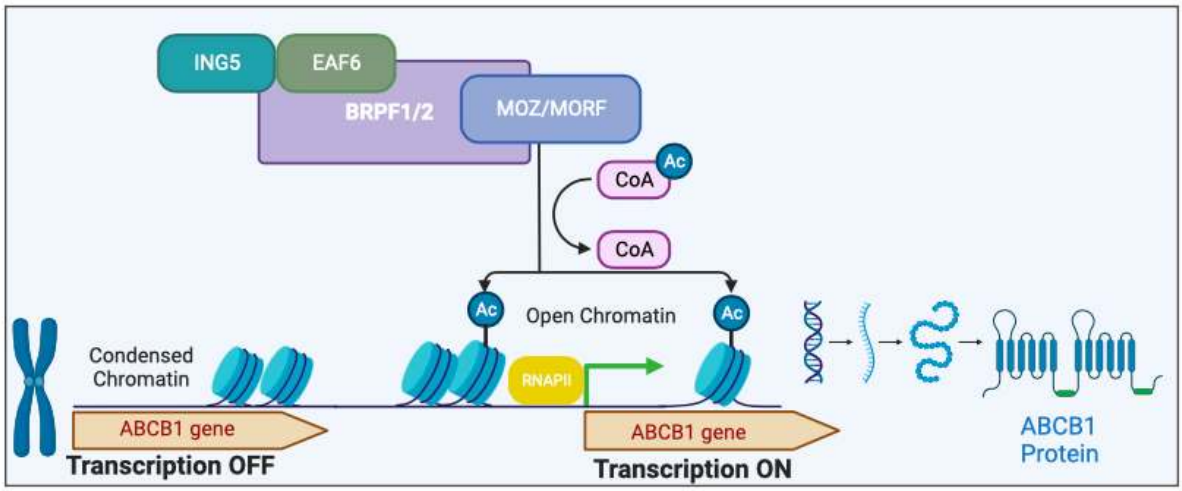

Figure 4.2: The model for *ABCB1* gene expression through H3K27ac mediated by BRPF complexes. Figure created with biorender.com.

4.2 Comparison of Results to Previous Studies

Our findings align with previous studies that have shown the potential of epigenetic regulation in reversing taxane resistance. The inhibition of BRPF proteins demonstrated efficacy in resensitizing taxane-resistant CRPCa cells, consistent with previous research using an epigenetic drug library and epi-targeted CRISPR screens.

According to a research, the development of resistance to Dtx appears to coincide with increased levels of TNFA (Sprowl et al., 2012). This resistance is associated with reduced sensitivity to the cytotoxic effects of TNFA, degradation of TNFR1 (TNF receptor 1), and activation of survival pathways mediated by TNFR2 (TNF receptor 2) through the activation of NFKB (Sprowl et al., 2012). In a study, it was discovered that both TNFA and taxol have the ability to degrade IκBα, resulting in the activation of NFKB. The activation of NFKB by TNFA and taxol can be prevented by using distinct inhibitors that target the NFKB pathway (Sprowl et al., 2012). Additionally, the stability of microtubules plays a role in the activation of NFKB by TNFA and taxol, as the reduction of microtubule stability diminishes their capacity to activate NFKB (Jackman et al., 2009).

NFKB is a transcription factor that regulates numerous genes involved in cell survival, inflammation, and immune responses (Oeckinghaus & Ghosh, 2009). NFKB transcription factor promotes drug resistance by increasing MDR1 expression (Bentires-Alj et al., 2003). At lower concentrations of taxanes (3 to 5 nM), the activation of NFKB-dependent cell-survival pathways by TNFA seems to play a significant role in the development of resistance to taxanes. However, at higher concentrations (≥ 15 nM) of Dtx, the drug causes an increase in *ABCB1* expression, which leads to a decrease in the amount of Dtx accumulated in cells. As a result, the production of TNFA stimulated by Dtx is reduced (Sprowl et al., 2012). The positive enrichment of this gene set suggests that the reversion of taxane resistance via BRPF inhibition might involve the activation of TNFA signaling via NFKB.

Computed overlaps analysis using the Hallmark Collection of GSEA (MSigDB) database revealed EMT as a positively enriched gene set among the intersecting 145 genes in the Figure 3.21A. EMT is a biological process that promotes cellular plasticity and is associated with increased invasiveness and metastasis in cancer. Numerous phenotypic changes, including cell morphological changes, loss of adhesion, and acquisition of stem cell-like characteristics, are caused by the changes in gene expression during EMT (Lamouille et al., 2014). EMT is known to be mediated by a number of important signaling pathways, including transforming growth factor beta (TGF-β), Wnt, Notch, and Hedgehog (Gonzalez & Medici, 2014). Drug resistance is promoted by the overexpression of EMT-TFs like Twist, Snail, and FOXC2, which induced EMT, increased the promoter activity and expression of ABC transporters (Saxena et al., 2011). Our findings in wound healing assay and adhesion assays indicate that there might be transcriptomic changes related to EMT and apical junction from taxane sensitive to resistant. We identified DEGs such as SERPINE1 that might contribute to EMT phenotype and loss of adhesion in taxane resistant cells.

The complement system, which was positively enriched in Computed overlaps analysis using the Hallmark Collection of GSEA (MSigDB) among the intersecting 145 genes in the Figure 3.22A is a crucial component of innate immunity, has been recognized as a protective mechanism against cancer cells over the years. Manipulating complement

effector functions in the cancer setting provides an opportunity to enhance monoclonal antibody-based immunotherapies. However, recent research has revealed the dual role of the complement system as inducer of tumor growth in chronic, persistent inflammation known as inflammaging (Netti et al., 2021). The identification of this pathway suggests its significance in the context of taxane resistance reversion. The identification of inflammation gene set suggests the presence of a dynamic interplay between immune cells, cytokines, and tumor microenvironment components that contribute to the reversal of drug resistance. IL2 is a cytokine known to regulate immune responses and cellular proliferation. Activation of the STAT5 pathway downstream of IL2 signaling can impact gene expression and cell survival (Abbas, 2020). The positive enrichment of this pathway highlights its potential contribution to overcoming taxane resistance.

Overall, the identified pathways, such as TNFA signaling via NFKB and IL2 STAT5 signaling, have connections to taxane resistance and microtubules through their involvement in cellular processes that influence cell survival, proliferation, and gene expression. Inhibition of BRPF may affect these pathways, leading to the restoration of sensitive transcriptomic profiles and potentially overcoming taxane resistance.

AML and many other cancers have been linked to the SWI/SNF chromatin remodeling complex in recent research (Hohmann et al., 2016). In particular, it has been discovered that this complex's ATPase subunit BRG1 is essential for promoting the expression of Myc, a key gene in AML. Several subunits of SWI/SNF complex, including BRG1, BRM, PBRM1, BRD7, and BRD9, contain chromatin reader domains that may be targeted. According to a recent study, BRD9 functions as a subunit of the SWI/SNF complexes in AML cells, where it exploits its bromodomain to encourage MYC expression and cell growth (Hohmann et al., 2016). Chromosomal translocations involving the MOZ gene are associated with poor prognosis in AML (Katsumoto et al., 2022). Overexpression of HOXA9, HOXA10, and MEIS1 is observed in AML patients with MOZ fusions. Researchers discovered that MOZ-TIF2 forms a stable complex with BRPF1, leading to increased HOX gene expression through MOZ-dependent histone acetylation (Shima et al., 2014). Depletion of BRPF1 or loss of MOZ's histone acetyltransferase activity prevents HOX gene dysregulation and leukemia development caused by MOZ-TIF2 (Shima et al., 2014). Activation of the BRPF1/HOX pathway via MOZ's activity is critical for MOZ-TIF2-induced AML (Shima et al., 2014). In our study, we investigated the role of BRPFs also in other types of cancer and found that inhibiting BRPFs led to increased vulnerability of K562 cells (Figure 3.30). This observation suggests that BRPFs play a crucial role in AML cell survival and proliferation, making them attractive targets for therapeutic intervention, and supports the relative literature on BRPFs role in AML. The observed sensitivity of AML cells to epigenetic drugs can potentially be attributed to their influence on the differentiation state of these cells. It has been well-documented that AML cells heavily rely on specific epigenetic modifiers to maintain their aberrant differentiation processes. By targeting these modifiers using epigenetic drugs, the

differentiation programs of AML cells can be disrupted, rendering them more vulnerable to therapeutic interventions (Gambacorta et al., 2019).

4.3 Implications of Results for Cancer Research and Treatment

The development, progression, and treatment resistance of tumors are all impacted by epigenetic regulation of cancer. Epigenetic changes are newly recognized as crucial to PCa growth, progression, and drug resistance. Moreover, epigenetic regulators are chromatin-binding proteins or enzymes that make them ideal therapeutic targets for small inhibitory compounds.

Obtained data indicated that pharmacological inhibition of BRPF reverts taxane resistance in CRPCa based on the results in Figure 3.7. Combination of taxanes and BRPF inhibition potentiate taxane resistant CRPCa cells. Epigenetic inhibitors, such as BRD inhibitors are already used in clinical studies (Ferri, Petosa, & McKenna, 2016); our findings with the underlying mechanism of actions may further provide future applications for taxane-resistant CRPCa therapy.

The results of this study have important implications for cancer research and treatment, particularly in the context of taxane-resistant CRPCa. The identification of BRPF proteins as molecular players involved in drug resistance provides insights into potential therapeutic targets. BRPF inhibition presents itself as a promising anticancer strategy to overcome taxane resistance and potentially improve treatment outcomes for patients with CRPCa.

Furthermore, our findings suggest that the mechanism underlying BRPF-mediated drug resistance involves the inhibition of drug efflux, specifically through the downregulation of *ABCB1*. This finding holds significant potential as it may provide an alternative approach to bypass the side effects associated with ABCB1 inhibitors. This knowledge opens up avenues for the development of effective therapies against taxane-resistant CRPCa, potentially utilizing BRPF inhibition in combination with taxane treatment.

4.4 Limitations of Study and Areas for Future Research

It is important to acknowledge the limitations of this study. First, the unsuccessful generation of BRPF1 knockout in resistant cells highlights the challenges in fully elucidating its role in taxane resistance. Further investigation is warranted to understand the specific functions and mechanisms of BRPF1 in drug resistance.

We encountered difficulties in performing ChIP sequencing with BRPF1. We tried CUT and RUN method as an alternative. In both experiments, we failed to yield DNA with high quality and quantity. Despite our efforts, we were unable to obtain reliable data regarding BRPF1's promoter occupancy with ChIP-sequencing. This limitation prevented us from fully assessing the role of BRPF1 in genomic occupancy and its potential

implications in chemotherapy resistance in CRPCa. Future studies should explore alternative techniques or optimize the ChIP sequencing protocol specifically for BRPF1 to overcome this limitation.

Secondly, we faced challenges in finding an antibody that specifically and efficiently recognizes BRPF2 for ChIP experiments. This limitation restricted our ability to investigate the promoter occupancy of BRPF2 and its potential association with H3K27ac in taxane resistance. Developing or identifying reliable antibodies targeting BRPF2 would be crucial for further investigations in this area.

Despite these limitations, our study provides valuable insights into the role of BRPFs in *ABCB1* promoter occupancy and its potential implications in chemotherapy resistance in CRPCa and TNBC. Future research should address these limitations and overcome the technical challenges to gain a more complete understanding of the role of BRPF1 and BRPF2, as well as their interactions with H3K27ac, in drug resistance mechanisms in CRPCa and TNBC.

Additionally, while the identified pathways and genes influenced by BRPF inhibition provide valuable insights, further studies are needed to comprehensively dissect their contributions to taxane resistance and their potential as therapeutic targets.

The vulnerability of K562 cells to BRPF inhibition opens up exciting prospects for future research and therapeutic development. Further investigations are warranted to elucidate the specific mechanisms by which BRPFs contribute to AML pathogenesis. Understanding the molecular interactions and downstream effects of BRPF inhibition in AML cells will provide valuable insights into the underlying mechanisms and potential therapeutic strategies.

Future research directions should focus on exploring the clinical applications of BRPF inhibition in taxane-resistant CRPCa. Preclinical and clinical studies are necessary to validate the efficacy of BRPF inhibitors and further investigate their safety profiles. Additionally, understanding the broader implications of BRPF-mediated drug resistance in other cancer types and identifying potential combination therapies could provide further advancements in cancer treatment strategies.

Chapter 5:
CONCLUSION

5.1 Summary of Study Findings and Implications

In this thesis, epigenetic modifications are spoken about in relation to taxane resistance and how they are increasingly being acknowledged as potential mediators of overcoming taxane resistance in PCa. When taxane-based medicines are employed to treat cancer, the emergence of drug resistance poses a significant challenge. The development of resistance mechanisms impairs the efficacy of taxane treatment, necessitating the research of alternative strategies to overcome this resistance.

In this study, our main goal was to learn more about the molecular processes behind the inhibition of BRPFs (bromodomain-containing reader proteins) in the reversal of taxane resistance. Several biological processes which are crucial for controlling epigenetic regulation, have been associated with transcriptional activation. In an effort to comprehend the effects of BRPF inhibition on taxane-resistant cancer cells, we targeted the expression of BRPF1 and BRPF2 using small pharmacologic inhibitors, siRNA, and CRISPR/Cas9 technologies. We used the Sulforhodamine B (SRB) assay to gauge cell viability. Second, we examined the cells' ability to form colonies using a colonogenic assay, which sheds light on their potential for clonogenicity and long-term survival. We used RNA-sequencing to get a thorough understanding of the molecular alterations brought about by BRPF inhibition. Using this method, we were able to compare taxane-resistant cells with and without BRPF inhibition in terms of their transcriptome differences, exposing changed gene expression patterns and possible BRPF downstream targets. We also used chromatin immunoprecipitation coupled with quantitative PCR (ChIP-qPCR) to find the direct target genes of BRPFs. Using this method, we were able to examine the genomic areas to which BRPF proteins bind and the effects of their inhibition on the expression of target genes. The results of this work demonstrate the important function of BRPF proteins in establishing taxane resistance and show that inhibiting these proteins can successfully overcome resistance and reestablish sensitivity to taxane treatment. BRPF inhibition is a novel and promising treatment approach in the fight against taxane resistance in CRPCa.

In summary, this study demonstrated that the inhibition of BRPF proteins effectively reverses taxane resistance in CRPCa cells. BRPF inhibition resensitizes taxane-resistant cells through the downregulation of *ABCB1* and suppression of drug efflux. The identification of key pathways and genes affected by BRPF inhibition provides important insights into the underlying mechanisms of taxane resistance and offers potential therapeutic targets for future interventions.

5.2 Recommendations for Future Research

Targeting epigenetic pathways appears an alternative strategy for overcoming drug resistance. Epigenetic alterations refer to changes in gene expression without altering the underlying DNA sequence. Epigenetic modifiers offer valuable therapeutic targets because they possess the ability to reverse or undo the epigenetic modifications that contribute to drug resistance. By intervening at the epigenetic level, we have the potential to restore the sensitivity of cancer cells to chemotherapy and improve patient responses. Furthermore, there is some tentative evidence that epigenetic alterations could be used as predictive biomarkers. To effectively treat drug-resistant cancers, it is crucial to target epigenetic regulators. By modulating the activity of these regulators, we can potentially overcome drug resistance and enhance treatment outcomes. One promising strategy is combining traditional chemotherapy with epigenetic modifiers. This approach aims to leverage the synergistic effects of chemotherapy drugs and epigenetic modulation to treat resistant tumors. In summary, the combination of chemotherapy with epigenetic inhibitors holds promise for treating drug-resistant tumors.

Based on the findings of this study, several recommendations for future research can be made. Further investigation into the specific functions of BRPF1 and its role in taxane resistance is needed to fully understand its contribution. Additionally, comprehensive studies are warranted to decipher the precise mechanisms by which BRPF inhibition influences the identified pathways and genes.

Overall, the findings from this study provide a foundation for future research of BRPFs in AML and in paclitaxel resistant TNBC. This research can focus on unraveling the functional significance of BRPF1, BRPF2 and H3K27ac, and their interplay in tumorigenesis and chemotherapy resistance. This future research can identify potential therapeutic targets to improve treatment outcomes for TNBC and AML patients.

Moreover, future research should focus on validating the efficacy and safety of BRPF inhibitors in preclinical and clinical settings. Exploring the clinical applications of BRPF inhibition, both as monotherapy and in combination with taxanes or other treatment modalities, holds promise for improving outcomes in taxane-resistant CRPCa patients.

5.3 Conclusion and Final Thoughts

In conclusion, this study highlights the potential of targeting BRPF proteins as a therapeutic approach to overcome taxane resistance in CRPCa. The findings contribute to our understanding of the molecular pathways involved in taxane resistance and provide a foundation for the development of effective therapies targeting BRPF-mediated drug resistance. The knowledge gained from this study may have broader implications for cancer research and treatment beyond CRPCa. Further exploration of BRPF inhibition and its impact on other cancer types and drug resistance mechanisms could pave the way for the development of novel therapeutic strategies in the fight against cancer.

BIBLIOGRAPHY

Abbas, A. K. (2020). The Surprising Story of IL-2: From Experimental Models to Clinical Application. *American Journal of Pathology*, *190*(9), 1776–1781. https://doi.org/10.1016/j.ajpath.2020.05.007

Alberts, B., Johnson, A., Lewis, J., Raff, M., Roberts, K., & Walter, P. (2002). Chromosomal DNA and Its Packaging in the Chromatin Fiber. Retrieved from https://www.ncbi.nlm.nih.gov/books/NBK26834/

Avril, T., Vauléon, E., & Chevet, E. (2017). Endoplasmic reticulum stress signaling and chemotherapy resistance in solid cancers. *Oncogenesis*, *6*(8), e373. https://doi.org/10.1038/oncsis.2017.72

Bailey, T. L. (2021). STREME: accurate and versatile sequence motif discovery. *Bioinformatics (Oxford, England)*, *37*(18), 2834–2840. https://doi.org/10.1093/bioinformatics/btab203

Bamborough, P., Barnett, H. A., Becher, I., Bird, M. J., Chung, C.-W., Craggs, P. D., … Watson, R. J. (2016). GSK6853, a Chemical Probe for Inhibition of the BRPF1 Bromodomain. *ACS Medicinal Chemistry Letters*, *7*(6), 552–557. https://doi.org/10.1021/acsmedchemlett.6b00092

Bentires-Alj, M., Barbu, V., Fillet, M., Chariot, A., Relic, B., Jacobs, N., … Bours, V. (2003). NF-κB transcription factor induces drug resistance through MDR1 expression in cancer cells. *Oncogene 2003 22:1*, *22*(1), 90–97. https://doi.org/10.1038/sj.onc.1206056

Berezovska, O. P., Glinskii, A. B., Yang, Z., Li, X.-M., Hoffman, R. M., & Glinsky, G. V. (2006). Essential role for activation of the Polycomb group (PcG) protein chromatin silencing pathway in metastatic prostate cancer. *Cell Cycle (Georgetown, Tex.)*, *5*(16), 1886–1901. https://doi.org/10.4161/cc.5.16.3222

Biersack, B., Nitzsche, B., & Höpfner, M. (2022). HDAC inhibitors with potential to overcome drug resistance in castration-resistant prostate cancer. *Cancer Drug Resistance (Alhambra, Calif.)*, *5*(1), 64–79. https://doi.org/10.20517/cdr.2021.105

Biswas, S., & Rao, C. M. (2018). Epigenetic tools (The Writers, The Readers and The Erasers) and their implications in cancer therapy. *European Journal of Pharmacology*, *837*, 8–24. https://doi.org/10.1016/j.ejphar.2018.08.021

Blagosklonny, M. V. (2003). Targeting cancer cells by exploiting their resistance. *Trends in Molecular Medicine*, *9*(7), 307–312. https://doi.org/10.1016/s1471-

4914(03)00111-4

Borrow, J., Stanton, V. P., Andresen, J. M., Becher, R., Behm, F. G., Chaganti, R. S., … Housman, D. E. (1996). The translocation t(8;16)(p11;p13) of acute myeloid leukaemia fuses a putative acetyltransferase to the CREB-binding protein. *Nature Genetics*, *14*(1), 33–41. https://doi.org/10.1038/ng0996-33

Cao, R., Wang, L., Wang, H., Xia, L., Erdjument-Bromage, H., Tempst, P., … Zhang, Y. (2002). Role of histone H3 lysine 27 methylation in Polycomb-group silencing. *Science (New York, N.Y.)*, *298*(5595), 1039–1043. https://doi.org/10.1126/science.1076997

Carlson, S., & Glass, K. C. (2014). The MOZ histone acetyltransferase in epigenetic signaling and disease. *Journal of Cellular Physiology*, *229*(11), 1571–1574. https://doi.org/10.1002/jcp.24617

Carroll, T. S., Liang, Z., Salama, R., Stark, R., & de Santiago, I. (2014). Impact of artifact removal on ChIP quality metrics in ChIP-seq and ChIP-exo data. *Frontiers in Genetics*, *5*, 75. https://doi.org/10.3389/fgene.2014.00075

Cheng, C. L.-H., Tsang, F. H.-C., Wei, L., Chen, M., Chin, D. W.-C., Shen, J., … Wong, C.-M. (2021). Bromodomain-containing protein BRPF1 is a therapeutic target for liver cancer. *Communications Biology*, *4*(1), 888. https://doi.org/10.1038/s42003-021-02405-6

Choi, E., Buie, J., Camacho, J., Sharma, P., & de Riese, W. T. W. (2022). Evolution of Androgen Deprivation Therapy (ADT) and Its New Emerging Modalities in Prostate Cancer: An Update for Practicing Urologists, Clinicians and Medical Providers. *Research and Reports in Urology*, *14*, 87–108. https://doi.org/10.2147/RRU.S303215

Clermont, P.-L., Crea, F., Chiang, Y. T., Lin, D., Zhang, A., Wang, J. Z. L., … Helgason, C. D. (2016). Identification of the epigenetic reader CBX2 as a potential drug target in advanced prostate cancer. *Clinical Epigenetics*, *8*(1), 16. https://doi.org/10.1186/s13148-016-0182-9

Crea, F., Duhagon Serrat, M. A., Hurt, E. M., Thomas, S. B., Danesi, R., & Farrar, W. L. (2011). BMI1 silencing enhances docetaxel activity and impairs antioxidant response in prostate cancer. *International Journal of Cancer*, *128*(8), 1946–1954. https://doi.org/10.1002/ijc.25522

Creyghton, M. P., Cheng, A. W., Welstead, G. G., Kooistra, T., Carey, B. W., Steine, E.

J., … Jaenisch, R. (2010). Histone H3K27ac separates active from poised enhancers and predicts developmental state. *Proceedings of the National Academy of Sciences*, *107*(50), 21931–21936. https://doi.org/10.1073/pnas.1016071107

Dabkeviciene, D., Jonusiene, V., Zitkute, V., Zalyte, E., Grigaitis, P., Kirveliene, V., & Sasnauskiene, A. (2015). The role of interleukin-8 (CXCL8) and CXCR2 in acquired chemoresistance of human colorectal carcinoma cells HCT116. *Medical Oncology (Northwood, London, England)*, *32*(12), 258. https://doi.org/10.1007/s12032-015-0703-y

de Morrée, E. S., Böttcher, R., van Soest, R. J., Aghai, A., de Ridder, C. M., Gibson, A. A., … van Weerden, W. M. (2016). Loss of SLCO1B3 drives taxane resistance in prostate cancer. *British Journal of Cancer*, *115*(6), 674–681. https://doi.org/10.1038/bjc.2016.251

Domingo-Domenech, J., Vidal, S. J., Rodriguez-Bravo, V., Castillo-Martin, M., Quinn, S. A., Rodriguez-Barrueco, R., … Cordon-Cardo, C. (2012). Suppression of acquired docetaxel resistance in prostate cancer through depletion of notch- and hedgehog-dependent tumor-initiating cells. *Cancer Cell*, *22*(3), 373–388. https://doi.org/10.1016/j.ccr.2012.07.016

Dulak, A. M., Stojanov, P., Peng, S., Lawrence, M. S., Fox, C., Stewart, C., … Bass, A. J. (2013). Exome and whole-genome sequencing of esophageal adenocarcinoma identifies recurrent driver events and mutational complexity. *Nature Genetics*, *45*(5), 478–486. https://doi.org/10.1038/ng.2591

Feng, S., & De Carvalho, D. D. (2022). Clinical advances in targeting epigenetics for cancer therapy. *The FEBS Journal*, *289*(5), 1214–1239. https://doi.org/10.1111/febs.15750

Ferri, E., Petosa, C., & McKenna, C. E. (2016). Bromodomains: Structure, function and pharmacology of inhibition. *Biochemical Pharmacology*, *106*, 1–18. https://doi.org/10.1016/J.BCP.2015.12.005

Gambacorta, V., Gnani, D., Vago, L., & Di Micco, R. (2019). Epigenetic Therapies for Acute Myeloid Leukemia and Their Immune-Related Effects. *Frontiers in Cell and Developmental Biology*, *7*, 207. https://doi.org/10.3389/fcell.2019.00207

Gao, Y., Li, J.-Y., Mao, J.-Y., Zhou, J.-F., Jiang, L., & Li, X.-P. (2022). Comprehensive Analysis of CRIP1 Expression in Acute Myeloid Leukemia. *Frontiers in Genetics*, *13*, 923568. https://doi.org/10.3389/fgene.2022.923568

Gao, Z., Zhang, J., Bonasio, R., Strino, F., Sawai, A., Parisi, F., … Reinberg, D. (2012). PCGF homologs, CBX proteins, and RYBP define functionally distinct PRC1 family complexes. *Molecular Cell*, *45*(3), 344–356. https://doi.org/10.1016/j.molcel.2012.01.002

Ge, J., Yu, W., Li, J., Ma, H., Wang, P., Zhou, Y., … Shi, G. (2021). USP16 regulates castration-resistant prostate cancer cell proliferation by deubiquitinating and stablizing c-Myc. *Journal of Experimental & Clinical Cancer Research : CR*, *40*(1), 59. https://doi.org/10.1186/s13046-021-01843-8

Genovese, I., Ilari, A., Assaraf, Y. G., Fazi, F., & Colotti, G. (2017). Not only P-glycoprotein: Amplification of the ABCB1-containing chromosome region 7q21 confers multidrug resistance upon cancer cells by coordinated overexpression of an assortment of resistance-related proteins. *Drug Resistance Updates*, *32*, 23–46. https://doi.org/10.1016/J.DRUP.2017.10.003

Gonzalez, D. M., & Medici, D. (2014). Signaling mechanisms of the epithelial-mesenchymal transition. *Science Signaling*, *7*(344), re8. https://doi.org/10.1126/SCISIGNAL.2005189

Grasso, C. S., Wu, Y.-M., Robinson, D. R., Cao, X., Dhanasekaran, S. M., Khan, A. P., … Tomlins, S. A. (2012). The mutational landscape of lethal castration-resistant prostate cancer. *Nature*, *487*(7406), 239–243. https://doi.org/10.1038/nature11125

Hobor, S., Van Emburgh, B. O., Crowley, E., Misale, S., Di Nicolantonio, F., & Bardelli, A. (2014). TGFα and amphiregulin paracrine network promotes resistance to EGFR blockade in colorectal cancer cells. *Clinical Cancer Research : An Official Journal of the American Association for Cancer Research*, *20*(24), 6429–6438. https://doi.org/10.1158/1078-0432.CCR-14-0774

Hohmann, A. F., Martin, L. J., Minder, J. L., Roe, J.-S., Shi, J., Steurer, S., … Vakoc, C. R. (2016). Sensitivity and engineered resistance of myeloid leukemia cells to BRD9 inhibition. *Nature Chemical Biology*, *12*(9), 672–679. https://doi.org/10.1038/nchembio.2115

Hour, T.-C., Chung, S.-D., Kang, W.-Y., Lin, Y.-C., Chuang, S.-J., Huang, A.-M., … Pu, Y.-S. (2015). EGFR mediates docetaxel resistance in human castration-resistant prostate cancer through the Akt-dependent expression of ABCB1 (MDR1). *Archives of Toxicology*, *89*(4), 591–605. https://doi.org/10.1007/s00204-014-1275-x

Hui, D. H. F., Tam, K. J., Jiao, I. Z. F., & Ong, C. J. (2019). Semaphorin 3C as a Therapeutic Target in Prostate and Other Cancers. *International Journal of Molecular Sciences*, *20*(3). https://doi.org/10.3390/ijms20030774

Jackman, R. W., Rhoads, M. G., Cornwell, E., & Kandarian, S. C. (2009). Microtubule-mediated NF-kappaB activation in the TNF-alpha signaling pathway. *Experimental Cell Research*, *315*(19), 3242–3249. https://doi.org/10.1016/j.yexcr.2009.08.020

Jones, P. A., & Baylin, S. B. (2007). The epigenomics of cancer. *Cell*, *128*(4), 683–692. https://doi.org/10.1016/j.cell.2007.01.029

Kalender Atak, Z., Imrichova, H., Svetlichnyy, D., Hulselmans, G., Christiaens, V., Reumers, J., … Aerts, S. (2017). Identification of cis-regulatory mutations generating de novo edges in personalized cancer gene regulatory networks. *Genome Medicine*, *9*(1), 80. https://doi.org/10.1186/s13073-017-0464-7

Katsumoto, T., Aikawa, Y., Iwama, A., Ueda, S., Ichikawa, H., Ochiya, T., & Kitabayashi, I. (2006). MOZ is essential for maintenance of hematopoietic stem cells. *Genes & Development*, *20*(10), 1321–1330. https://doi.org/10.1101/gad.1393106

Katsumoto, T., Ogawara, Y., Yamagata, K., Aikawa, Y., Goitsuka, R., Nakamura, T., & Kitabayashi, I. (2022). MOZ is critical for the development of MOZ/MLL fusion-induced leukemia through regulation of Hoxa9/Meis1 expression. *Blood Advances*, *6*(19), 5527–5537. https://doi.org/10.1182/bloodadvances.2020003490

Ketchart, W., Ogba, N., Kresak, A., Albert, J. M., Pink, J. J., & Montano, M. M. (2011). HEXIM1 is a critical determinant of the response to tamoxifen. *Oncogene*, *30*(33), 3563–3569. https://doi.org/10.1038/onc.2011.76

Kim, H., & Ronai, Z. A. (2020). PRMT5 function and targeting in cancer. *Cell Stress*, *4*(8), 199–215. https://doi.org/10.15698/cst2020.08.228

Kitabayashi, I., Aikawa, Y., Nguyen, L. A., Yokoyama, A., & Ohki, M. (2001). Activation of AML1-mediated transcription by MOZ and inhibition by the MOZ-CBP fusion protein. *The EMBO Journal*, *20*(24), 7184–7196. https://doi.org/10.1093/emboj/20.24.7184

Klein, B. J., Cox, K. L., Jang, S. M., Côté, J., Poirier, M. G., & Kutateladze, T. G. (2020). Molecular Basis for the PZP Domain of BRPF1 Association with Chromatin. *Structure*, *28*(1), 105-110.e3. https://doi.org/10.1016/j.str.2019.10.014

Kosaka, T., Miyajima, A., Shirotake, S., Suzuki, E., Kikuchi, E., & Oya, M. (2011).

Long-term androgen ablation and docetaxel up-regulate phosphorylated Akt in castration resistant prostate cancer. *The Journal of Urology*, *185*(6), 2376–2381. https://doi.org/10.1016/j.juro.2011.02.016

KP, L. (2016). Mechanistic diversity in ATP-binding cassette (ABC) transporters. *Nature Structural & Molecular Biology*, *23*(6). https://doi.org/10.1038/NSMB.3216

Lamouille, S., Xu, J., & Derynck, R. (2014). Molecular mechanisms of epithelial-mesenchymal transition. *Nature Reviews. Molecular Cell Biology*, *15*(3), 178–196. https://doi.org/10.1038/NRM3758

Langmead, B., & Salzberg, S. L. (2012). Fast gapped-read alignment with Bowtie 2. *Nature Methods*, *9*(4), 357–359. https://doi.org/10.1038/nmeth.1923

Laue, K., Daujat, S., Crump, J. G., Plaster, N., Roehl, H. H., Kimmel, C. B., … Hammerschmidt, M. (2008). The multidomain protein Brpf1 binds histones and is required for Hox gene expression and segmental identity. *Development*, *135*(11), 1935–1946. https://doi.org/10.1242/dev.017160

Li, Z., Li, B., Yu, H., Wang, P., Wang, W., Hou, P., … Bai, J. (2022). DNMT1-mediated epigenetic silencing of TRAF6 promotes prostate cancer tumorigenesis and metastasis by enhancing EZH2 stability. *Oncogene*, *41*(33), 3991–4002. https://doi.org/10.1038/s41388-022-02404-9

Lin, G., Huang, T., Zhang, X., & Wang, G. (2022). Deubiquitinase USP35 stabilizes BRPF1 to activate mevalonate (MVA) metabolism during prostate tumorigenesis. *Cell Death Discovery*, *8*(1), 453. https://doi.org/10.1038/s41420-022-01231-x

Liu, B., Pan, S., Xiao, Y., Liu, Q., Xu, J., & Jia, L. (2018). LINC01296/miR-26a/GALNT3 axis contributes to colorectal cancer progression by regulating O-glycosylated MUC1 via PI3K/AKT pathway, *37*(1), 316. Retrieved from https://jeccr.biomedcentral.com/articles/10.1186/s13046-018-0994-x

Liu, C., Zhu, Y., Lou, W., Nadiminty, N., Chen, X., Zhou, Q., … Gao, A. C. (2013). Functional p53 determines docetaxel sensitivity in prostate cancer cells. *The Prostate*, *73*(4), 418–427. https://doi.org/10.1002/pros.22583

Liu, Y., Zheng, C., Huang, Y., He, M., Xu, W. W., & Li, B. (2021). Molecular mechanisms of chemo- and radiotherapy resistance and the potential implications for cancer treatment. *MedComm*, *2*(3), 315–340. https://doi.org/10.1002/mco2.55

Lledo, P. M., Vernier, P., Vincent, J. D., Mason, W. T., & Zorec, R. (1993). Inhibition

of Rab3B expression attenuates Ca(2+)-dependent exocytosis in rat anterior pituitary cells. *Nature*, *364*(6437), 540–544. https://doi.org/10.1038/364540a0

Loyola, A., & Almouzni, G. (2004). Histone chaperones, a supporting role in the limelight. *Biochimica et Biophysica Acta*, *1677*(1–3), 3–11. https://doi.org/10.1016/j.bbaexp.2003.09.012

Ludyga, N., Englert, S., Pflieger, K., Rauser, S., Braselmann, H., Walch, A., … Aubele, M. (2013). The impact of Cysteine-Rich Intestinal Protein 1 (CRIP1) in human breast cancer. *Molecular Cancer*, *12*(1), 28. https://doi.org/10.1186/1476-4598-12-28

Maloney, S. M., Hoover, C. A., Morejon-Lasso, L. V, & Prosperi, J. R. (2020). Mechanisms of Taxane Resistance. *Cancers*, *12*(11), 3323. https://doi.org/10.3390/cancers12113323

McLean, C. Y., Bristor, D., Hiller, M., Clarke, S. L., Schaar, B. T., Lowe, C. B., … Bejerano, G. (2010). GREAT improves functional interpretation of cis-regulatory regions. *Nature Biotechnology*, *28*(5), 495–501. https://doi.org/10.1038/nbt.1630

McMillin, D. W., Hewes, B., Gangadharan, B., Archer, D. R., Mittler, R. S., & Spencer, H. T. (2006). Complete regression of large solid tumors using engineered drug-resistant hematopoietic cells and anti-CD137 immunotherapy. *Human Gene Therapy*, *17*(8), 798–806. https://doi.org/10.1089/hum.2006.17.798

Meier, J. C., Tallant, C., Fedorov, O., Witwicka, H., Hwang, S.-Y., van Stiphout, R. G., … Knapp, S. (2017a). Selective Targeting of Bromodomains of the Bromodomain-PHD Fingers Family Impairs Osteoclast Differentiation. *ACS Chemical Biology*, *12*(10), 2619–2630. https://doi.org/10.1021/acschembio.7b00481

Meier, J. C., Tallant, C., Fedorov, O., Witwicka, H., Hwang, S.-Y., van Stiphout, R. G., … Knapp, S. (2017b). Selective Targeting of Bromodomains of the Bromodomain-PHD Fingers Family Impairs Osteoclast Differentiation. *ACS Chemical Biology*, *12*(10), 2619–2630. https://doi.org/10.1021/acschembio.7b00481

Moore, S. D. P., Herrick, S. R., Ince, T. A., Kleinman, M. S., Dal Cin, P., Morton, C. C., & Quade, B. J. (2004). Uterine leiomyomata with t(10;17) disrupt the histone acetyltransferase MORF. *Cancer Research*, *64*(16), 5570–5577. https://doi.org/10.1158/0008-5472.CAN-04-0050

Netti, G. S., Franzin, R., Stasi, A., Spadaccino, F., Dello Strologo, A., Infante, B., … Stallone, G. (2021). Role of Complement in Regulating Inflammation Processes in

Renal and Prostate Cancers. *Cells*, *10*(9). https://doi.org/10.3390/cells10092426

Obi, J. O., Lubula, M. Y., Cornilescu, G., Henrickson, A., McGuire, K., Evans, C. M., … Glass, K. C. (2020). The BRPF1 bromodomain is a molecular reader of di-acetyllysine. *Current Research in Structural Biology*, *2*, 104–115. https://doi.org/10.1016/j.crstbi.2020.05.001

Oeckinghaus, A., & Ghosh, S. (2009). The NF-κB Family of Transcription Factors and Its Regulation. *Cold Spring Harbor Perspectives in Biology*, *1*(4). https://doi.org/10.1101/CSHPERSPECT.A000034

Paradisi, A., Creveaux, M., Gibert, B., Devailly, G., Redoulez, E., Neves, D., … Mehlen, P. (2013). Combining chemotherapeutic agents and netrin-1 interference potentiates cancer cell death. *EMBO Molecular Medicine*, *5*(12), 1821–1834. https://doi.org/10.1002/emmm.201302654

Peterson, C. L., & Tamkun, J. W. (1995). The SWI-SNF complex: a chromatin remodeling machine? *Trends in Biochemical Sciences*, *20*(4), 143–146. https://doi.org/10.1016/s0968-0004(00)88990-2

Poplawski, A., Hu, K., Lee, W., Natesan, S., Peng, D., Carlson, S., … Glass, K. C. (2014). Molecular insights into the recognition of N-terminal histone modifications by the BRPF1 bromodomain. *Journal of Molecular Biology*, *426*(8), 1661–1676. https://doi.org/10.1016/j.jmb.2013.12.007

Ramírez, F., Ryan, D. P., Grüning, B., Bhardwaj, V., Kilpert, F., Richter, A. S., … Manke, T. (2016). deepTools2: a next generation web server for deep-sequencing data analysis. *Nucleic Acids Research*, *44*(W1), W160–W165. https://doi.org/10.1093/nar/gkw257

Rebello, R. J., Oing, C., Knudsen, K. E., Loeb, S., Johnson, D. C., Reiter, R. E., … Bristow, R. G. (2021). Prostate cancer. *Nature Reviews Disease Primers*, *7*(1), 9. https://doi.org/10.1038/s41572-020-00243-0

Rees, D. C., Johnson, E., & Lewinson, O. (2009). ABC transporters: the power to change. *Nature Reviews Molecular Cell Biology*, *10*(3), 218–227. https://doi.org/10.1038/nrm2646

Rengasamy, M., Zhang, F., Vashisht, A., Song, W.-M., Aguilo, F., Sun, Y., … Walsh, M. J. (2017). The PRMT5/WDR77 complex regulates alternative splicing through ZNF326 in breast cancer. *Nucleic Acids Research*, *45*(19), 11106–11120. https://doi.org/10.1093/nar/gkx727

Sánchez, C., Mercado, A., Contreras, H. R., Mendoza, P., Cabezas, J., Acevedo, C., … Castellón, E. A. (2011). Chemotherapy sensitivity recovery of prostate cancer cells by functional inhibition and knock down of multidrug resistance proteins. *The Prostate*, *71*(16), 1810–1817. https://doi.org/10.1002/pros.21398

Saxena, M., Stephens, M. A., Pathak, H., & Rangarajan, A. (2011). Transcription factors that mediate epithelial-mesenchymal transition lead to multidrug resistance by upregulating ABC transporters. *Cell Death & Disease*, *2*(7). https://doi.org/10.1038/CDDIS.2011.61

Sella, A., Sternberg, C., Kovel, S., Yarom, N., & Skoneczna, I. (2007). Progression after docetaxel-based chemotherapy in androgen-independent prostate cancer. *Urological Oncology*. https://doi.org/10.1111/j.1464-410X.2007.07037.x

Semenas, J., Allegrucci, C., Boorjian, S. A., Mongan, N. P., & Persson, J. L. (2012). Overcoming drug resistance and treating advanced prostate cancer. *Current Drug Targets*, *13*(10), 1308–1323. https://doi.org/10.2174/138945012802429615

Shang, Z., Yu, J., Sun, L., Tian, J., Zhu, S., Zhang, B., … Niu, Y. (2019). LncRNA PCAT1 activates AKT and NF-κB signaling in castration-resistant prostate cancer by regulating the PHLPP/FKBP51/IKKα complex. *Nucleic Acids Research*, *47*(8), 4211–4225. https://doi.org/10.1093/nar/gkz108

Shima, H., Yamagata, K., Aikawa, Y., Shino, M., Koseki, H., Shimada, H., & Kitabayashi, I. (2014). Bromodomain-PHD finger protein 1 is critical for leukemogenesis associated with MOZ-TIF2 fusion. *International Journal of Hematology*, *99*(1), 21–31. https://doi.org/10.1007/s12185-013-1466-x

Si, M., & Lang, J. (2018). The roles of metallothioneins in carcinogenesis. *Journal of Hematology & Oncology*, *11*(1), 107. https://doi.org/10.1186/s13045-018-0645-x

Siegel, R. L., Miller, K. D., Fuchs, H. E., & Jemal, A. (2022). Cancer statistics, 2022. *CA: A Cancer Journal for Clinicians*, *72*(1), 7–33. https://doi.org/10.3322/caac.21708

Singh, S. K., Apata, T., Gordetsky, J. B., & Singh, R. (2019). Docetaxel Combined with Thymoquinone Induces Apoptosis in Prostate Cancer Cells via Inhibition of the PI3K/AKT Signaling Pathway. *Cancers*, *11*(9). https://doi.org/10.3390/cancers11091390

Sprowl, J. A., Reed, K., Armstrong, S. R., Lanner, C., Guo, B., Kalatskaya, I., … Parissenti, A. M. (2012a). Alterations in tumor necrosis factor signaling pathways

are associated with cytotoxicity and resistance to taxanes: a study in isogenic resistant tumor cells. *Breast Cancer Research : BCR*, *14*(1), R2. https://doi.org/10.1186/bcr3083

Sprowl, J. A., Reed, K., Armstrong, S. R., Lanner, C., Guo, B., Kalatskaya, I., … Parissenti, A. M. (2012b). Alterations in tumor necrosis factor signaling pathways are associated with cytotoxicity and resistance to taxanes: a study in isogenic resistant tumor cells. *Breast Cancer Research : BCR*, *14*(1), R2. https://doi.org/10.1186/BCR3083

Suarez-Arnedo, A., Torres Figueroa, F., Clavijo, C., Arbeláez, P., Cruz, J. C., & Muñoz-Camargo, C. (2020). An image J plugin for the high throughput image analysis of in vitro scratch wound healing assays. *PLOS ONE*, *15*(7), e0232565. https://doi.org/10.1371/journal.pone.0232565

Sun, T., Bi, F., Liu, Z., & Yang, Q. (2020). SLC7A2 serves as a potential biomarker and therapeutic target for ovarian cancer. *Aging*, *12*(13), 13281–13296. https://doi.org/10.18632/aging.103433

Tao, W., Shi, J.-F., Zhang, Q., Xue, B., Sun, Y.-J., & Li, C.-J. (2013). Egr-1 enhances drug resistance of breast cancer by modulating MDR1 expression in a GGPPS-independent manner. *Biomedicine & Pharmacotherapy = Biomedecine & Pharmacotherapie*, *67*(3), 197–202. https://doi.org/10.1016/j.biopha.2013.01.001

Taverna, S. D., Li, H., Ruthenburg, A. J., Allis, C. D., & Patel, D. J. (2007a). How chromatin-binding modules interpret histone modifications: lessons from professional pocket pickers. *Nature Structural & Molecular Biology*, *14*(11), 1025–1040. https://doi.org/10.1038/nsmb1338

Taverna, S. D., Li, H., Ruthenburg, A. J., Allis, C. D., & Patel, D. J. (2007b). How chromatin-binding modules interpret histone modifications: lessons from professional pocket pickers. *Nature Structural & Molecular Biology*, *14*(11), 1025–1040. https://doi.org/10.1038/nsmb1338

Terris, B., Blaveri, E., Crnogorac-Jurcevic, T., Jones, M., Missiaglia, E., Ruszniewski, P., … Lemoine, N. R. (2002). Characterization of gene expression profiles in intraductal papillary-mucinous tumors of the pancreas. *The American Journal of Pathology*, *160*(5), 1745–1754. https://doi.org/10.1016/S0002-9440(10)61121-2

Terry, S., Ploussard, G., Allory, Y., Nicolaiew, N., Boissière-Michot, F., Maillé, P., … Vacherot, F. (2009). Increased expression of class III beta-tubulin in castration-

resistant human prostate cancer. *British Journal of Cancer*, *101*(6), 951–956. https://doi.org/10.1038/sj.bjc.6605245

Thadani-Mulero, M., Nanus, D. M., & Giannakakou, P. (2012). Androgen receptor on the move: boarding the microtubule expressway to the nucleus. *Cancer Research*, *72*(18), 4611–4615. https://doi.org/10.1158/0008-5472.CAN-12-0783

Tsai, H.-C., Chang, A.-C., Tsai, C.-H., Huang, Y.-L., Gan, L., Chen, C.-K., … Tang, C.-H. (2019). CCN2 promotes drug resistance in osteosarcoma by enhancing ABCG2 expression. *Journal of Cellular Physiology*, *234*(6), 9297–9307. https://doi.org/10.1002/jcp.27611

Tsunedomi, R., Yoshimura, K., Kimura, Y., Nishiyama, M., Fujiwara, N., Matsukuma, S., … Nagano, H. (2022). Elevated expression of RAB3B plays important roles in chemoresistance and metastatic potential of hepatoma cells. *BMC Cancer*, *22*(1), 260. https://doi.org/10.1186/s12885-022-09370-1

Ullah, M., Pelletier, N., Xiao, L., Zhao, S. P., Wang, K., Degerny, C., … Yang, X.-J. (2008). Molecular architecture of quartet MOZ/MORF histone acetyltransferase complexes. *Molecular and Cellular Biology*, *28*(22), 6828–6843. https://doi.org/10.1128/MCB.01297-08

Varambally, S., Dhanasekaran, S. M., Zhou, M., Barrette, T. R., Kumar-Sinha, C., Sanda, M. G., … Chinnaiyan, A. M. (2002). The polycomb group protein EZH2 is involved in progression of prostate cancer. *Nature*, *419*(6907), 624–629. https://doi.org/10.1038/nature01075

Vidal, S. J., Rodriguez-Bravo, V., Quinn, S. A., Rodriguez-Barrueco, R., Lujambio, A., Williams, E., … Domingo-Domenech, J. (2015). A targetable GATA2-IGF2 axis confers aggressiveness in lethal prostate cancer. *Cancer Cell*, *27*(2), 223–239. https://doi.org/10.1016/j.ccell.2014.11.013

Wang, J., Seebacher, N., Shi, H., Kan, Q., Duan, Z., Wang, J., … Duan, Z. (2017). Novel strategies to prevent the development of multidrug resistance (MDR) in cancer. *Oncotarget*, *8*(48), 84559–84571. https://doi.org/10.18632/oncotarget.19187

Wang, K., Zhu, X., Zhang, K., Yin, Y., Chen, Y., & Zhang, T. (2018). Interleukin-6 contributes to chemoresistance in MDA-MB-231 cells via targeting HIF-1α. *Journal of Biochemical and Molecular Toxicology*, *32*(3), e22039. https://doi.org/10.1002/jbt.22039

Wang, L., Skotland, T., Berge, V., Sandvig, K., & Llorente, A. (2017). Exosomal proteins as prostate cancer biomarkers in urine: From mass spectrometry discovery to immunoassay-based validation. *European Journal of Pharmaceutical Sciences : Official Journal of the European Federation for Pharmaceutical Sciences*, *98*, 80–85. https://doi.org/10.1016/j.ejps.2016.09.023

Wang, Q., Li, M., Wu, T., Zhan, L., Li, L., Chen, M., … Yu, G. (2022). Exploring Epigenomic Datasets by ChIPseeker. *Current Protocols*, *2*(10). https://doi.org/10.1002/cpz1.585

Wang, R., Sumarpo, A., Saiki, Y., Chen, N., Sunamura, M., & Horii, A. (2016). ABCB1 Is Upregulated in Acquisition of Taxane Resistance: Lessons from Esophageal Squamous Cell Carcinoma Cell Lines. *The Tohoku Journal of Experimental Medicine*, *240*(4), 295–301. https://doi.org/10.1620/tjem.240.295

Wang, Y., Huang, Z., Chen, C. Z., Liu, C., Evans, C. P., Gao, A. C., … Chen, H.-W. (2020). Therapeutic Targeting of MDR1 Expression by RORγ Antagonists Resensitizes Cross-Resistant CRPC to Taxane via Coordinated Induction of Cell Death Programs. *Molecular Cancer Therapeutics*, *19*(2), 364–374. https://doi.org/10.1158/1535-7163.MCT-19-0327

Wein, L., & Loi, S. (2017). Mechanisms of resistance of chemotherapy in early-stage triple negative breast cancer (TNBC). *The Breast*, *34*, S27–S30. https://doi.org/10.1016/J.BREAST.2017.06.023

Wen, H., Kim, Y. C., Snyder, C., Xiao, F., Fleissner, E. A., Becirovic, D., … Wang, S. M. (2014). Family-specific, novel, deleterious germline variants provide a rich resource to identify genetic predispositions for BRCAx familial breast cancer. *BMC Cancer*, *14*(1), 470. https://doi.org/10.1186/1471-2407-14-470

Wu, T. Y. H., Hassig, C., Wu, Y., Ding, S., & Schultz, P. G. (2004). Design, synthesis, and activity of HDAC inhibitors with a N-formyl hydroxylamine head group. *Bioorganic & Medicinal Chemistry Letters*, *14*(2), 449–453. https://doi.org/10.1016/j.bmcl.2003.10.055

Xin, L., Liu, C., Liu, Y., Mansel, R. E., Ruge, F., Davies, E., … Martin, T. A. (2021). SIKs suppress tumor function and regulate drug resistance in breast cancer. *American Journal of Cancer Research*, *11*(7), 3537–3557. Retrieved from http://www.ncbi.nlm.nih.gov/pubmed/34354859

Yan, K., Rousseau, J., Littlejohn, R. O., Kiss, C., Lehman, A., Rosenfeld, J. A., …

Yang, X.-J. (2017). Mutations in the Chromatin Regulator Gene BRPF1 Cause Syndromic Intellectual Disability and Deficient Histone Acetylation. *The American Journal of Human Genetics*, *100*(1), 91–104. https://doi.org/10.1016/J.AJHG.2016.11.011

Yan, K., Rousseau, J., Machol, K., Cross, L. A., Agre, K. E., Gibson, C. F., … Yang, X.-J. (2020). Deficient histone H3 propionylation by BRPF1-KAT6 complexes in neurodevelopmental disorders and cancer. *Science Advances*, *6*(4). https://doi.org/10.1126/sciadv.aax0021

Yang, X-J, & Ullah, M. (2007). MOZ and MORF, two large MYSTic HATs in normal and cancer stem cells. *Oncogene*, *26*(37), 5408–5419. https://doi.org/10.1038/sj.onc.1210609

Yang, Xiang-Jiao. (2015). MOZ and MORF acetyltransferases: Molecular interaction, animal development and human disease. *Biochimica et Biophysica Acta*, *1853*(8), 1818–1826. https://doi.org/10.1016/j.bbamcr.2015.04.014

You, L., Li, L., Zou, J., Yan, K., Belle, J., Nijnik, A., … Yang, X.-J. (2016). BRPF1 is essential for development of fetal hematopoietic stem cells. *The Journal of Clinical Investigation*, *126*(9), 3247–3262. https://doi.org/10.1172/JCI80711

You, L., Yan, K., Zou, J., Zhao, H., Bertos, N. R., Park, M., … Yang, X.-J. (2015). The chromatin regulator Brpf1 regulates embryo development and cell proliferation. *The Journal of Biological Chemistry*, *290*(18), 11349–11364. https://doi.org/10.1074/jbc.M115.643189

Zahra, R., Furqan, M., Ullah, R., Mithani, A., Saleem, R. S. Z., & Faisal, A. (2020). A cell-based high-throughput screen identifies inhibitors that overcome P-glycoprotein (Pgp)-mediated multidrug resistance. *PLOS ONE*, *15*(6), e0233993. https://doi.org/10.1371/journal.pone.0233993

Zhang, G., Liu, X., Li, J., Ledet, E., Alvarez, X., Qi, Y., … Zhang, H. (2015). Androgen receptor splice variants circumvent AR blockade by microtubule-targeting agents. *Oncotarget*, *6*(27), 23358–23371. https://doi.org/10.18632/oncotarget.4396

Zhang, Q., Lei, L., & Jing, D. (2020). Knockdown of SERPINE1 reverses resistance of triple-negative breast cancer to paclitaxel via suppression of VEGFA. *Oncology Reports*, *44*(5), 1875–1884. https://doi.org/10.3892/or.2020.7770

Zhong, B., Sallman, D. A., Gilvary, D. L., Pernazza, D., Sahakian, E., Fritz, D., … Djeu, J. Y. (2010). Induction of clusterin by AKT--role in cytoprotection against

docetaxel in prostate tumor cells. *Molecular Cancer Therapeutics*, *9*(6), 1831–1841. https://doi.org/10.1158/1535-7163.MCT-09-0880

Zhu, Y., Liu, C., Nadiminty, N., Lou, W., Tummala, R., Evans, C. P., & Gao, A. C. (2013). Inhibition of ABCB1 Expression Overcomes Acquired Docetaxel Resistance in Prostate Cancer. *Molecular Cancer Therapeutics*, *12*(9), 1829–1836. https://doi.org/10.1158/1535-7163.MCT-13-0208